수의학 박사학위 논문

Proteomic profiling of cuprizone-induced demyelination in the mouse hippocampus

마우스 해마에서
cuprizone 에 의한 탈수초화 과정 중의
단백체 분석

2023 년 2 월

서울대학교 대학원
수의학과 수의생명과학 전공
(수의조직학)
한 규 리

A Dissertation for the Degree of Doctor of Philosophy

Proteomic profiling of cuprizone-induced demyelination in the mouse hippocampus

February 2023

Kyu Ri Hahn

Supervisor: Prof. Yeo Sung Yoon, D.V.M., Ph.D.

Department of Veterinary Medicine
Veterinary Biomedical Sciences
(Veterinary Histology)

The Graduate School of Seoul National University

Proteomic profiling of cuprizone-induced demyelination in the mouse hippocampus

지도교수 윤 여 성

이 논문을 수의학박사 학위논문으로 제출함
2022 년 11 월

서울대학교 대학원
수의학과 수의생명과학전공
(수의조직학)
한 규 리

한규리의 수의학박사 학위논문을 인준함

2022 년 12 월

위 원 장 _____ (인)

부위원장 _____ (인)

위 원 _____ (인)

위 원 _____ (인)

위 원 _____ (인)

ABSTRACT

Proteomic profiling of cuprizone-induced demyelination in the mouse hippocampus

By
Kyu Ri Hahn

Graduate School of Seoul National University

Supervisor: Prof. Yeo Sung Yoon, D.V.M., Ph.D.

Multiple sclerosis is characterized by the autoimmune attack on myelin sheath in the central nervous system. The cuprizone model, which induces demyelination, has been widely used in multiple sclerosis research. In the present experiment, I sought to examine the changes in hippocampal proteomic profiles during demyelination and remyelination using the cuprizone model.

First, the experimental animals were divided into three groups: a group receiving normal chow diet for 8 weeks (control), a group receiving cuprizone-supplemented

diet for 8 weeks, and a group receiving normal chow diet for 3 weeks following cuprizone-supplemented diet for 5 weeks.

The cuprizone-supplemented diet significantly reduced myelin sheath, cell proliferation, neuroblast differentiation, and cAMP response element-binding protein (CREB) signaling in the hippocampus. Meanwhile, cessation of cuprizone intake significantly ameliorated the reduction in myelin sheath, cell proliferation, neuroblast differentiation, and CREB signaling in the hippocampus.

Next, two-dimensional gel electrophoresis (2DE) and liquid chromatography-tandem mass spectrometry (LC-MS/MS)-based quantification methods were applied for hippocampal protein profiling following demyelination and remyelination. Expression of various proteins in the hippocampus was altered by over two-folds following cuprizone intake or termination.

Among the identified proteins, the expression of only ketimine reductase mu-crystallin (CRYM) and protein disulfide isomerase A3 precursor (PDIA3) was decreased after cuprizone intake and increased after cuprizone termination. To validate the protein expression patterns in the hippocampus, immunohistochemical staining was performed. Both PDIA3 and CRYM were significantly downregulated in hippocampal CA1 region upon demyelination and upregulated upon remyelination. Immunostaining of PDIA3 and CRYM in the hippocampus was weakened during demyelination and intensified during remyelination. Overall, the results of protein analysis and immunostaining were consistent.

Furthermore, I investigated the protective effects of CRYM and PDIA3 against cuprizone-induced demyelination in the hippocampus. To ease the crossing of proteins through the blood–brain barrier, I synthesized Tat peptide-fusion proteins,

including Tat-CRYM and Tat-PDIA3. The experimental animals were divided into four groups: a control group, a group receiving cuprizone diet, a group receiving Tat-CRYM plus cuprizone diet, and a group receiving Tat-PDIA3 plus cuprizone diet. Immunofluorescence staining revealed that the reduction in proliferating cell count and neuroblast differentiation was alleviated in groups receiving Tat-CRYM and Tat-PDIA3, respectively, compared with those in the group receiving cuprizone alone. Meanwhile, significant ameliorative effects on myelin basic protein expression and CREB signaling in the hippocampus were noted only in the group receiving Tat-PDIA3 plus cuprizone. These results suggest that Tat-PDIA3 ameliorates cuprizone-induced demyelination and reduction in hippocampal neurogenesis by promoting phosphorylation in CREB signaling.

In conclusion, cuprizone intake reduces myelin sheath, cell proliferation, neuroblast differentiation, and CREB signaling in the hippocampus, while cuprizone termination ameliorates these effects during remyelination. Through hippocampal proteomic analysis during demyelination and remyelination, the existence of CRYM and PDIA3, the only proteins whose expression was suppressed during demyelination and promoted during remyelination, was confirmed, and immunostaining corroborated these findings. Administration of both CRYM and PDIA3 in the demyelinated state improved cell proliferation and neuroblast differentiation in the hippocampus, while PDIA3 administration alone improved myelin and CREB signaling. In addition, hippocampal neurogenesis is closely related to the growth of neurons and phosphorylation in CREB signaling. Therefore, PDIA3 may be useful for the prevention or treatment of demyelination, suggesting its therapeutic potential in multiple sclerosis.

Keywords: Neurogenesis, Hippocampus, Multiple sclerosis, Cuprizone, Demyelination, Remyelination, Ketimine reductase mu-crystallin, Protein disulfide isomerase A3 precursor

Student number: 2016-21756

LIST OF ABBREVIATION

2DE	Two-dimensional gel electrophoresis
AGC	Automatic gain control
AHN	Adult hippocampal neurogenesis
ANOVA	One-way analysis of variance
CNX	Calnexin
CPZ	Cuprizone
CRYM	Ketimine reductase mu-crystallin
CTL	Normal chow diet-fed mice
Cu	CPZ-supplemented diet-fed mice
Cu+CRYM	CPZ-supplemented diet-fed mice with injection of Tat-CRYM
Cu+N	Normal diet group for 3 weeks after CPZ-diet for 5 weeks
Cu+PDIA3	CPZ-supplemented diet-fed with injection of Tat-PDIA3
DCX	Doublecortin
DG	Dentate gyrus
DI	Deionized
DW	Distilled water
GCL	Granular cell layer
HSP10	10 kDa heat shock protein
Iba-1	Ionized calcium-binding adapter molecule 1
LASP1	LIM and SH3 domain protein 1
LC-MS/MS	Liquid chromatography-tandem mass spectrometry

MBP	Myelin basic protein
ML	Molecular layer
MS	Multiple sclerosis
PB	Phosphate buffer
PBS	Phosphate-buffered saline
pCREB	Phosphorylated cAMP response element binding protein at Ser133
PDIA3	Protein disulfide isomerase A3 precursor
PoL	Polymorphic layer
ROD	Relative optical density
SGZ	Subgranular zone

CONTENTS

LIST OF FIGURES

Figure 13. Overview of Tat-CRYM and Tat-PDIA3 fusion proteins and confirmation of the delivery of these proteins to the mouse hippocampus with immunohistochemical staining for His-tag.

Figure 14. MBP immunohistochemical staining in the hippocampus of group fed normal chow diet (CTL), group fed CPZ diet (Cu), group fed CPZ diet and administered Tat-CRYM injection (Cu+CRYM), and group fed CPZ diet and administered Tat-PDIA3 injection (Cu+PDIA3).

Figure 15. Iba-1 immunohistochemical staining in the hippocampus of group fed normal chow diet (CTL), group fed CPZ diet (Cu), group fed CPZ diet and administered Tat-CRYM injection (Cu+CRYM), and group fed CPZ diet and administered Tat-PDIA3 injection (Cu+PDIA3).

Figure 16. Ki67 immunohistochemical staining in the hippocampal DG of group fed normal chow diet (CTL), group fed CPZ diet (Cu), group fed CPZ diet and administered Tat-CRYM injection (Cu+CRYM), and group fed CPZ diet and administered Tat-PDIA3 injection (Cu+PDIA3).

Figure 17. DCX immunohistochemical staining in the hippocampal DG of group fed normal chow diet (CTL), group fed CPZ diet (Cu), group fed CPZ diet and administered Tat-CRYM injection (Cu+CRYM), and group fed CPZ diet and administered Tat-PDIA3 injection (Cu+PDIA3).

Figure 18. pCREB staining in the hippocampal DG of group fed normal chow diet (CTL), group fed CPZ diet (Cu), group fed CPZ diet and administered Tat-CRYM injection (Cu+CRYM), and group fed CPZ diet and administered Tat-PDIA3 injection (Cu+PDIA3).

LIST OF TABLES

INTRODUCTION

The hippocampus—one of the important parts of the limbic system—plays pivotal roles in learning and memory. In particular, it performs crucial functions in transforming short-term memory into long-term memory and, likewise, in spatial cognition (Castilla-Ortega et al., 2011; Eichenbaum, 2017). Adult hippocampal neurogenesis (AHN) is characterized by the continuous production of neural stem cells in certain brain regions, including the subventricular zone of the lateral ventricle and subgranular zone (SGZ) of the dentate gyrus (DG) in the hippocampus (Gage, 2002; Kempermann et al., 1997). The DG can be divided into three layers based on the structure: the molecular layer (ML), granular cell layer (GCL), and polymorphic layer (PoL). The ML constitutes the dendrites of granule cells and axons derived from the entorhinal cortex. The GCL is formed by the cell bodies of granule cells, where dendrites enter the ML and accept input signals from the perforant pathway of the entorhinal cortex. The PoL, the deepest layer of the DG, constitutes the axons of granule cells and mossy fibers with abundant intervening neurons (Amaral et al., 2007; Toni and Schinder, 2015).

Newly generated granule cells are produced from neural stem cells in the SGZ through the processes of proliferation, differentiation, and maturation. Type 1 cells are called radial glial cells because of their morphology. Type 2 cells are characterized by the most potent proliferative potential and are believed to be immediate precursor cells during transition from glial to neuronal lineages. Finally, type 3 cells (i.e., neuroblasts) depart the cell cycle and differentiate into immature neurons. Thereafter, the maturation of newly generated neurons is characterized by

rapid axonal and dendritic growth and elevated synaptic plasticity. Axons of mature neurons expand into the pyramidal cells of hippocampal CA3 region (Beckervordersandforth et al., 2015; Kempermann et al., 2015), and these integrated neurons are involved in the function of neural circuitry in the hippocampus (Mu et al., 2011).

Myelin allows neuron to transmit information faster, because the myelination of axons propagates the action potential by jumping node to node. Demyelination disease is any condition that damages the nerve fibers in the brain. For instance, multiple sclerosis (MS) is characterized by autoimmune-mediated attack on the myelin sheath, which hinders the ability of nerves to transmit messages properly, with the risk of subsequent degeneration. In many patients with MS, nerve damage and extensive demyelination in the hippocampus have been reported as pathological features (Guimarães and Sá, 2012). Although drugs may help reduce the disease progression, the symptoms of MS cannot be reversed, and the mechanisms underlying tissue damage and the ameliorative effects of these drugs are only partly understood.

Cuprizone (CPZ), a copper chelator, has been widely used to induce the damage and loss of myelin and oligodendrocytes in the brain (Matsushima and Morell, 2001), including the hippocampus (Kim et al., 2019). Repeated exposure to CPZ is indicative of gray matter demyelinating disease, resembling the condition in MS, which causes amnesia (Lassmann, 2018; Omotoso et al., 2019); it has also been used in the process of remyelination. Meanwhile, termination of CPZ has been reported to result in strong remyelination within a few days (Skripuletz et al., 2015). In previous studies using mouse models, CPZ treatment significantly suppressed

myelin basic protein (MBP) levels in the hippocampus, thereby reducing cell proliferation and neuroblast differentiation in the DG (Kim et al., 2019; Hahn et al., 2022).

Several approaches exist for the analysis of CPZ-induced demyelination in multiple brain regions (Sen et al., 2021; Werner et al., 2010). For instance, Szilagyi et al. (2020) used proteomics to study demyelination and remyelination in the corpus callosum. However, no systemic approaches have been employed to assess hippocampal protein changes in the presence of clear CPZ-induced demyelination (Matsushima and Morell, 2001) and AHN reduction. Therefore, I sought to examine the modulations in hippocampal protein profiles during demyelination and remyelination induced by CPZ exposure for 8 weeks or CPZ exposure for 5 weeks, followed by CPZ termination for 3 weeks.

In the present experiment, two-dimensional gel electrophoresis (2DE) and liquid chromatography-tandem mass spectrometry (LC-MS/MS)-based quantification methods were applied to evaluate evident proteins changes following the intake of CPZ-supplemented and/or normal diet. Among the identified and significantly altered proteins, those whose expression was suppressed after CPZ intake but promoted after CPZ termination were further analyzed, and their effects on CPZ-induced demyelination were assessed as a step toward the treatment of demyelination disease.

MATERIALS AND METHODS

Experimental design I

Experimental animals

Four-week-old male C57BL/6N mice were obtained from the Central Lab Animal Inc. (Seoul, South Korea). All animals were maintained at 22 ± 1℃ and 60% ± 5% humidity under a 12 h/12 h light/dark cycle; food and water were provided *ad libitum* until the end of experiment. All experimental protocols were approved by the Institutional Animal Care and Use Committee of the Seoul National University (SNU-190314-12-2 and SNU-190906-2). Animal handling and management conformed to guidelines established under the current international laws and policies (NIH Guide for the Care and Use of Laboratory Animals, NIH Publication No. 85-23, 1985, revised 1996). All experimental processes were performed to minimize the number of animals used and the suffering of experimental animals caused by the research procedure. The animals were divided into three groups: a group receiving normal chow diet for 8 weeks (CTL), a group receiving CPZ-supplemented diet for 8 weeks (Cu), and a group receiving normal diet for 3 weeks following CPZ-supplemented diet for 5 weeks (Cu+N). The CPZ-supplemented diet contained 0.2% CPZ (Sigma-Aldrich, St. Louis, MO, USA) in AIN-76-based chow diet, as described in a previous study (Hahn et al., 2022).

2DE

Following treatment with CPZ diet for 8 weeks or CPZ diet for 5 weeks, followed by normal diet for 3 weeks, the mice were anesthetized with a mixture of alfaxalone

(75 mg/kg; Careside, Seongnam, South Korea) and xylazine (10 mg/kg; Bayer Korea, Seoul, South Korea). Hippocampal tissues were isolated from the brains and suspended in a mixture of buffer described elsewhere (Jung et al., 2020). 2DE was performed as follows (Park et al., 2002). First, sample aliquots in buffer (7 M urea, 2 M thiourea, 4.5% 3-((3-cholamidopropyl) dimethylammonio)-1-propanesulfonate, 100 mM dithioerythritol, and 40 mM Tris [pH 8.8]) were applied to immobilized pH 3–10 nonlinear gradient strips (Amersham Biosciences, Uppsala, Sweden). Isoelectric focusing was regulated at 80,000 Vh. For second dimension, electrophoresis was performed with 9–16% linear gradient polyacrylamide gels (18 cm × 20 cm × 1.5 mm) at constant 40 mA per gel for approximately 5 h. For protein fixation, the gels were incubated in 40% methanol and 5% phosphoric acid for 1 h and stained using Coomassie brilliant blue GG-250 for 12 h. After de-staining with distilled water (DW), the gels were scanned in a densitometer (GS710; Bio-Rad, Richmond, CA, USA) and converted into electronic files. The results were analyzed with Image Master Platinum 5.0 (Amersham Biosciences).

Peptide analysis using LC-MS/MS

For peptide analysis, Easy n-LC (Thermo Fisher, San Jose, CA, USA) and LTQ Orbitrap XL mass spectrometer (Thermo Fisher) equipped up with a nano-electrospray source were used. Using a C18 nanopore column (150 mm × 0.1 mm, 3 μm pore size; Agilent), the samples were separated. For LC separation, mobile phase A (0.1% formic acid and 3% acetonitrile in DI water) and mobile phase B (0.1% formic acid in acetonitrile) were used. The chromatography gradient was scheduled for a linear increase from 0% B to 60% B in 9 min, 60% B to 90% B in 1 min, and

3% B in 5 min at the flow rate of 1,800 nL·min-1. The mass spectra were obtained through data-dependent acquisition with a full mass scan (380–1700 m/z) and 10 MS/MS scans. For MS1 full scans, the orbitrap resolution was 15,000 and the automatic gain control (AGC) was 2×10^5; for MS/MS with LTQ, AGC was 1×10^4.

Database search

Using the MASCOT search engine (Matrix Science Inc., Boston, MA, USA), peptide sequences present in the protein sequence database were identified. The database search criteria were as follows: taxonomy = *Mus musculus*; fixed modification = carbamidomethylation at cysteine residues; variable modification = oxidization at methionine residues; maximum allowed missed cleavage = 2; MS tolerance = 10 ppm; and MS/MS tolerance = 0.8 Da. The peptides were processed at a significance threshold of $p < 0.05$.

The "score" in each table is the MASCOT score, calculated as follows: SCORE = $-10 \times \ln 10(P)$, where P is the molecular weight search score.

Tissue processing and immunostaining

The animals were perfused with 0.1 M phosphate-buffered saline (PBS, pH 7.4), followed by 4% paraformaldehyde in 0.1 M phosphate buffer (PB, pH 7.4). The mouse brains were dissected and fixed in 4% paraformaldehyde for 12 h at 4℃. Then, the brains were incubated overnight in 30% sucrose solution. Next, 30-μm-thick sections of the brains were obtained with a cryostat (Leica, Wetzlar, Germany) and stored in a preservative containing 30% glycerol, 30% ethyl glycol, 10% $2PO_4$, and 30% DW at 4℃ until use. The sections were subjected to overnight

immunostaining at 4°C with the following primary antibodies: rabbit anti-Ki67 (1:1,000; Abcam, Cambridge, UK), rabbit anti-doublecortin (DCX, 1:2,000; Abcam), rabbit anti-myelin basic protein (MBP, 1:1,000; Abcam), rabbit anti-phosphorylated cAMP response element binding protein at Ser133 (pCREB, 1:1,000; Cell Signaling Technology Inc., Beverly, MA, USA), mouse anti-ketimine reductase mu-crystallin (CRYM, 1:250; Santa Cruz Biotechnology Inc., Santa Cruz, CA, USA), and rabbit anti-protein disulfide isomerase A3 precursor (PDIA3, 1:1000; Thermo Fisher Scientific; Invitrogen, Waltham, MA, USA).

Data quantification and statistical analysis

All immunoreactive structures were analyzed using ImageJ 1.53 (NIH, Bethesda, MD, USA). Four sections of the brain located between 1.70 and 2.46 mm from the bregma at 180 μm intervals were used to analyze the number or immunoreactivity of the immunohistochemically stained structures (Paxinos, 2001).

Optical densities of CRYM, PDIA3, MBP, and DCX were evaluated as the sum of gray scale (0–255) and pixel number using ImageJ. The number of Ki67- and pCREB-immunoreactive nuclei was in the SGZ of DG bounded by the GCL was determined. The resultant data were represented as mean ± standard deviation and statistically analyzed using GraphPad Prism 5.01 (GraphPad Software Inc., La Jolla, CA, USA), as previously described (Hahn et al., 2022). The relative optical density (ROD) was described as the percentage of the control value. One-way analysis of variance (ANOVA), followed by Bonferroni post hoc test, was performed, and a $p < 0.05$ was considered significant.

Experimental design II

Experimental animals

Four-week-old male C57BL/6N mice were obtained from the Central Lab Animal Inc. (Seoul). All animals were maintained at 22 ± 1°C and 60% ± 5% humidity under a 12 h/12 h light/dark cycle; food and water were provided *ad libitum* until the end of experiment. All experimental protocols were approved by the Institutional Animal Care and Use Committee of the Seoul National University (SNU-210917-2). Animal handling and management conformed to guidelines established under the current international laws and policies (NIH Guide for the Care and Use of Laboratory Animals, NIH Publication No. 85-23, 1985, revised 1996). All experimental processes were performed to minimize the number of animals used and suffering of the experimental animals caused by the research procedure. The animals were divided into four groups: CTL, Cu, CPZ-supplemented diet-fed mice with Tat-CRYM injection (Cu+CRYM), and CPZ-supplemented diet-fed mice with Tat-PDIA3 injection (Cu+PDIA3). The CPZ-supplemented diet was provided for 8 weeks, and Tat-CRYM (3 $mg \cdot kg^{-1}$) or Tat-PDIA3 (3 $mg \cdot kg^{-1}$) was administered intraperitoneally once a day for the 4 final weeks.

Expression vector construction

To facilitate the intracellular delivery and blood–brain barrier crossing of the CRYM and PDIA3 proteins in the mouse hippocampus, Tat-CRYM and Tat-PDIA3 were prepared. As described previously (Yoo et al., 2017, 2019), polymerase chain reaction (PCR) was performed using primers for CRYM and PDIA3 cDNAs. The PCR product was subcloned into a TA cloning vector and ligated to a Tat expression

vector. Each of the plasmids with Tat-CRYM and Tat-PDIA3 was transformed into *Escherichia coli* BL21 cells and confirmed. Proteins purified using the Nib+ → Ni2+-nitrilotriacetic acid sepharose affinity column with PD-10 column chromatography (Amersham) were processed using Detoxi-Gel™ endotoxin removal gel (Pierce, Rockford, IL, USA). The final Tat-CRYM and Tat-PDIA3 proteins were confirmed by western blotting with the rabbit anti-His-Tag antibody (1:200, Novus Biologicals, Centennial, CO, USA).

Tissue processing and immunofluorescence staining

Following treatment the CPZ diet plus Tat-CRYM or Tat-PDIA3, the mice were anesthetized with a mixture of alfaxalone (75 mg/kg; Careside) and xylazine (10 mg/kg; Bayer Korea). The animals were perfused transcardially with 0.1M PBS (pH 7.4) and 4% paraformaldehyde in 0.1 M PB (pH 7.4). The brains were dissected and further fixed for 12 h in the same fixative containing 4% paraformaldehyde, followed by overnight incubation in 30% sucrose solution. Next, 30-μm-thick sections were obtained with a cryostat (Leica) and stored in a preservative containing 30% glycerol, 30% ethyl glycol, 10% $2PO_4$, and 30% DW at 4℃ until use. After washing with PBS, the sections were incubated with the following primary antibodies, as described previously (Hahn et al., 2022; Jung et al., 2020): rabbit anti-His-Tag (1:200; Novus), rabbit anti-Ki67 (1:1,000; Abcam), rabbit anti-DCX (1:2,000; Abcam), rabbit anti-MBP (1:1,000; Abcam), rabbit anti-pCREB (1:1,000; Cell Signaling Technology Inc.), and rabbit anti-Iba-1 (1:500; Wako, Osaka, Japan). Thereafter, the sections were incubated with Cy3-conjugated anti-rabbit IgG for 2 h.

Data quantification and statistical analysis

All immunoreactive structures were analyzed using ImageJ 1.53 (NIH, Bethesda, MD, USA). Four sections located between 1.70 and 2.46 mm from the bregma at 180 μm intervals were used to analyze the number of immunohistochemically stained structures (Paxinos, 2001).

Optical densities of His-Tag, MBP, Iba-1, and DCX were evaluated as the sum of gray scale (0–255) and pixel number using ImageJ (version 1.53; National Institutes of Health), and the number of Ki67- and pCREB-immunoreactive nuclei was in the SGZ of DG bounded by the GCL was determined. The resultant data were presented as mean ± standard deviation and statistically analyzed using GraphPad Prism 5.01 (GraphPad Software Inc., La Jolla, CA, USA), as previously described (Jung et al., 2019; Hahn et al., 2022). ROD was defined as percentage of the control value. The results were subjected to ANOVA, followed by Bonferroni post hoc test, and a $p < 0.05$ was considered statistically significant.

RESULTS

Experiment I

Effects of demyelination and remyelination on MBP immunoreactivity in the hippocampus

Immunostaining was performed using MBP to examine the changes in myelin sheath following demyelination induced by the CPZ-supplemented diet and remyelination following switch to the normal diet. In the CTL group, strong MBP immunoreactivity was noted in the alveus and stratum lacunosum-moleculare of the hippocampal CA1 region, mossy fibers of the hippocampal CA3 region, and SGZ of the DG compared with that in the other groups (Figure 1A). In contrast, weak MBP immunoreactivity was observed in the DG in the Cu group, which was significantly lower (53.8% of CTL) than that in the CTL group (Figure 1B and 1D). In the Cu+N group, MBP immunoreactivity was significantly increased compared with that in the Cu group (Figure 1C). The mean percentage of ROD was 80.8% in the Cu+N group compared with 100% in the CTL group (Figure 1D).

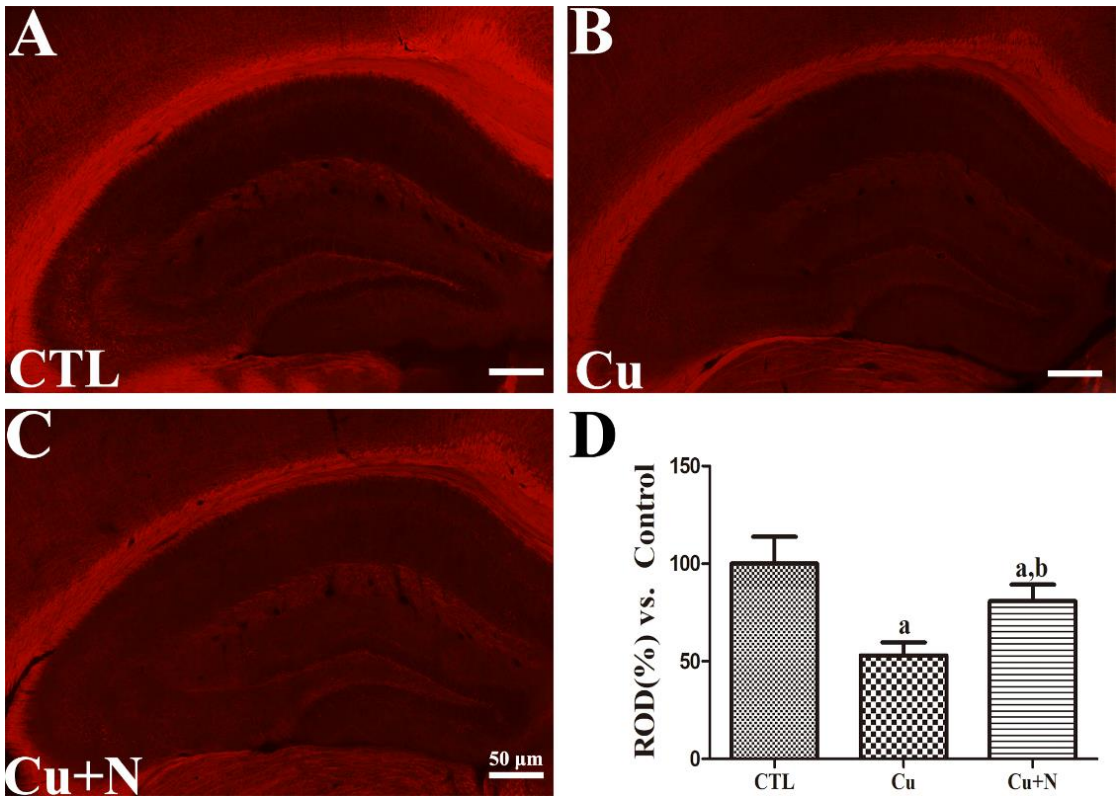

Figure 1. MBP immunohistochemical staining in the hippocampus of (A) group fed normal chow diet for 8 weeks (CTL), (B) group fed CPZ diet for 8 weeks (Cu), and (C) group fed normal diet for 3 weeks after CPZ diet for 5 weeks (Cu+N). (D) ROD represents the percentage of MBP immunoreactivity in the hippocampus in the CTL group. Scale bar = 50 μm. (n = 5 per group; $^{a}p < 0.05$, significantly different from the CTL group; $^{b}p < 0.05$, significantly different from the Cu group). All data are presented as mean ± standard deviation.

Effects of demyelination and remyelination on cell proliferation in the DG

To confirm cell proliferation in the DG, Ki67 immunohistochemical staining was performed after demyelination induced by the CPZ diet and remyelination induced by switch to the normal diet. In the CTL group, the highest number of the Ki67-positive cells were located in the SGZ of the DG (27 cells; Figure 2A, 2D, and 2G). In the Cu group, a few Ki67-positive cells were noted in the SGZ (Figure 2B and 2E), and their number was significantly lower (12.6 cells) than that in the CTL group (Figure 2G). In the Cu+N group, 21.8 Ki67-positive cells were detected in the SGZ, and this number was significantly higher than that in the Cu group (Figure 2C, 2F, and 2G).

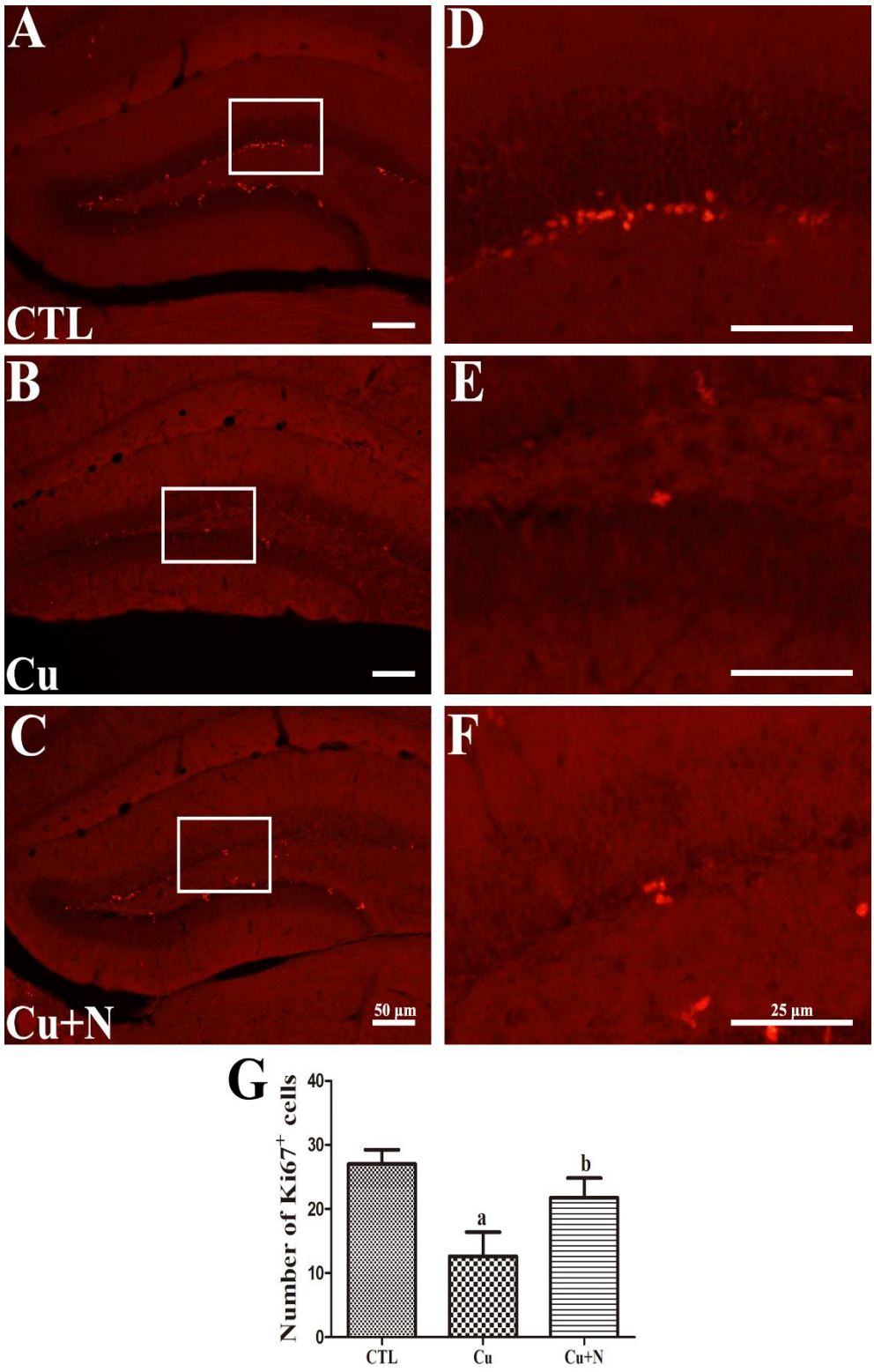
A
CTL
D
B
Cu
E
C
Cu+N
50 μm
F
25 μm
G
Number of Ki67+ cells
40
30
20
10
0
a
b
CTL
Cu
Cu+N

Figure 2. Ki67 immunohistochemical staining in the DG of (A, D) group fed normal chow diet for 8 weeks (CTL), (B, E) group fed CPZ diet for 8 weeks (Cu), and (C, F) group fed normal diet for 3 weeks after CPZ diet for 5 weeks (Cu+N). (D, E, F) High magnification of boxed areas in (A), (B), and (C), respectively. (G) Number of Ki67-postivie cells in the SGZ of DG. Scale bar = 50 μm (A, B, and C) and 25 μm (D, E, and F) (n = 5 per group; $^{a}p < 0.05$, significantly different from the CTL group; $^{b}p < 0.05$, significantly different from the Cu group). All data are presented as mean ± standard deviation.

Effects of demyelination and remyelination on neuroblast differentiation in the DG

DCX immunostaining was performed to observe the number of differentiated neuroblasts in the DG. In the CTL group, the highest number of cell bodies of DCX-immunoreactive neuroblasts was recorded in the SGZ, and their well-developed dendrites extended into the ML of DG (Figure 3A and 3D). In the Cu group, the number of DCX-immunoreactive neuroblasts in the DG was clearly reduced, and their dendrites were poorly developed (Figure 3B and 3E). In the Cu+N group, the number of DCX-immunoreactive neuroblasts was higher than that in the Cu group (Figure 3C and 3F). In the Cu group, DCX immunoreactivity was 25.7% of that in the CTL group, indicating a significant reduction. Conversely, in the Cu+N group, DCX immunoreactivity was 73.0% of that in the CTL group, indicating significant increase compared with the value in the Cu group but significantly decrease compared with the value in the CTL group (Figure 3G).

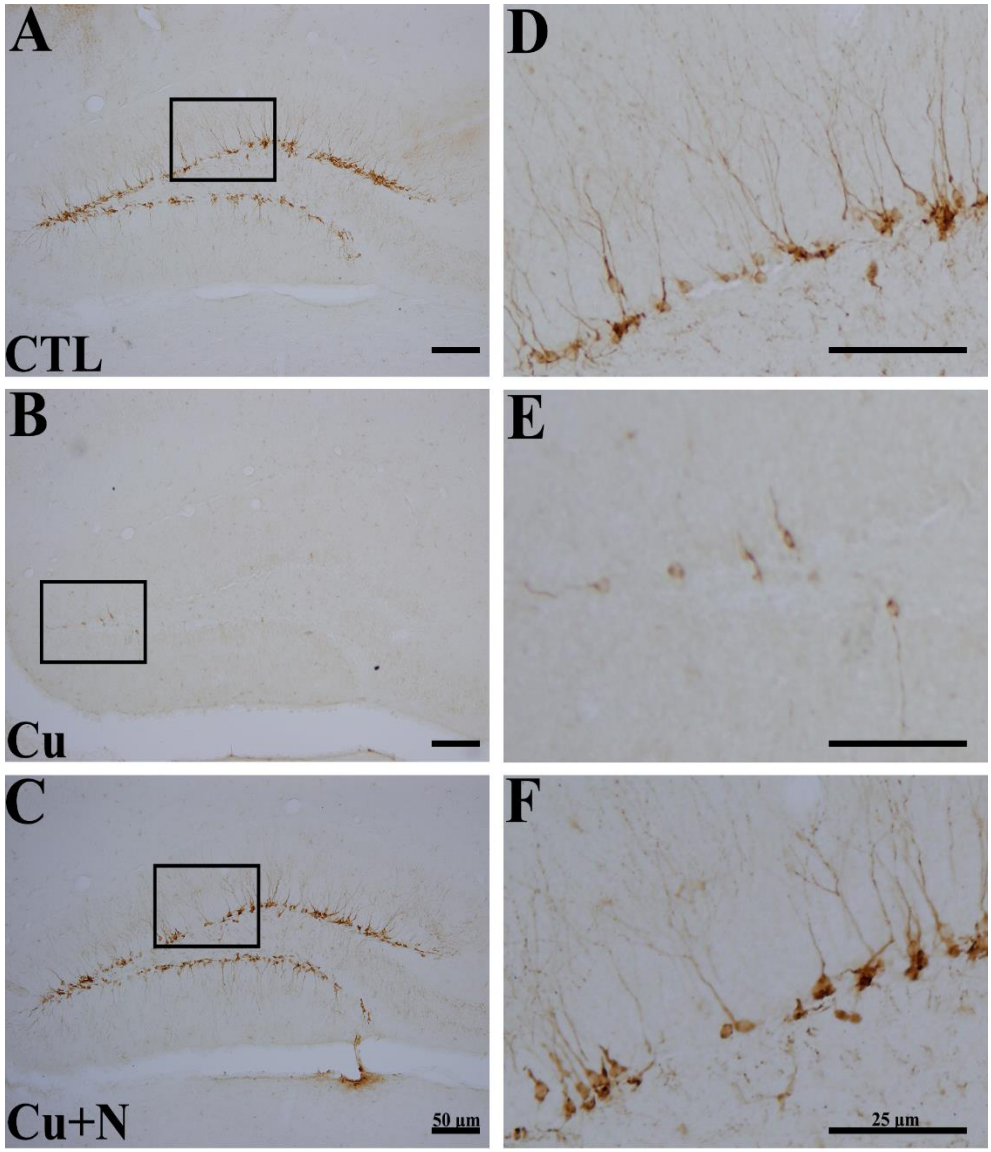
A
CTL
D
B
Cu
E
C
Cu+N
50 μm
F
25 μm
G
ROD(%) vs. Control
150
100
50
0
a
a,b
CTL
Cu
Cu+N

Figure 3. DCX immunohistochemical staining in the hippocampal DG of (A, D) group fed normal chow diet for 8 weeks (CTL), (B, E) group fed CPZ diet for 8 weeks (Cu), and (C, F) group fed normal diet for 3 weeks after CPZ diet for 5 weeks (Cu+N). (D, E, F) High magnification of boxed areas in (A), (B), and (C), respectively. (G) ROD is described as the percentage of DCX immunoreactivity in the DG of the CTL group. Scale bar = 50 μm (A, B, C) and 25 μm (D, E, F). (n = 5 per group; $^{a}p < 0.05$, significantly different from the CTL group; $^{b}p < 0.05$, significantly different from the Cu group). All data are presented as mean ± standard deviation.

Effects of demyelination and remyelination on phosphorylation in the CREB signaling in the DG

pCREB immunostaining was performed to examine phosphorylation in the CREB signaling in the DG after demyelination and remyelination. In the CTL group, abundant pCREB-positive nuclei were detected in the SGZ of DG (69 nuclei; Figure 4A and 4D). In the Cu group, a few pCREB-positive nuclei detected found in the SGZ, and this number was significantly lower than that in the CTL group (Figure 4B and 4D). In the Cu+N group, significantly higher number of pCREB-positive nuclei were detected in the DG than that in the Cu group (Figure 4C and 4D).

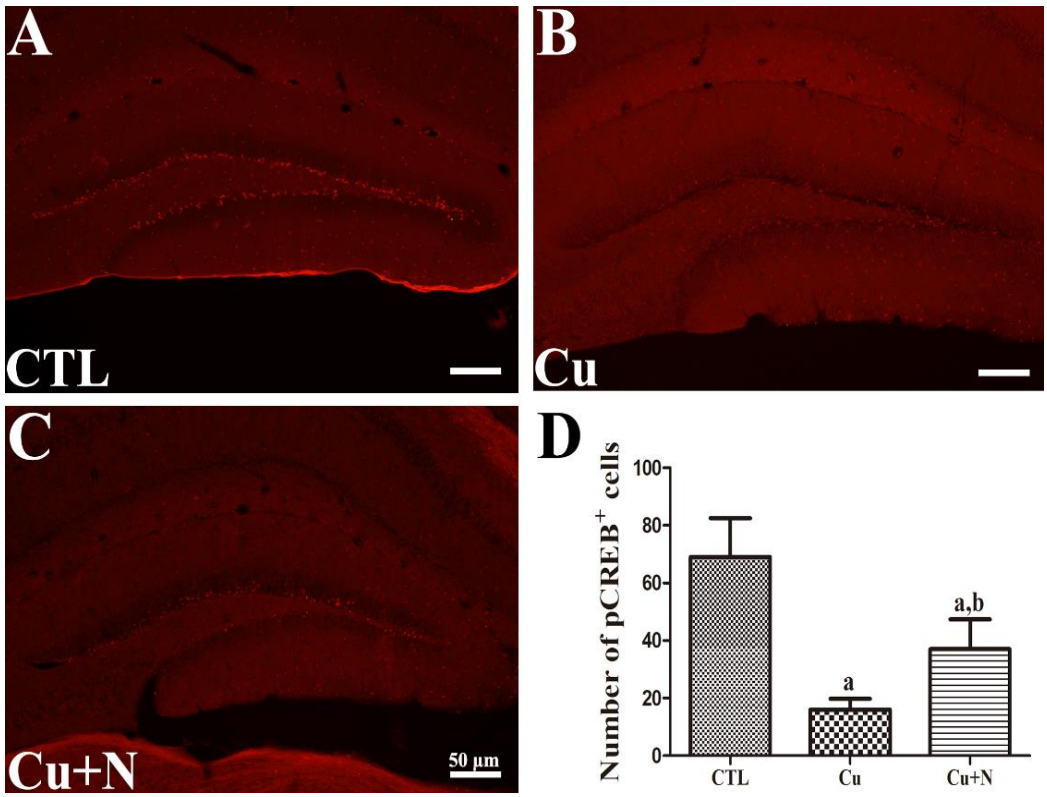

Figure 4. Immunohistochemical staining of pCREB in the hippocampal DG of (A) group fed normal chow diet for 8 weeks (CTL), (B) group fed CPZ diet for 8 weeks (Cu), and (C) group fed normal diet for 3 weeks after CPZ diet for 5 weeks (Cu+N). (D) The number of pCREB-positive nuclei detected in the SGZ of DG is shown. Scale bar = 50 μm (n = 5 per group; $^{a}p < 0.05$, significantly different from the CTL group; $^{b}p < 0.05$, significantly different from the Cu group). All data are presented as mean ± standard deviation.

Effect of demyelination on protein profiles in the hippocampus

To elucidate the effect of demyelination on protein profiles in the hippocampus, 2DE was performed and changes in proteins after the intake and termination of CPZ diet were examined. In the CTL group, 556 spots were detected, while in the Cu group, 636 spots were detected on 2DE gels. Among these proteins, 509 spots were shared between the two groups, and respectively 18 and 28 spots in the Cu group showed more than two-fold increase and decrease in density compared with those in the CTL group (Figure 5). Enlarged images of gels confirmed the increase or decrease in the density of spots in the Cu group compared to that in the CTL group (Figures 6 and 7).

For protein identification, LC-MS/MS and MASCOT search were performed. Among the 18 and 28 spots, respectively 17 and 22 proteins were identified, as presented in Tables 1A and 1B.

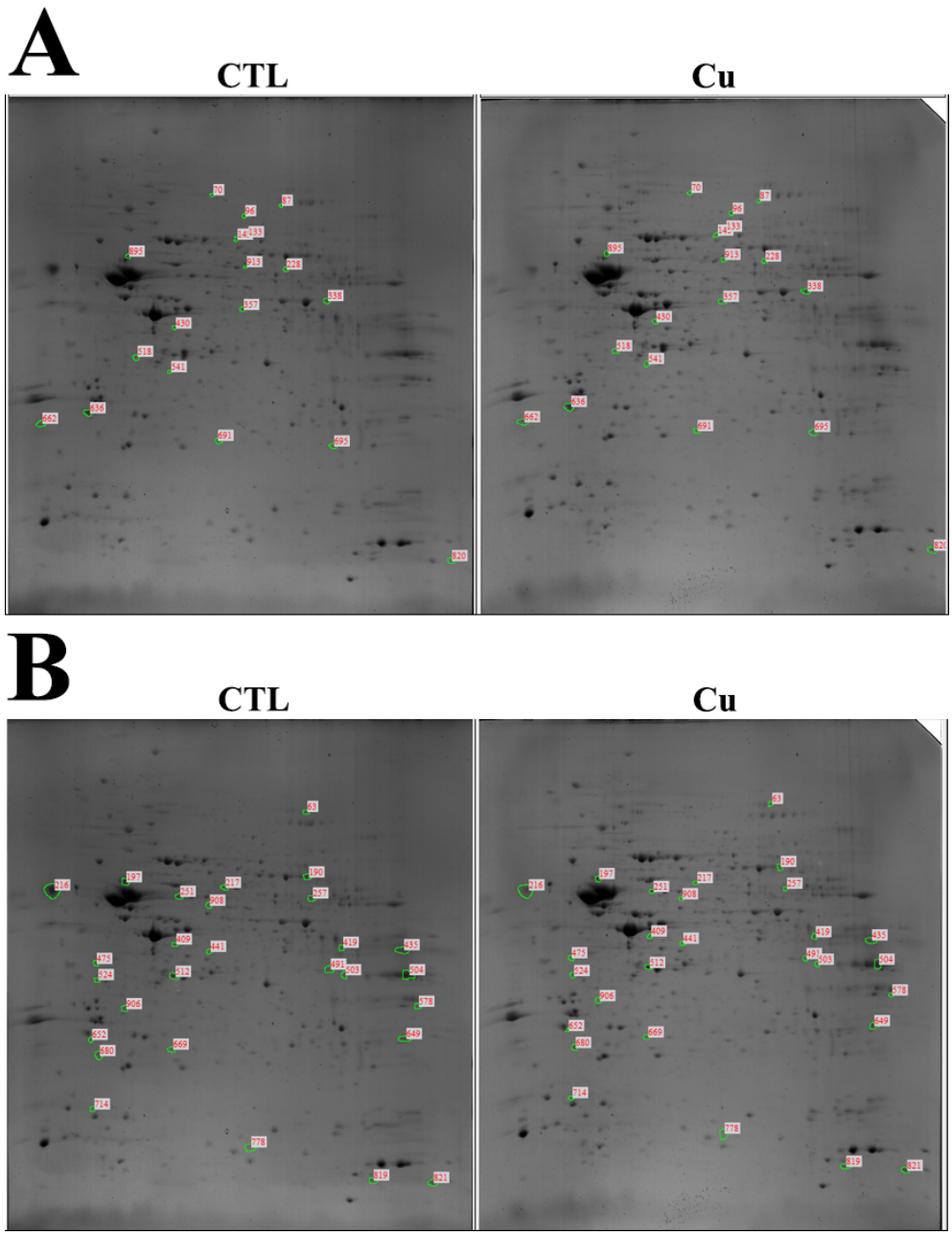

Figure 5. Spots on 2DE gels corresponding to hippocampal proteins extracted from group fed normal chow diet (CTL) and group fed CPZ diet (Cu) for 8 weeks. The density of spots in (A) was increased and that of spots in (B) was decreased by over two-folds in the Cu group compared with that in the CTL group.

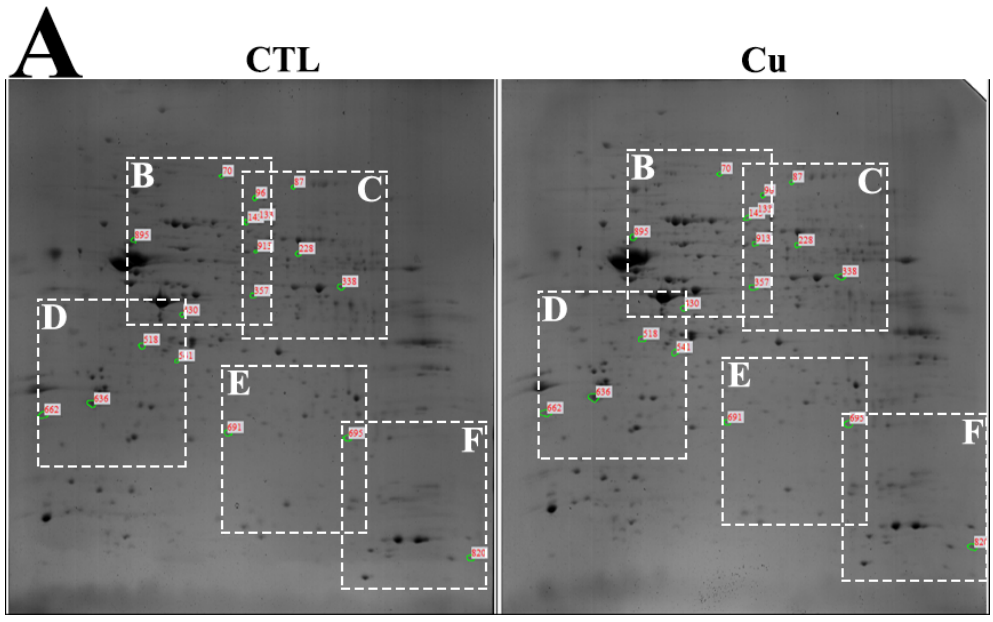
A
CTL
Cu
B
C
D
E
F

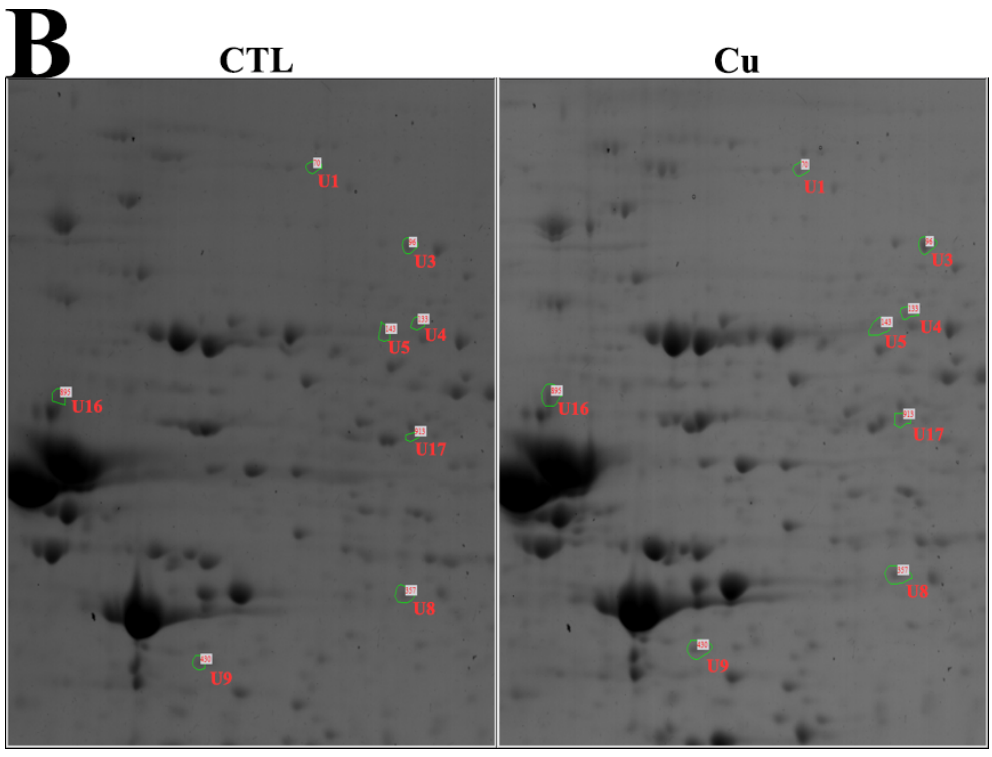
B
CTL
Cu
U1
U3
U4
U5
U16
U17
U8
U9

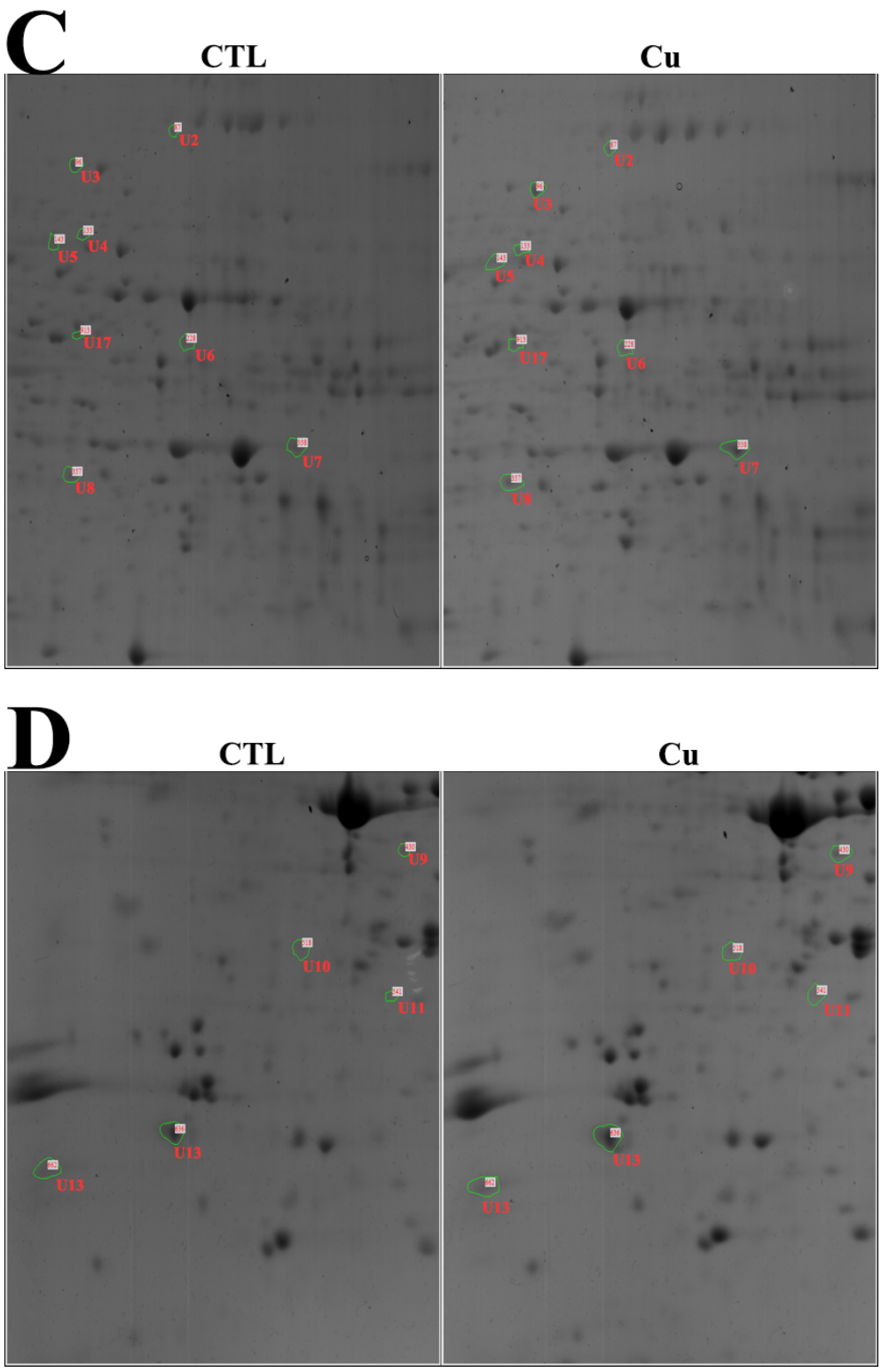
C
CTL
Cu
U2
U3
U4
U5
U17
U6
U7
U8
D
CTL
Cu
U9
U10
U11
U13
U13

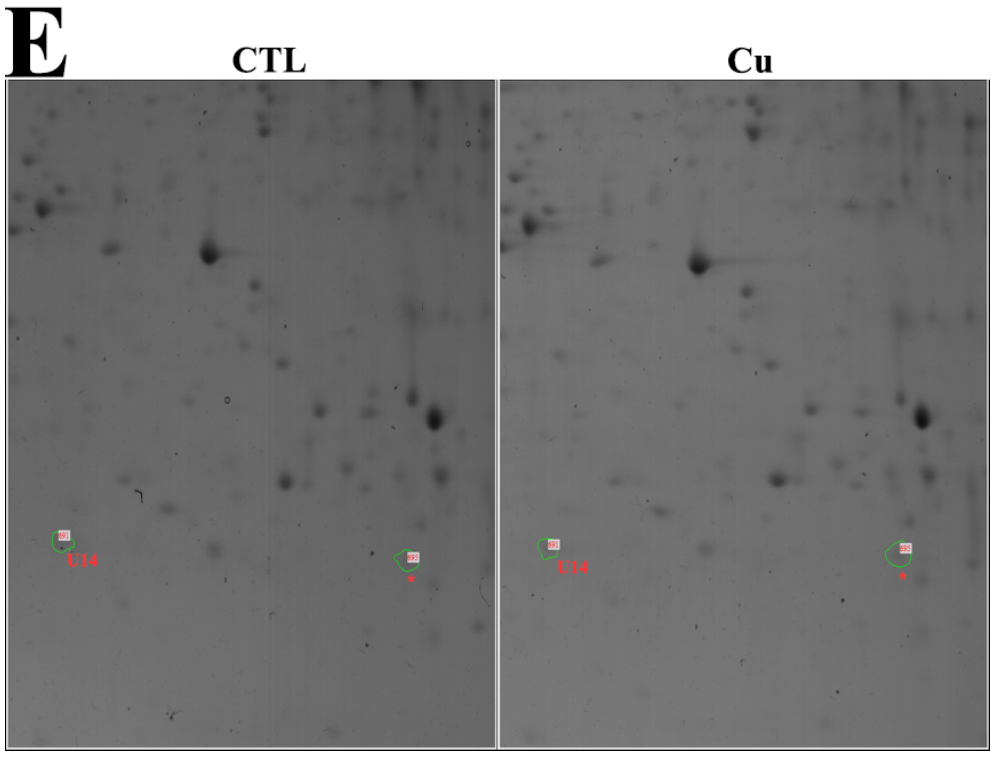
E
CTL
Cu
U14
U14

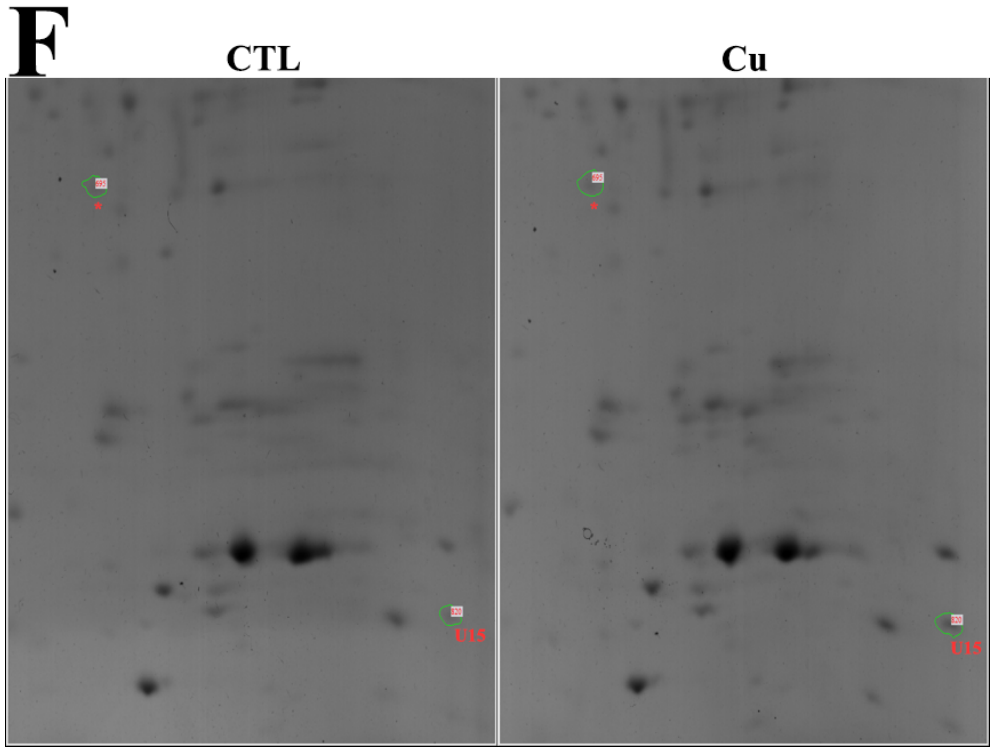
F
CTL
Cu
U15
U15

Figure 6. Enlarged gel images of spots whose density increased by over two-folds in the group fed CPZ diet (Cu) compared with that group fed normal chow diet (CTL). (A) Each region of magnified area in the full 2DE gel image is shown in (B), (C), (D), (E), and (F). Each spot is assigned a unique number from U1 to U17. *No significant hits to report.

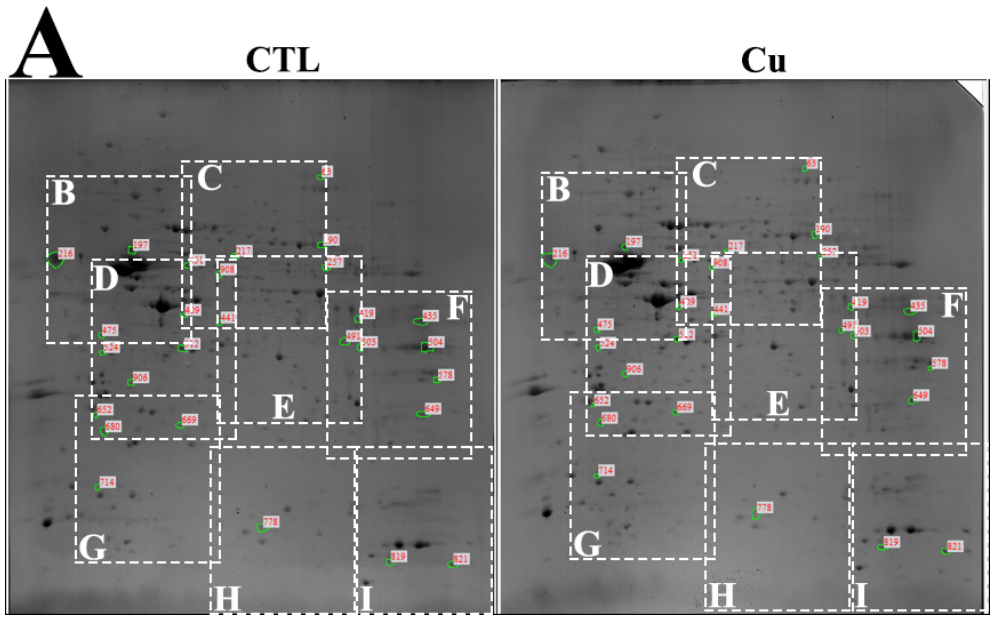
A
CTL
Cu
B
C
D
E
F
G
H
I

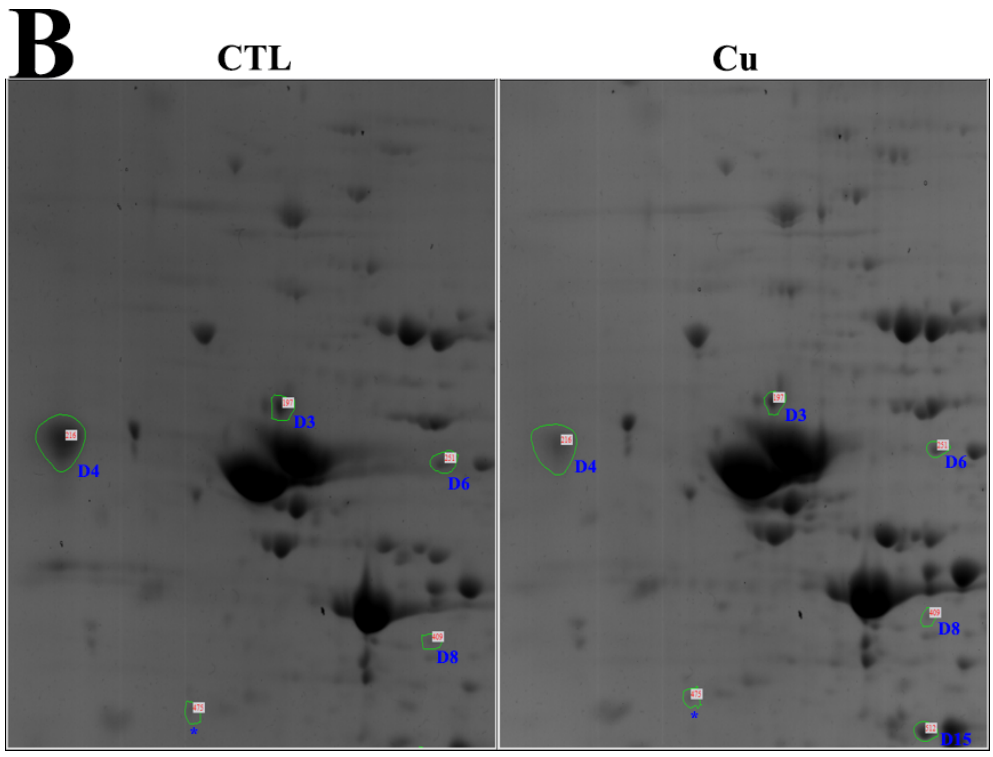
B
CTL
Cu
D3
D4
D6
D8
D15

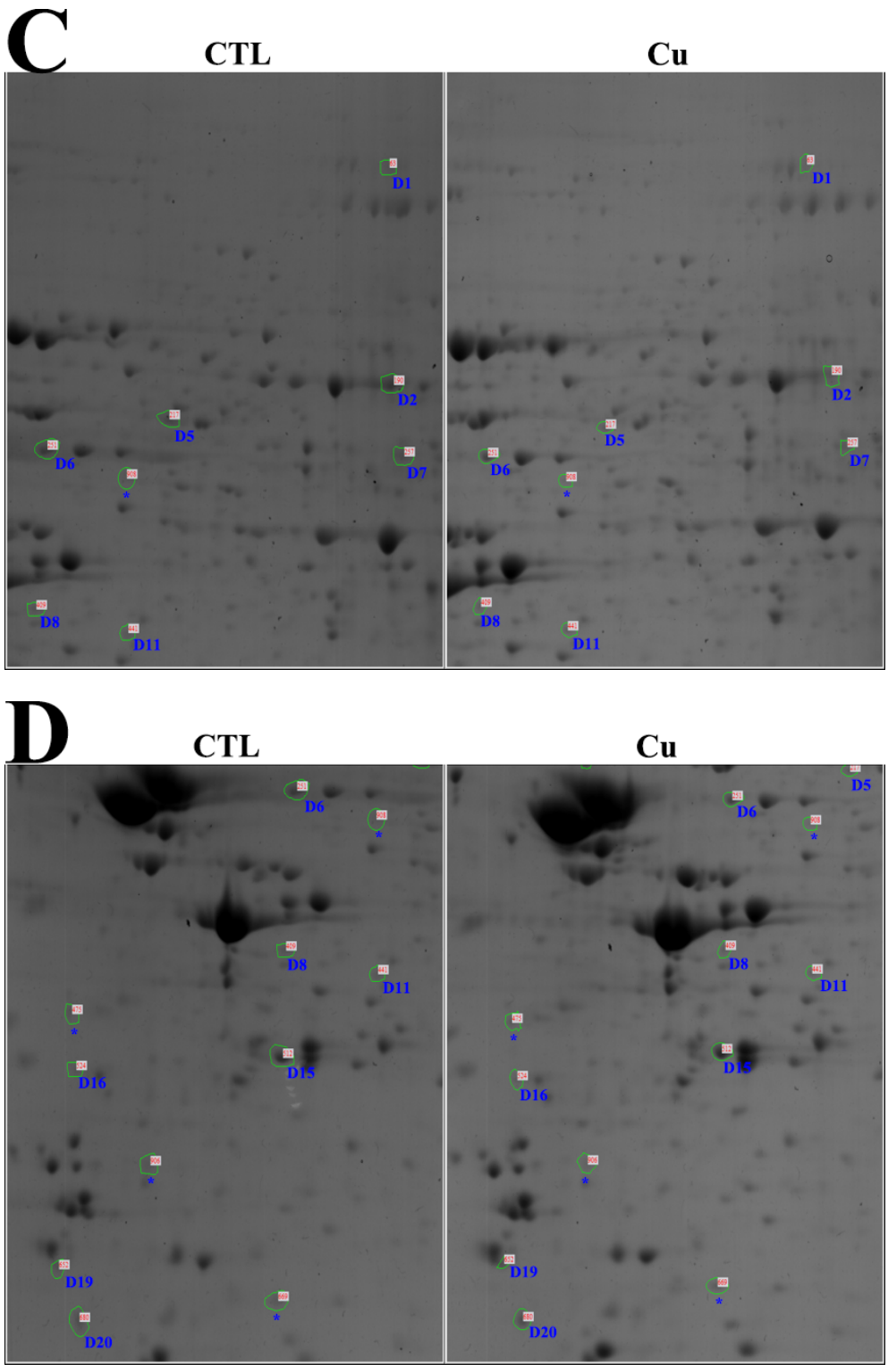
C
CTL
Cu
D1
D2
D5
D6
D7
D8
D11
D
CTL
Cu
D5
D6
D8
D11
D15
D16
D19
D20

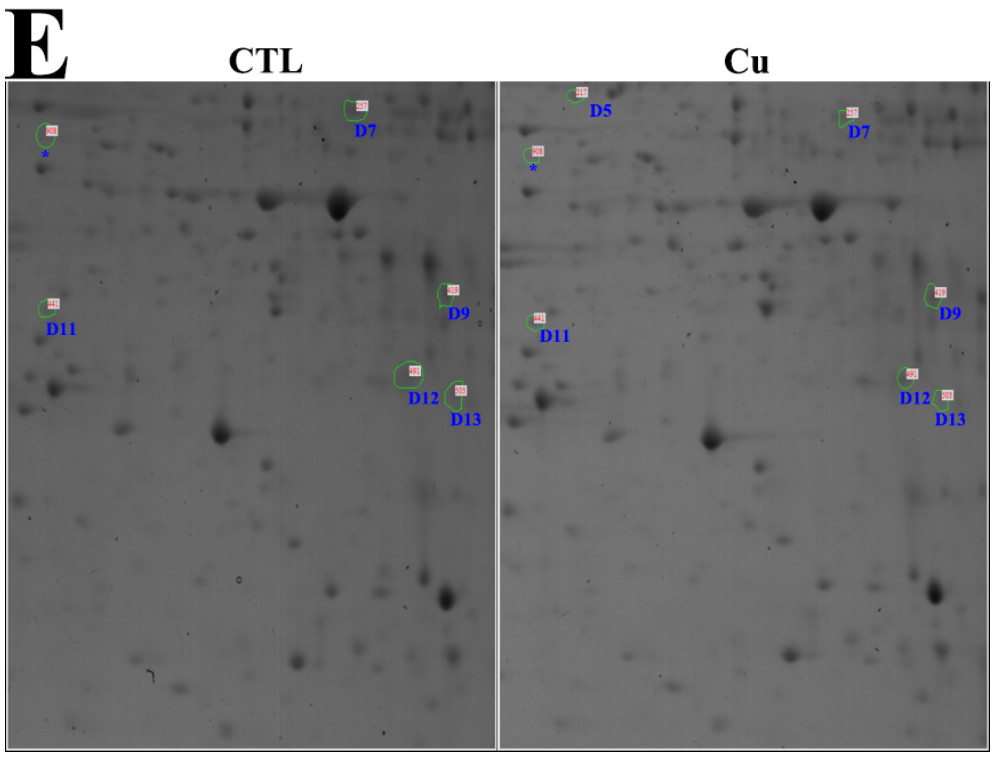
E
CTL
Cu
D5
D7
D9
D11
D12
D13

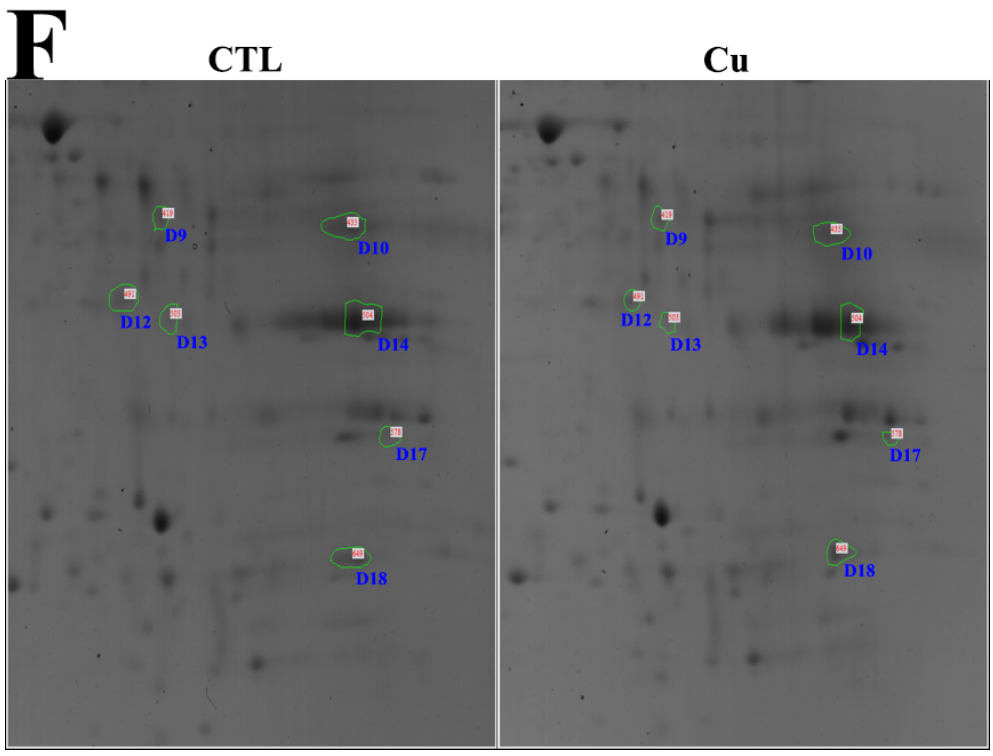
F
CTL
Cu
D9
D10
D12
D13
D14
D17
D18

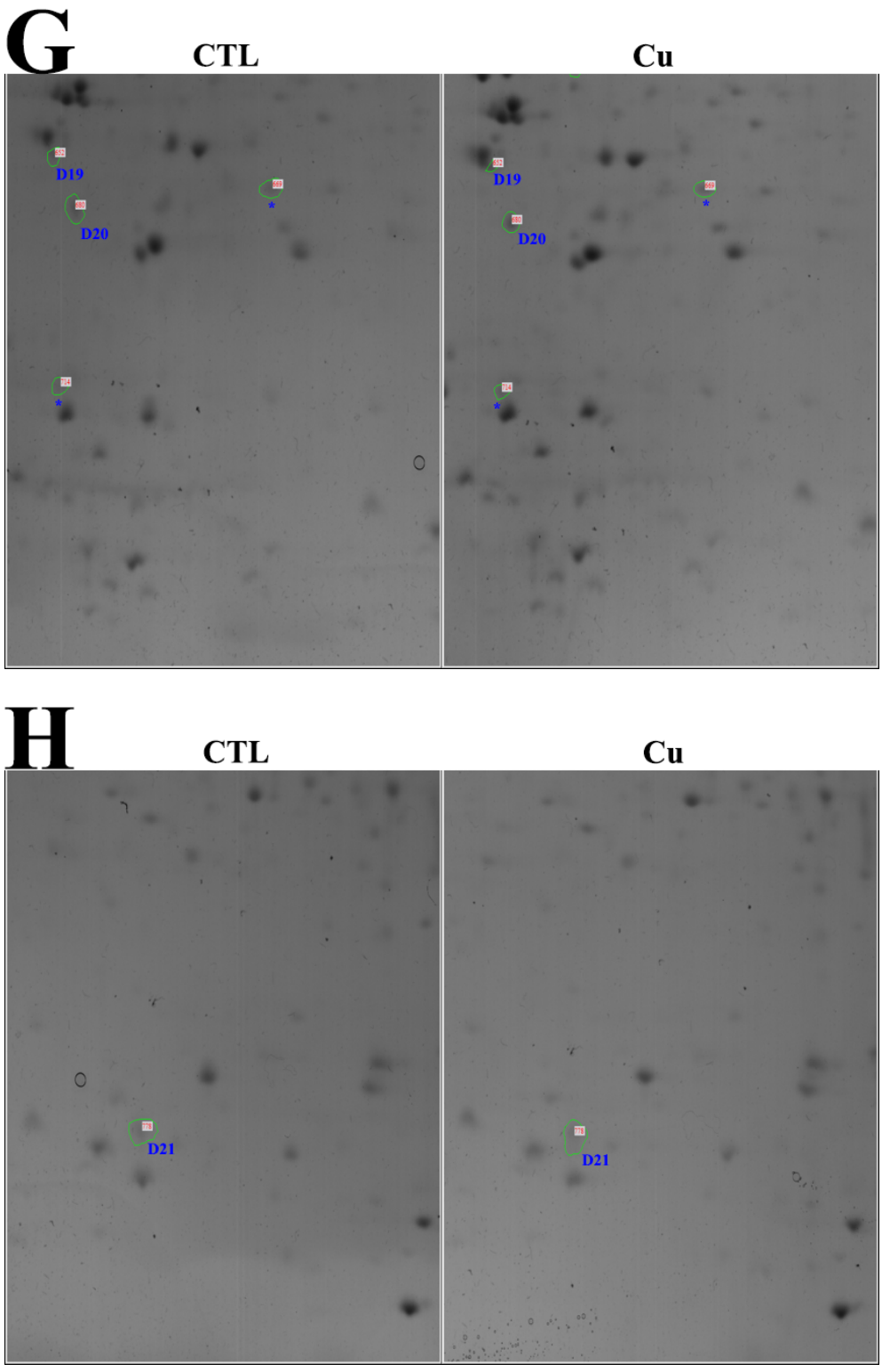
G
CTL
Cu
D19
D20
D19
D20
H
CTL
Cu
D21
D21

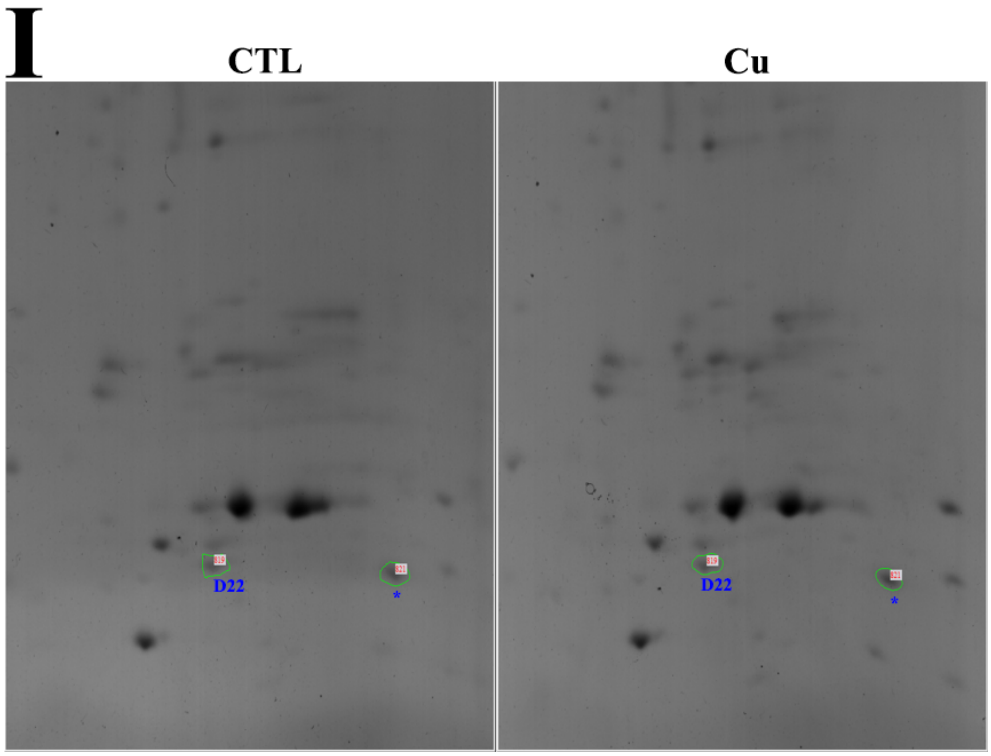

Figure 7. Enlarged gel images of spots whose density decreased by over two-folds in the group fed CPZ diet (Cu) compared with that in the group fed normal chow diet (CTL). (A) Each region of magnified area in the full 2DE gel image is shown in (B), (C), (D), (E), (F), (G), (H), and (I). Each spot is assigned a unique number from D1 to D22. *No significant hits to report.

Table 1. List of identified proteins with increased or decreased expression in the group fed normal chow diet (CTL) or CPZ diet (Cu)

A **Increased**

Spot no.	Protein no.	Accession no., Protein Name	Score	Mr (kDa)	pI Value	Matched peptide	Sequence Coverage (%)	Cu/CTL Ratio
70	U1	BAA08446.1, APG-1	69	95.285	5.53	2	1	2.06
87	U2	BAC65593.1, mKIAA0567 protein, partial	100	64.566	8.87	2	3	2.48
96	U3	NP_083949.2, MICOS complex subunit Mic60 isoform 1	1285	84.247	6.18	65	28	2.19
133	U4	AAH06685.1, Trap1 protein, partial	46	80.370	6.25	1	1	2.09
143	U5	NP_031534.2, V-type proton ATPase catalytic subunit A	120	55.958	5.64	3	4	2.17
228	U6	EDL04922.1, Fyn proto-oncogene, isoform CRA_b	41	65.162	6.69	1	1	2.14
338	U7	EDL27268.1, mCG127690	165	29.719	9.10	5	13	2.09
357	U8	EDL31457.1, mitogen activated protein kinase kinase 2, isoform CRA_b	31	43818	6.24	1	1	2.71
430	U9	NP_032165.3, guanine nucleotide-binding protein G(q) subunit alpha	73	42.416	5.48	2	4	2.34
518	U10	NP_080230.2, glycerol-3-phosphate phosphatase	134	34.975	5.24	4	8	3.07
541	U11	NP_038499.2, annexin A4	86	36.178	5.43	2	6	2.48
636	U12	ABL01512.1, beta-actin, partial	79	13.588	5.93	2	23	1.99
662	U13	EDL02536.1, RAB5C, member RAS oncogene family, isoform CRA_b, partial	117	29.779	8.72	2	8	1.97
691	U14	Q9DBP5.1, UMP-CMP kinase	37	22.379	5.68	1	6	2.32
820	U15	EDL20118.1, mCG13600, isoform CRA_b	56	5.864	8.01	1	24	2.06
895	U16	NP_058587.1, serine/threonine-protein phosphatase 2A 65 kDa regulatory subunit A alpha isoform	212	66.077	5.00	6	6	2.14
913	U17	AAH18545.1, Hspd1 protein	34	27.112	4.76	1	3	2.11

B **Decreased**

Spot no.	Protein no.	Accession no., Protein Name	Score	Mr (kDa)	pI Value	Matched peptide	Sequence Coverage (%)	CTL/Cu Ratio
63	D1	EDL24836.1, mCG6358	310	117.727	6.43	7	6	2.29
190	D2	NP_034085.2, dihydropyrimidinase-related protein 2	138	62.638	5.95	3	5	4.42
197	D3	EDL29822.1, guanosine diphosphate (GDP) dissociation inhibitor 1, isoform CRA_a, partial	1066	56.133	4.92	59	26	2.20
216	D4	EDL04152.1, mCG18413, isoform CRA_b, partial	365	51.572	4.98	27	10	3.28
217	D5	NP_031978.2, protein disulfide-isomerase A3 precursor	187	55.902	5.61	4	8	2.16
251	D6	NP_476561.1, V-type proton ATPase subunit B, brain isoform	317	568.85	5.57	16	11	2.04
257	D7	NP_038709.1, synapsin-2 isoform IIb	46	52.818	7.62	1	1	3.22
409	D8	NP_001091.1, actin, alpha skeletal muscle	46	42.366	5.23	1	2	2.19
419	D9	CAA30275.1, aspartate aminotransferase	342	46.489	6.68	8	16	2.11
435	D10	NP_031769.2, collagen alpha-2(I) chain preproprotein	84	129.992	9.27	3	1	2.16
441	D11	AAH11036.1, Bisphosphate 3'-nucleotidase 1	52	33.564	5.58	2	2	2.18
491	D12	AGZ02590.1, sirtuin-2 isoform 3, partial	44	46.987	5.15	1	3	2.76
503	D13	EDL00035.1, mCG117541	162	33.094	6.71	5	11	2.06
504	D14	AAH92267.1, Glyceraldehyde-3-phosphate dehydrogenase	480	36.102	8.44	24	24	2.12
512	D15	NP_057878.1, ketimine reductase mu-crystallin	791	33.673	5.44	38	31	2.13
524	D16	NP_057878.1, ketimine reductase mu-crystallin	182	33.673	5.44	4	13	1.96
578	D17	NP_031536.2, V-type proton ATPase subunit E 1	207	26.202	8.44	9	16	2.20
649	D18	EDL01936.1, mCG131602, isoform CRA_a, partial	550	29.222	8.31	23	40	2.33
652	D19	NP_003072.2, synaptosomal-associated protein 25 isoform SNAP25A	28	23.549	4.74	1	3	2.62
680	D20	NP_004152.1 ras-related protein Rab-1A isoform 1	210	22.891	5.93	6	20	1.98
778	D21	EDL23025.1 mCG5289	42	15.402	5.74	1	6	2.47
819	D22	NP_032329.1 10 kDa heat shock protein, mitochondrial	76	10.956	7.93	2	23	2.43

Effect of remyelination on protein profiles in the hippocampus

To elucidate the effect of remyelination on protein profiles in the hippocampus, 2DE of the Cu and Cu+N groups was performed. In the Cu and Cu+N groups, respectively 522 and 570 spots were detected; of these, 454 spots were shared between the two groups, and respectively 26 and 29 spots in the Cu+N group showed over two-fold increase and decrease in density compared with those in the Cu group (Figure 8). Enlarged images of the gels confirmed the increase or decrease in the density of spots in the Cu+N group compared with that in the Cu group (Figures 9 and 10).

Using LC-MS/MS and MASCOT search, 19 and 25 proteins were identified, as presented as Table 2.

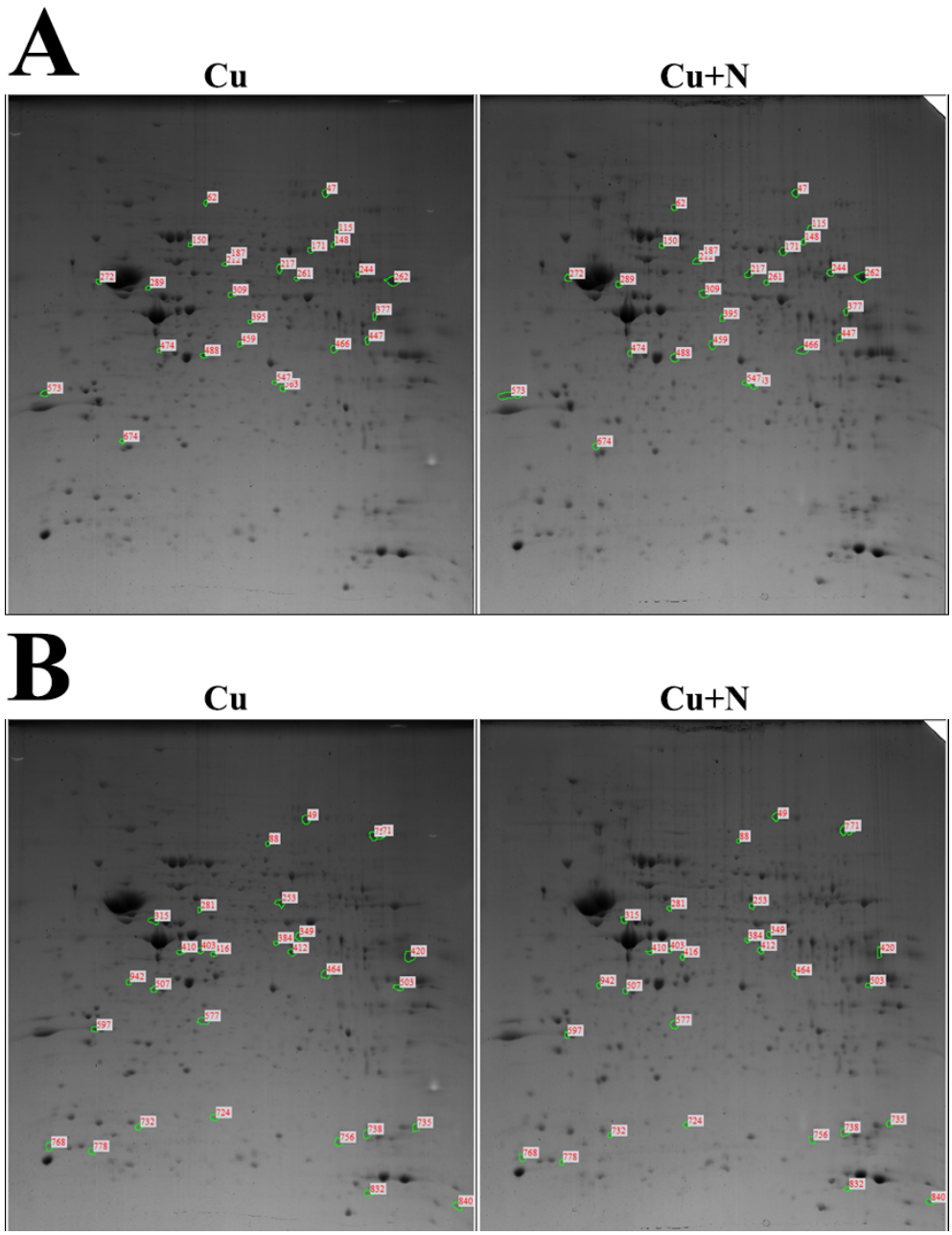

Figure 8. Spots on 2DE gel corresponding to hippocampal proteins extracted from the group fed CPZ diet (Cu) for 8 weeks and the group fed normal diet for 3 weeks after CPZ diet for 5 weeks (Cu+N). Spots in (A) showed increase and those in (B) showed decrease in density by over two-folds in the Cu+N group compared with that in the Cu group.

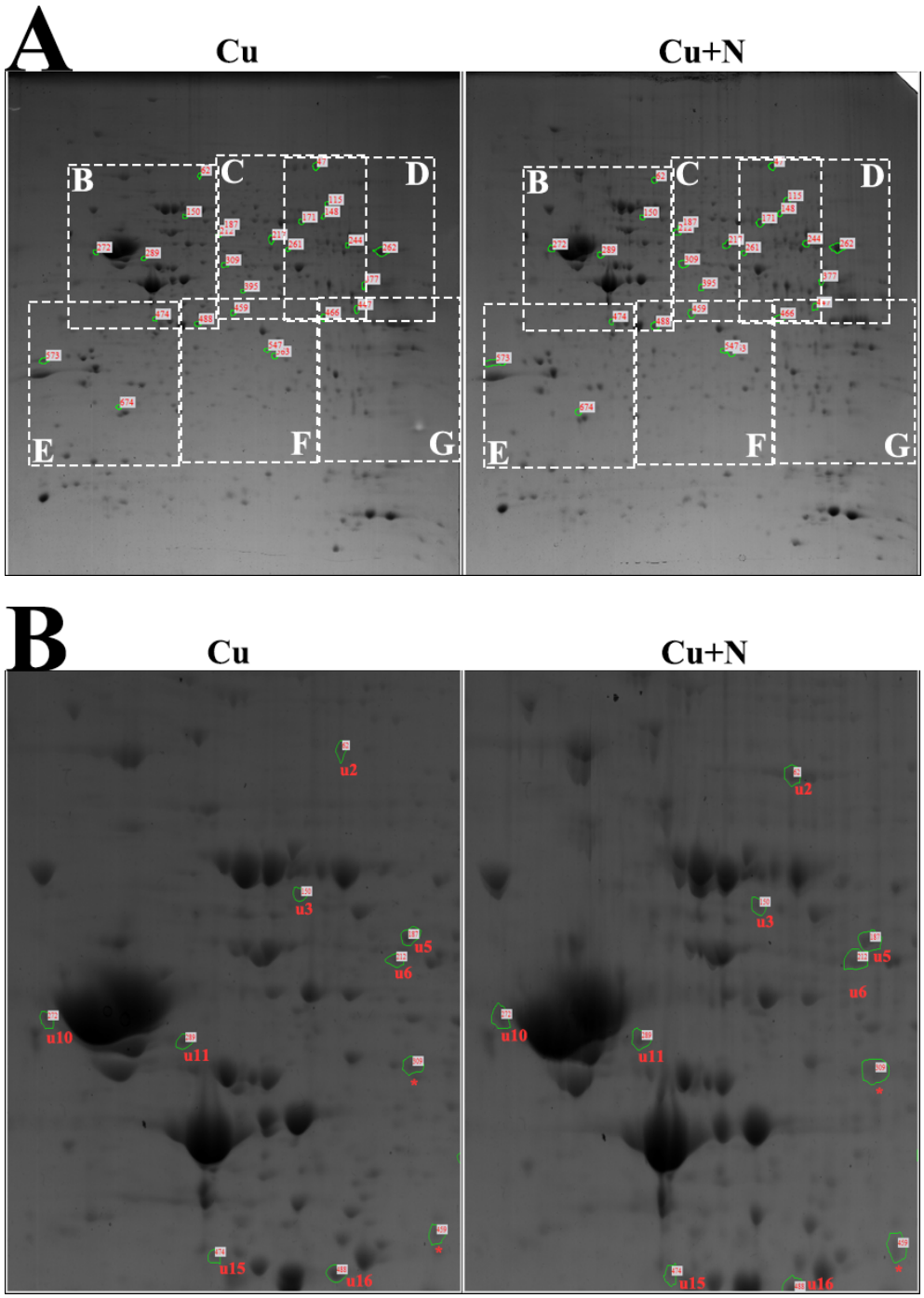
A
Cu
Cu+N
B
C
D
E
F
G
B
Cu
Cu+N
u2
u3
u5
u6
u10
u11
u15
u16

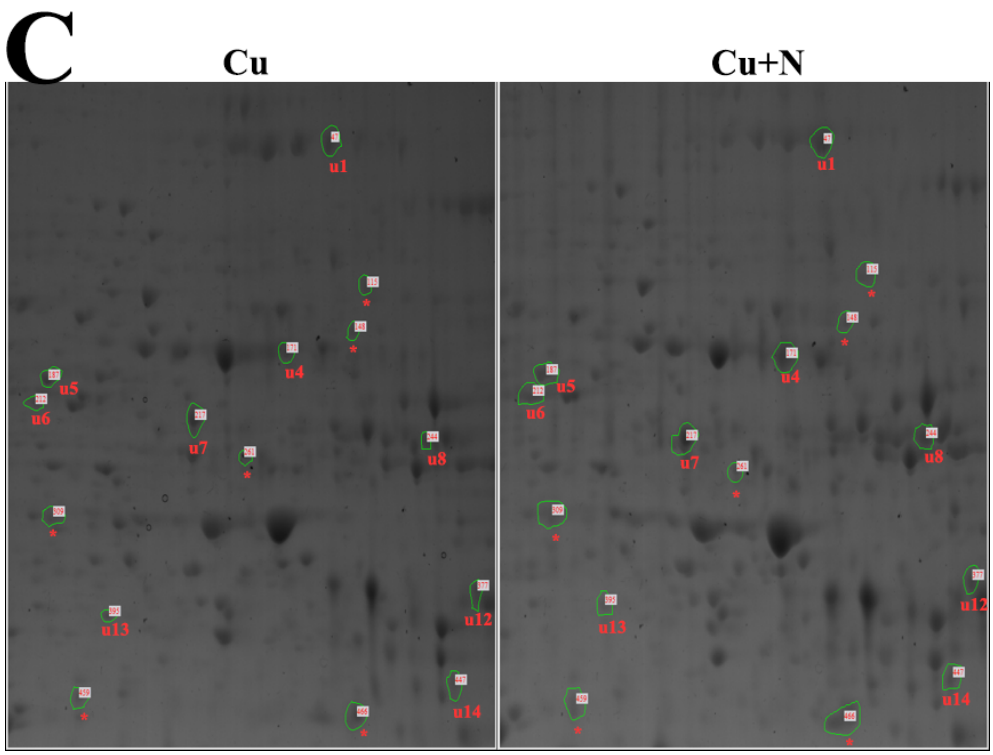
C
Cu
Cu+N
u1
u4
u5
u6
u7
u8
u12
u13
u14

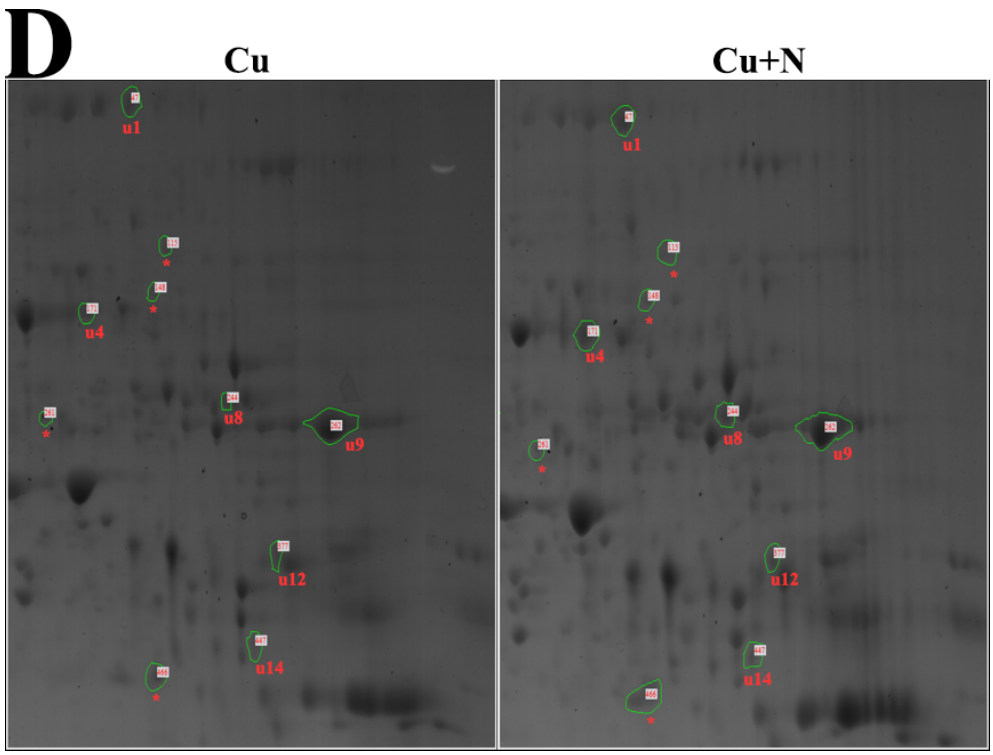
D
Cu
Cu+N
u1
u4
u8
u9
u12
u14

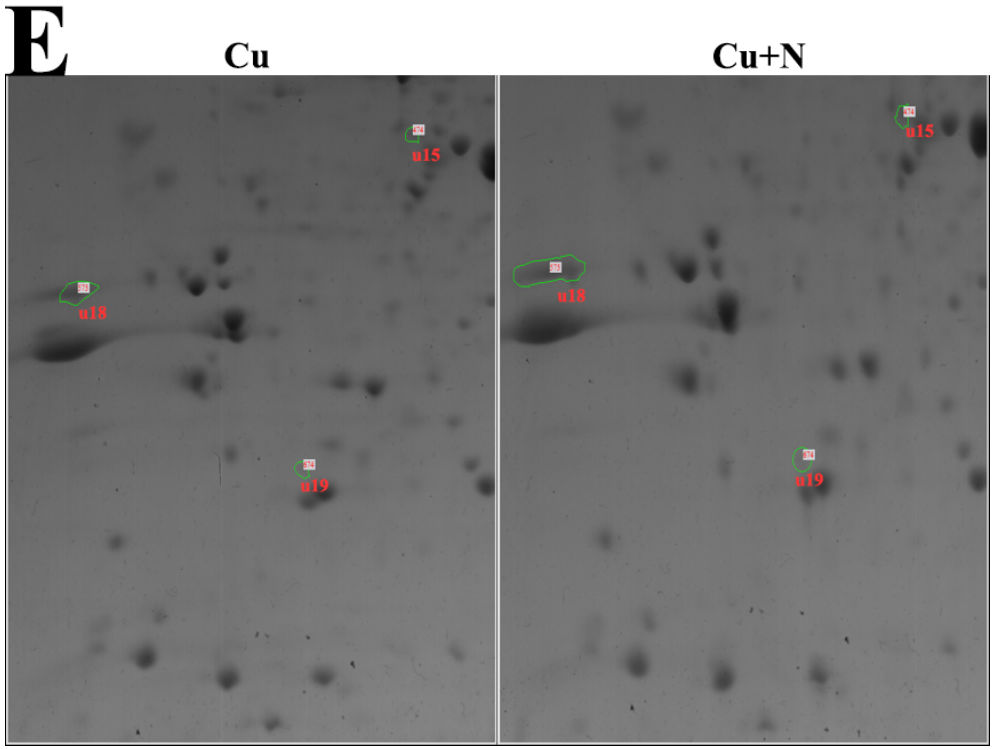
E
Cu
Cu+N
u15
u18
u19
u15
u18
u19

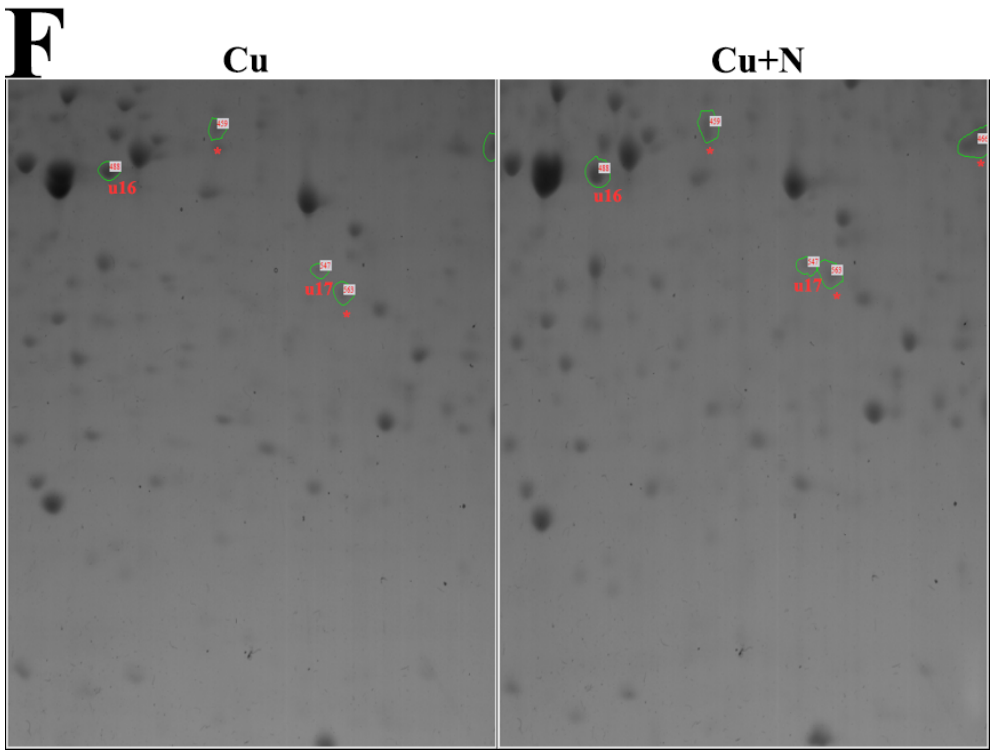
F
Cu
Cu+N
u16
u17
u16
u17

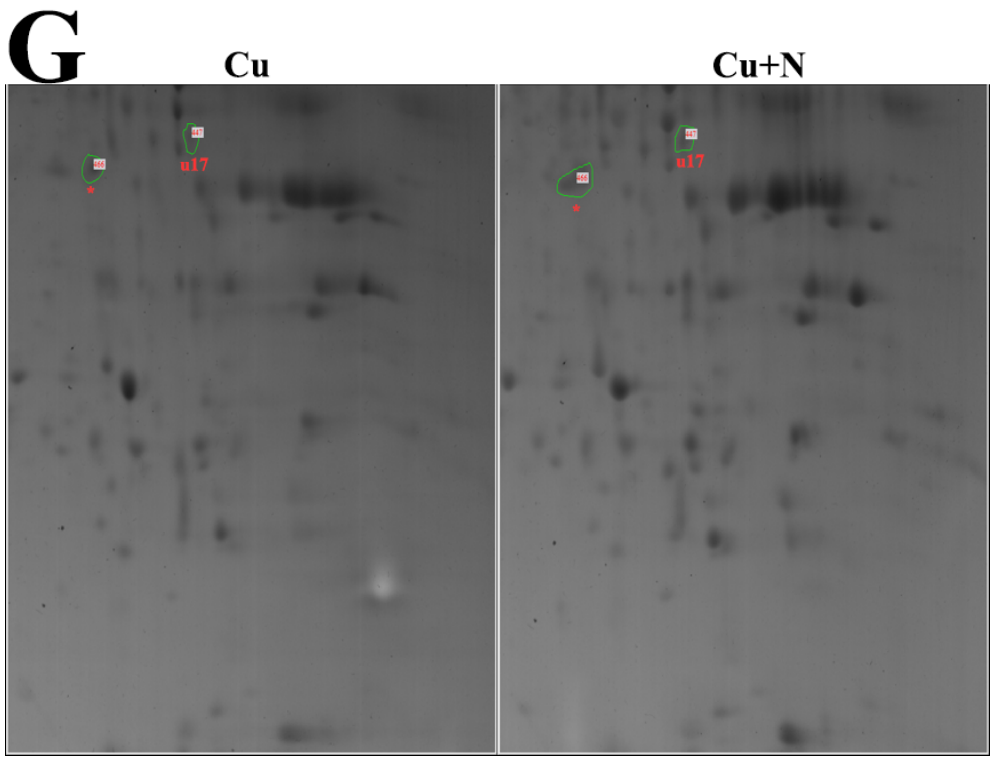

Figure 9. Enlarged gel images of spots whose density increased by over two-folds in the group fed CPZ diet for 8 weeks (Cu) compared with that in the group fed normal diet for 3 weeks after CPZ diet for 5 weeks (Cu+N). (A) Each region of magnified area in the full 2DE gel image is shown in (B), (C), (D), (E), (F), and (G). Each spot is assigned a unique number from u1 to u19. *No significant hits to report.

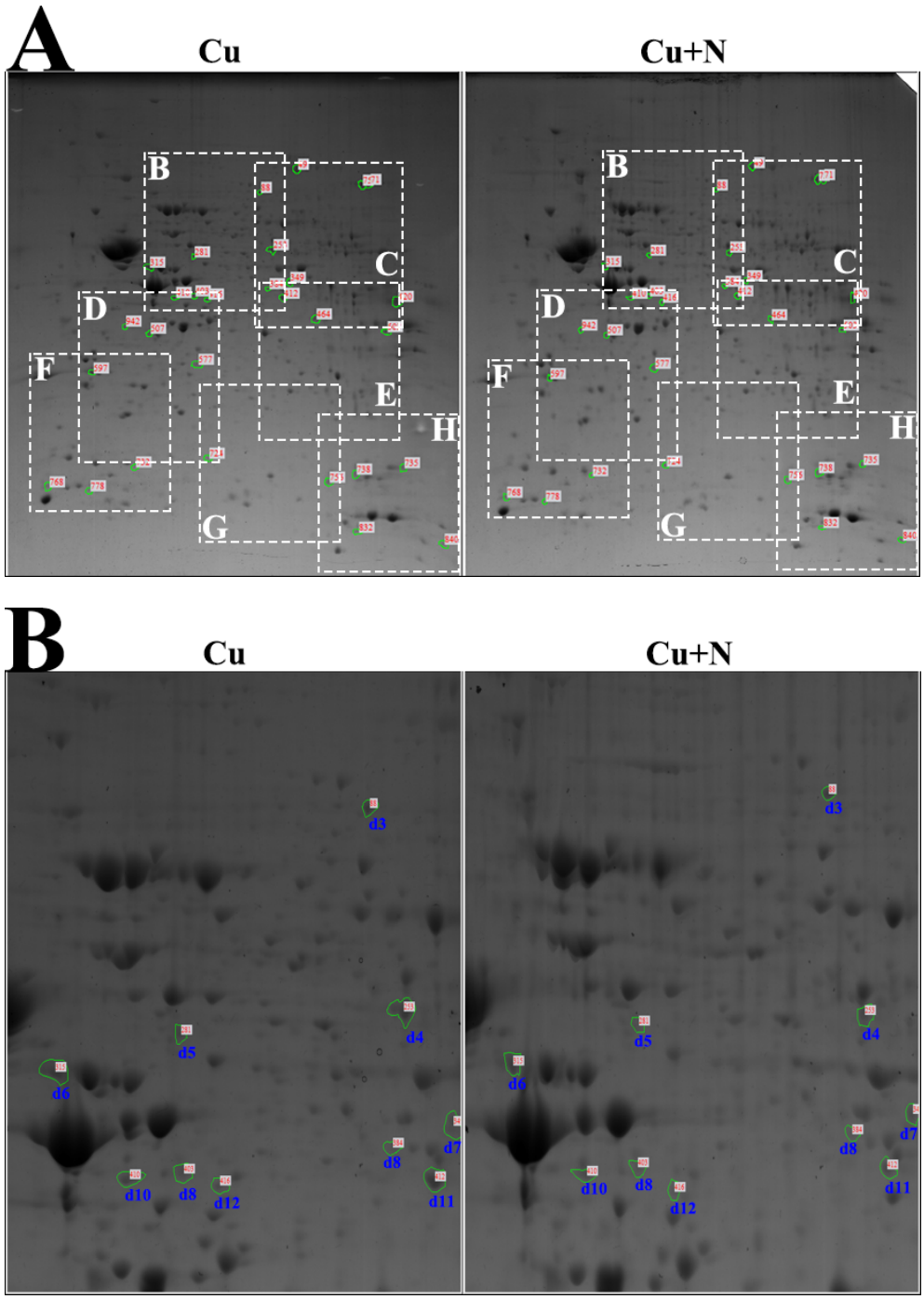
A
Cu
Cu+N
B
C
D
E
F
G
H
B
Cu
Cu+N
d3
d4
d5
d6
d7
d8
d10
d8
d12
d11

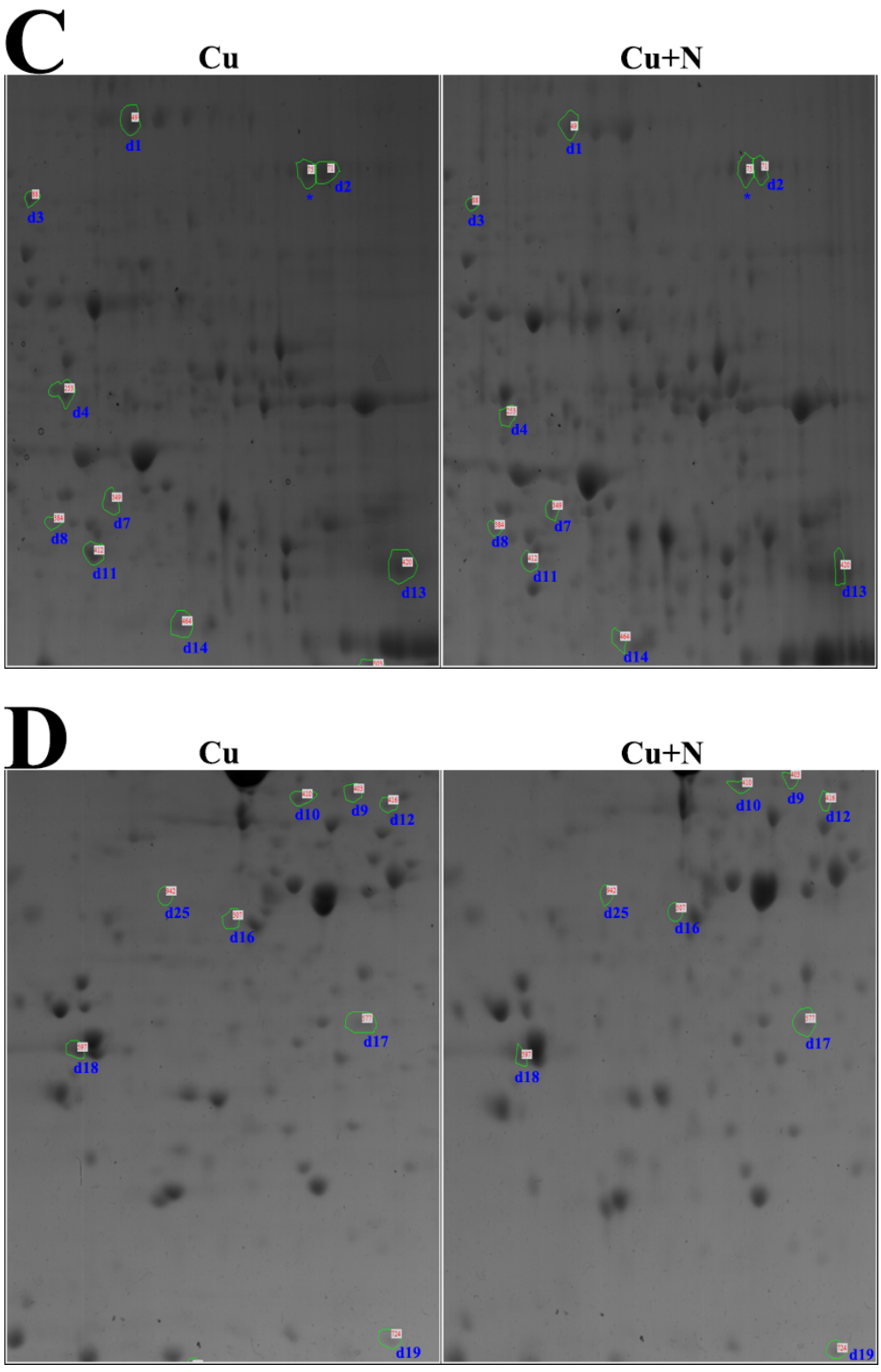
C
Cu
Cu+N
d1
d2
d3
d4
d7
d8
d11
d13
d14
D
Cu
Cu+N
d10
d9
d12
d25
d16
d17
d18
d19

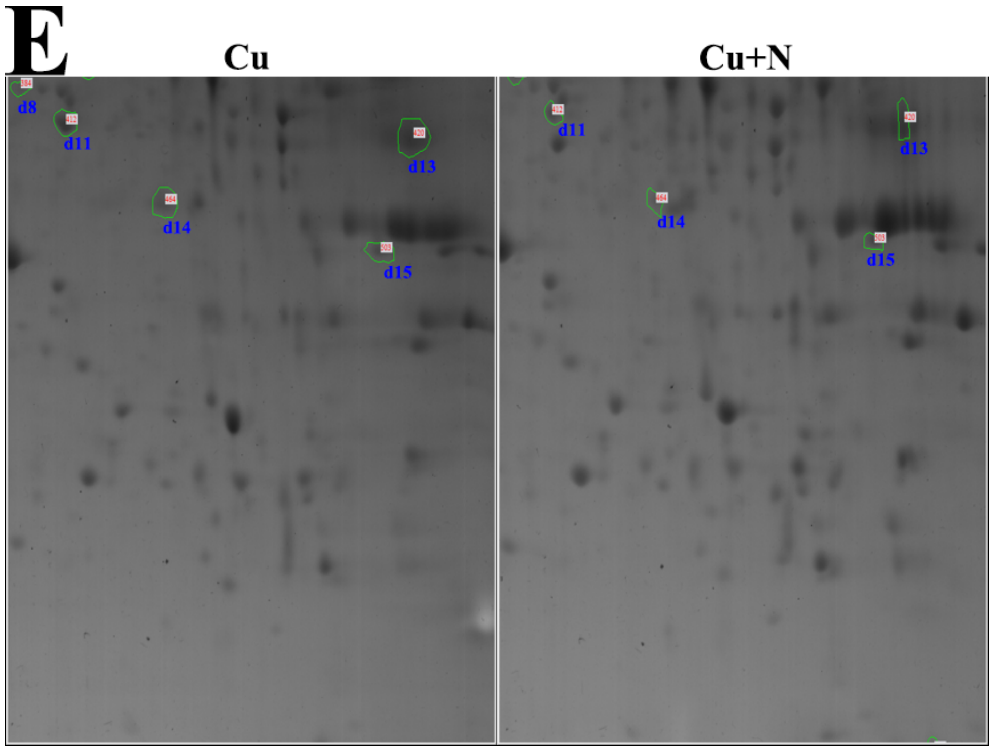
E
Cu
Cu+N
d8
d11
d13
d14
d15
d11
d13
d14
d15

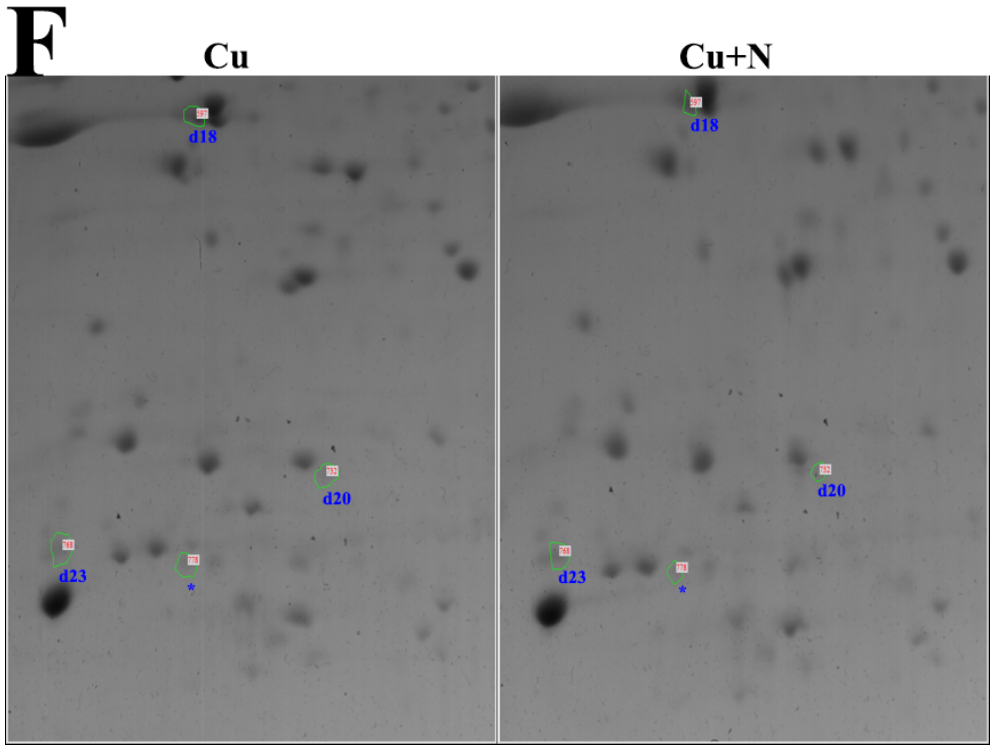
F
Cu
Cu+N
d18
d20
d23
*
d18
d20
d23
*

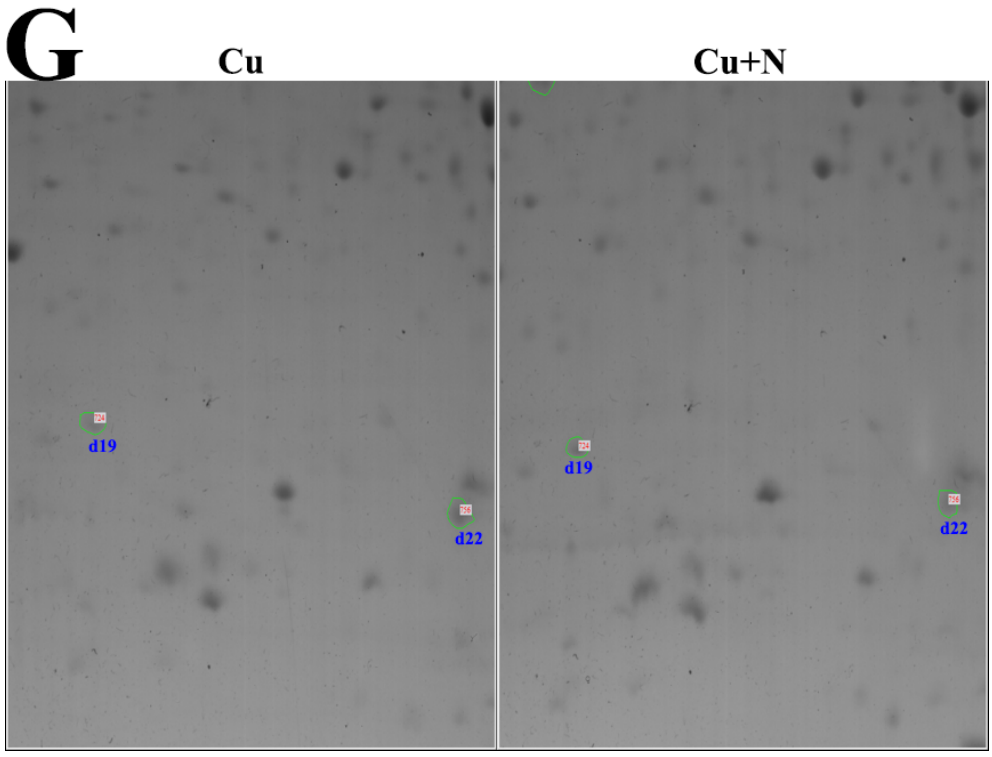
G
Cu
Cu+N
d19
d22
d19
d22

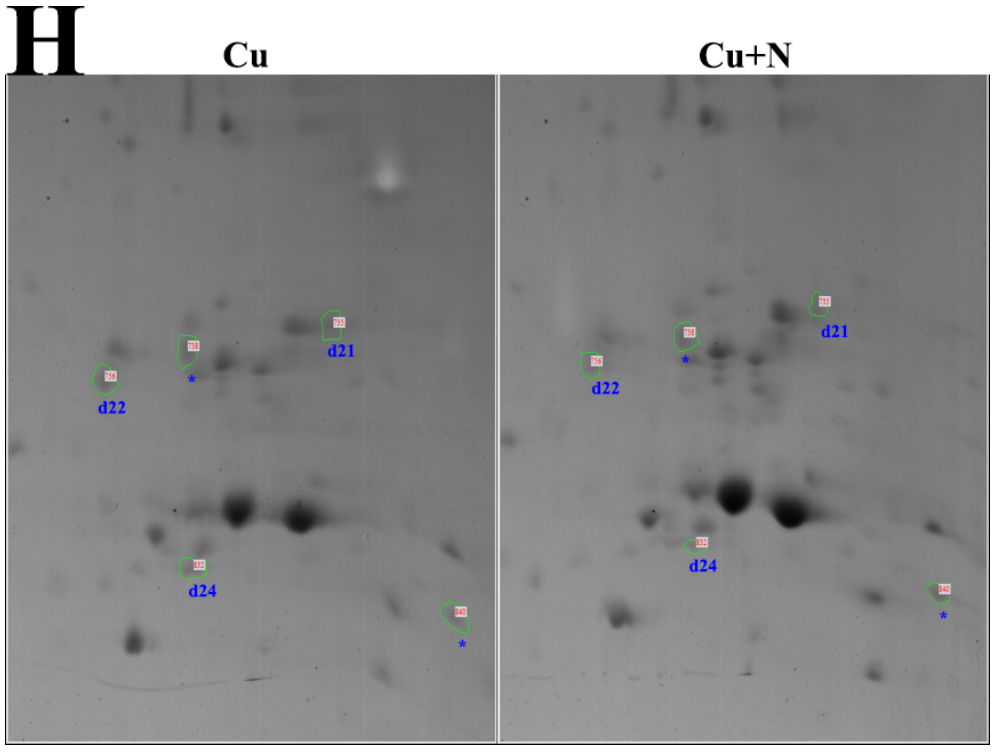
H
Cu
Cu+N
d21
d22
d24
*
d21
d22
d24
*

Figure 10. Enlarged gel images of spots whose density decreased by over two-folds in group fed CPZ diet for 8 weeks (Cu) compared with that in the group fed normal diet for 3 weeks after CPZ diet for 5 weeks (Cu+N). (A) Each region of magnified area in the full 2DE gel image is shown in (B), (C), (D), (E), (F), (G), and (H). Each spot is assigned a unique number from d1 to d25. *No significant hits to report.

Table 2. List of identified proteins with increased or decreased expression in the group fed CPZ diet for 8 weeks (Cu) and the group fed normal diet for 3 weeks after CPZ diet for 5 weeks (Cu+N)

A **Increased**

Spot no.	Protein no.	Accession no., Protein name	Score	Mr (kDa)	pI Value	Matched peptide	Sequence Coverage (%)	Cu+N/Cu Ratio
47	u1	XP_006497712.2, PREDICTED: dynamin-1 isoform X1	2064	97.906	6.57	66	35	1.98
62	u2	AAH94462.1, Aconitase 2, mitochondrial	323	86.036	8.08	8	8	2.22
150	u3	EDL16325.1, p21 (CDKN1A)-activated kinase 1, isoform CRA_c	103	59.643	6.02	3	5	2.29
171	u4	NP_034085.2, dihydropyrimidinase-related protein 2	279	62.638	5.95	16	10	2.77
187	u5	NP_031663.1, T-complex protein 1 subunit epsilon isoform 1	223	60.023	5.69	4	6	2.24
212	u6	NP_031978.2, protein disulfide-isomerase A3 precursor	765	57.099	5.88	24	30	2.44
217	u7	NP_031662.2, T-complex protein 1 subunit beta	1001	57.783	5.97	25	25	3.19
244	u8	NP_077150.1, succinyl-CoA:3-ketoacid coenzyme A transferase 1, mitochondrial precursor	75	52.636	8.98	2	4	2.21
262	u9	NP_031531.1, ATP synthase subunit alpha, mitochondrial precursor	1972	59.83	9.22	103	43	2.07
272	u10	NP_032950.1, cAMP-dependent protein kinase type II-alpha regulatory subunit	273	45.903	4.82	7	12	1.98
289	u11	AAA37238.1, synexin	517	50.192	5.91	23	19	2.11
377	u12	NP_032854.2, phosphoglycerate kinase 1	221	44.949	8.03	9	10	1.98
395	u13	NP_033015.1, transcriptional activator protein Pur-alpha	84	34.976	6.07	3	3	2.74
447	u14	EDL14930.1, acyl-CoA thioesterase 7, isoform CRA_b, partial	171	43.037	8.91	4	8	3.55
474	u15	NP_057878.1, ketimine reductase mu-crystallin	296	33.673	5.44	7	18	2.68
488	u16	EDL15010.1, guanine nucleotide binding protein, beta 1, isoform CRA_a, partial	140	38.494	5.61	3	7	2.26
547	u17	EDK99781.1, myeloid leukemia factor 2, partial	108	25.922	7.29	5	10	2.14
573	u18	NP_006752.1, 14-3-3 protein epsilon	459	29.326	4.63	15	36	2.21
674	u19	AAH13897.1, Proteasome (prosome, macropain) subunit, beta type 6	198	21.995	5.14	4	14	2.24

B **Decreased**

Spot no.	Protein no.	Accession no.	Score	Mr (kDa)	pI Value	Matched peptide	Sequence Coverage (%)	Cu/Cu+N Ratio
49	d1	NP_034195.2, dynamin-1 isoform 1	394	97.603	7.23	10	8	3.28
71	d2	AAH94462.1, Aconitase 2, mitochondrial	323	86.036	8.08	8	8	2.48
88	d3	NP_033536.2, ezrin	116	69.506	5.9	3	3	1.99
253	d4	NP_031662.2, T-complex protein 1 subunit beta	439	57.583	5.97	16	16	4.23
281	d5	AQS27607.1, hypothetical protein	105	55.349	5.44	2	4	1.97
315	d6	NP_034407.2, glial fibrillary acidic protein isoform 2	828	49.927	5.27	24	36	3.24
349	d7	EDL06107.1, mCG21063, isoform CRA_a	213	44.923	6.09	6	10	2.65
384	d8	AAH59848.1 Sept5 protein, partial	221	41.841	5.89	6	11	2.74
403	d9	NP_036131.1, COP9 signalosome complex subunit 4 isoform a	112	46.541	5.57	2	5	1.98
410	d10	NP_032165.3, guanine nucleotide-binding protein G(q) subunit alpha	427	42.416	5.48	10	23	2.66
412	d11	NP_033015.1, transcriptional activator protein Pur-alpha	666	34.976	6.07	21	25	4.46
416	d12	AAH11036.1, Bisphosphate 3'-nucleotidase 1	102	33.564	5.58	3	6	2.46
420	d13	NP_031464.1, fructose-bisphosphate aldolase A isoform 2	768	39.787	8.31	25	28	2.62
464	d14	NP_034818.1, LIM and SH3 domain protein 1	685	30.374	6.61	19	36	4.86
503	d15	AAC26867.1, heterogenous nuclear ribonucleoprotein A2/B1	619	36.028	8.67	19	36	2.05
507	d16	NP_062606.1, beta-soluble NSF attachment protein	196	33.878	5.32	6	12	2.04
577	d17	AAI00416.1, Transcription elongation factor A (SII)-like 5	118	22.096	5.95	2	9	2.08
597	d18	EDL08815.1, tyrosine 3-monooxygenase/tryptophan 5-monooxygenase activation protein, zeta polypeptide, isoform CRA_b, part	806	29.24	4.71	22	38	2.61
724	d19	BAB61894.1, stathmin	233	17.324	5.76	5	21	2.26
732	d20	NP_001961.1, eukaryotic translation initiation factor 5A-1 isoform B	118	17.094	5.08	3	14	4.79
735	d21	NP_031713.1, cofilin-1	178	18.776	8.22	4	19	5.00
756	d22	EDL15910.1, mCG145251, partial	329	17.412	6.78	11	37	1.96
768	d23	EDL02573.1, mCG144006, partial	137	55.01	5.14	4	5	2.05
832	d24	NP_032329.1, 10 kDa heat shock protein, mitochondrial	89	10.956	7.93	2	21	3.40
942	d25	NP_080230.2, glycerol-3-phosphate phosphatase	132	34.975	5.21	4	8	2.43

Functions of high-score proteins

To identify reliable proteins among the candidates, the identified proteins in each group were sorted according to the following criteria: scores exceeding 70 and 20 in MASCOT search and sequence coverage, respectively. High-scoring proteins in the CTL and Cu groups are listed in Table 3, and high-scoring proteins in the Cu and Cu+N groups are listed in Table 4.

As shown in Table 5, the selected high-scoring proteins were grouped by function as follows: (1) proteins involved in energy production, (2) proteins involved in genetic material, (3) proteins involved in signaling pathways and processes, (4) proteins involved in metabolic process, (5) proteins involved in protein folding, (6) proteins involved in cytoskeletal activity, (7) synaptic proteins, and (8) proteins involved in other activities. Proteins with no function were removed.

Table 3. List of high-scoring proteins in the group fed normal chow diet (CTL) and the group fed CPZ diet (Cu)

Increased

Spot no.	Protein no.	Accession no.	Protein Name	Score	Mr (kDa)	pI Value	Matched peptide	Sequence Coverage (%)	Cu/CTL Ratio
96	U3	NP_083949.2	MICOS complex subunit Mic60 isoform 1	1285	84.247	6.18	65	28	2.19
636	U7	ABL01512.1	beta-actin, partial	79	13.588	5.93	2	23	1.99
820	U15	EDL20118.1	mCG13600, isoform CRA_b	56	5.864	8.01	1	24	2.06

Decreased

Spot no.	Protein no.	Accession no.	Protein Name	Score	Mr (kDa)	pI Value	Matched peptide	Sequence Coverage (%)	CTL/Cu Ratio
197	D3	EDL29822.1	guanosine diphosphate (GDP) dissociation inhibitor 1, isoform CRA_a	1066	56.133	4.92	59	26	2.20
504	D14	AAH92267.1	Glyceraldehyde-3-phosphate dehydrogenase	480	36.102	8.44	24	24	2.12
512	D15	NP_057878.1	ketimine reductase mu-crystallin	791	33.673	5.44	38	31	2.13
649	D18	EDL01936.1	mCG131602, isoform CRA_a, partial	550	29.222	8.31	23	40	2.33
680	D20	NP_004152.1	ras-related protein Rab-1A isoform 1	210	22.891	5.93	6	20	1.98
819	D22	NP_032329.1	10 kDa heat shock protein, mitochondrial	76	10.956	7.93	2	23	2.43

Table 4. List of high-scoring proteins in the group fed CPZ diet for 8 weeks (Cu) and the group fed normal diet for 3 weeks after CPZ diet for 5 weeks (Cu+N)

Increased

Spot no.	Protein no.	Accession no.	Protein Name	Score	Mr (kDa)	pI Value	Matched peptide	Sequence Coverage (%)	Cu+N/Cu Ratio
47	u1	XP_006497712.2	dynamin-1 isoform X1	2064	97.906	6.57	66	35	1.98
212	u6	NP_031978.2	protein disulfide-isomerase A3 precursor	765	57.099	5.88	24	30	2.44
217	u7	NP_031662.2	T-complex protein 1 subunit beta	1001	57.783	5.97	25	25	3.19
262	u9	NP_031531.1	ATP synthase subunit alpha, mitochondrial precursor	1972	59.83	9.22	103	43	2.45
573	u18	NP_006752.1	14-3-3 protein epsilon	459	29.326	4.63	15	36	2.21

Decreased

Spot no.	Protein no.	Accession no.	Protein Name	Score	Mr (kDa)	pI Value	Matched peptide	Sequence Coverage (%)	Cu/Cu+N Ratio
315	d6	NP_034407.2	glial fibrillary acidic protein isoform 2	828	49.927	5.27	24	36	3.24
410	d10	NP_032165.3	guanine nucleotide-binding protein G(q) subunit alpha	427	42.416	5.48	10	23	2.66
412	d11	NP_033015.1	transcriptional activator protein Pur-alpha	666	34.976	6.07	21	25	4.46
420	d13	NP_031464.1	fructose-bisphosphate aldolase A isoform 2	768	39.787	8.31	25	28	2.62
464	d14	NP_034818.1	LIM and SH3 domain protein 1	685	30.374	6.61	19	36	4.86
503	d15	AAC26867.1	heterogenous nuclear ribonucleoprotein A2/B1	619	36.028	8.67	19	36	2.05
597	d18	EDL08815.1	tyrosine 3-monooxygenase/tryptophan 5-monooxygenase activation protein, zeta polypeptide, isoform CRA_b	806	29.24	4.71	22	38	2.61
724	d19	BAB61894.1	stathmin	233	17.324	5.76	5	21	2.26
756	d22	EDL15910.1	mCG145251, partial	329	17.412	6.78	11	37	1.96
832	d24	NP_032329.1	10 kDa heat shock protein, mitochondrial	89	10.956	7.93	2	21	3.40

Table 5. List of proteins in each functional category

Proteins involved in Energy production

	Spot no.	Protein no.	Accession no.	Protein Name	Score	Mr (kDa)	pI Value	Matched peptide	Sequence Coverage (%)	Ratio
CTL vs Cu	504	D14	AAH92267.1	Glyceraldehyde-3-phosphate dehydrogenase	480	36.102	8.44	24	24	-2.12
Cu vs Cu+N	262	u9	NP_031531.1	ATP synthase subunit alpha, mitochondrial precursor	1972	59.83	9.22	103	43	2.45

Protein involved in Genetic material

	Spot no.	Protein no.	Accession no.	Protein Name	Score	Mr (kDa)	pI Value	Matched peptide	Sequence Coverage (%)	Ratio
Cu vs Cu+N	412	d11	NP_033015.1	transcriptional activator protein Pur-alpha	666	34.976	6.07	21	25	-4.46
	503	d15	AAC26867.1	heterogenous nuclear ribonucleoprotein A2/B1	619	36.028	8.67	19	36	-2.05

Proteins involved in Signaling pathways and processes

	Spot no.	Protein no.	Accession no.	Protein Name	Score	Mr (kDa)	pI Value	Matched peptide	Sequence Coverage (%)	Ratio
CTL vs Cu	680	D20	NP_004152.1	ras-related protein Rab-1A isoform 1	210	22.891	5.93	6	20	-1.98
Cu vs Cu+N	573	u18	NP_006752.1	14-3-3 protein epsilon	459	29.326	4.63	15	36	2.21
	410	d10	NP_032165.3	guanine nucleotide-binding protein G(q) subunit alpha	427	42.416	5.48	10	23	-2.66
	597	d18	EDL08815.1	tyrosine 3-monooxygenase/tryptophan 5-monooxygenase activation protein, zeta polypeptide, isoform CRA_b	806	29.24	4.71	22	38	-2.61

Proteins involved in Metabolism process

	Spot no.	Protein no.	Accession no.	Protein Name	Score	Mr (kDa)	pI Value	Matched peptide	Sequence Coverage (%)	Ratio
CTL vs Cu	512	D15	NP_057878.1	ketimine reductase mu-crystallin	791	33.673	5.44	38	31	-2.13
Cu vs Cu+N	212	u6	NP_031978.2	protein disulfide-isomerase A3 precursor	765	57.099	5.88	24	30	2.44
	420	d13	NP_031464.1	fructose-bisphosphate aldolase A isoform 2	768	39.787	8.31	25	28	-2.62

Proteins involved in Protein folding

	Spot no.	Protein no.	Accession no.	Protein Name	Score	Mr (kDa)	pI Value	Matched peptide	Sequence Coverage (%)	Ratio
CTL vs Cu	819	D22	NP_032329.1	10 kDa heat shock protein, mitochondrial	76	10.956	7.93	2	23	-2.43
Cu vs Cu+N	832	d24			89				21	-3.40
	217	u7	NP_031662.2	T-complex protein 1 subunit beta	1001	57.783	5.97	25	25	3.19

Proteins involved in Cytoskeletal activity

	Spot no.	Protein no.	Accession no.	Protein Name	Score	Mr (kDa)	pI Value	Matched peptide	Sequence Coverage (%)	Ratio
CTL vs Cu	636	U7	ABL01512.1	beta-actin, partial	79	13.588	5.93	2	23	1.99
Cu vs Cu+N	464	d14	NP_034818.1	LIM and SH3 domain protein 1	685	30.374	6.61	19	36	-4.86

Proteins involved in Synaptic protein

	Spot no.	Protein no.	Accession no.	Protein Name	Score	Mr (kDa)	pI Value	Matched peptide	Sequence Coverage (%)	Ratio
Cu vs Cu+N	47	u1	XP_006497712.2	dynamin-1 isoform X1	2064	97.906	6.57	66	35	1.98
	315	d6	NP_034407.2	glial fibrillary acidic protein isoform 2	828	49.927	5.27	24	36	-3.24

Proteins involved in other activity

	Spot no.	Protein no.	Accession no.	Protein Name	Score	Mr (kDa)	pI Value	Matched peptide	Sequence Coverage (%)	Ratio
CTL vs Cu	96	U3	NP_083949.2	MICOS complex subunit Mic60 isoform 1	1285	84.247	6.18	65	28	2.19
	197	D3	EDL29822.1	guanosine diphosphate (GDP) dissociation inhibitor 1, isoform CRA_a	1066	56.133	4.92	59	26	-2.20
Cu vs Cu+N	724	d19	BAB61894.1	stathmin	233	17.324	5.76	5	21	-2.26

Proteins identified in both proteomic analyses

Proteins present in both lists of CTL *versus* Cu group and Cu *versus* Cu+N group are presented in Table 6. Expression of the 10 kDa heat shock protein (HSP10) was decreased in the CTL *versus* Cu group protein list as well as in the Cu *versus* Cu+N group protein list. Meanwhile, expression of the guanine nucleotide-binding protein G(q) subunit alpha was increased in the Cu group but decreased in the Cu+N group. Expression of PDIA3 and CRYM was decreased in the Cu group but increased in the Cu+N group.

Table 6. List of identical proteins in the protein lists

	Spot no.	Protein no.	Accession no.	Protein Name	Score	Mr (kDa)	pI Value	Matched peptide	Sequence Coverage (%)	Ratio
CTL vs Cu	819	D22	NP_032329.1	10 kDa heat shock protein, mitochondrial	76	10.956	7.93	2	23	-2.43
Cu vs Cu+N	832	d24			89			2	21	-3.40

	Spot no.	Protein no.	Accession no.	Protein Name	Score	Mr (kDa)	pI Value	Matched peptide	Sequence Coverage (%)	Ratio
CTL vs Cu	430	U9	NP_032165.3	guanine nucleotide-binding protein G(q) subunit alpha	73	42.416	5.48	2	4	2.34
Cu vs Cu+N	410	d10			427			10	23	-2.66

	Spot no.	Protein no.	Accession no.	Protein Name	Score	Mr (kDa)	pI Value	Matched peptide	Sequence Coverage (%)	Ratio
CTL vs Cu	217	D5	NP_031978.2	protein disulfide-isomerase A3 precursor	187	57.099	5.88	4	8	-2.16
Cu vs Cu+N	212	u6			765			24	30	2.44
CTL vs Cu	512	D15	NP_057878.1	ketimine reductase mu-crystallin	791	33.673	5.44	38	31	-2.13
Cu vs Cu+N	474	u15			296			7	18	2.68

Selection and validation of proteins

Among the identified proteins, the expression of CRYM and PDIA3 was decreased after demyelination and increased after remyelination, suggesting their close link to myelin survival or AHN. CRYM was detected at two different spots on 2DE gels in the CTL *versus* Cu group but at only one spot on 2DE gels in the Cu *versus* Cu+N group (Figure 11A).

The expression of these proteins was validated through immunohistochemical staining. CRYM immunoreactivity was detected in the pyramidal layers of the hippocampal CA1 and CA3 regions and the ML of DG in the CTL group (Figure 11B, 11C, and 11D). In the Cu group, weaker CRYM immunoreactivity was detected in the stratum pyramidale of CA1 and CA3 regions and ML of DG than that in the CTL group (Figure 11B, 11C, and 11D). Specifically, CRYM immunoreactivity in DG, CA1, and CA3 in the Cu group was significantly decreased to 53.6%, 69.2%, and 75.3%, respectively, of that in the CTL group (Figure 11E, 11F, and 11G). Moreover, CRYM immunoreactivity in DG, CA1, and CA3 in the Cu+N group was stronger than that in the Cu group (72.0%, 89.8%, and 90.3% of that in the CTL group) (Figure 11E, 11F, and 11G). Meanwhile, CRYM immunoreactivity in DG and CA1 in the Cu+N group was significantly stronger than that in the Cu group (Table 7).

On 2DE gels, PDIA3 spots showed stronger density in the Cu+N group than in the Cu group (Figure 12A). In the CTL group, PDIA3 immunoreactivity was primarily detected in the stratum pyramidale of CA1 and CA3 as well as in the GCL of DG (Figure 12B, 12C, and 12D). In the Cu group, the distribution pattern of PDIA3 spots was similar to that in the CTL group, although immunoreactivity in DG, CA1, and

CA3 in this group was significantly decreased compared with that in the CTL group (86.0%, 52.1% and 62.1%, respectively) (Figure 12E, 12F, and 12G). In the Cu+N group, PDIA3 immunoreactivity in all regions was stronger than that in the Cu group (96.4%, 81.6%, and 79.4% of that in the CTL group, respectively) (Figure 12E, 12F, and 12G). In the Cu+N group, PDIA3 immunoreactivity in CA1 and CA3 was significantly stronger than that in the Cu group (Table 7).

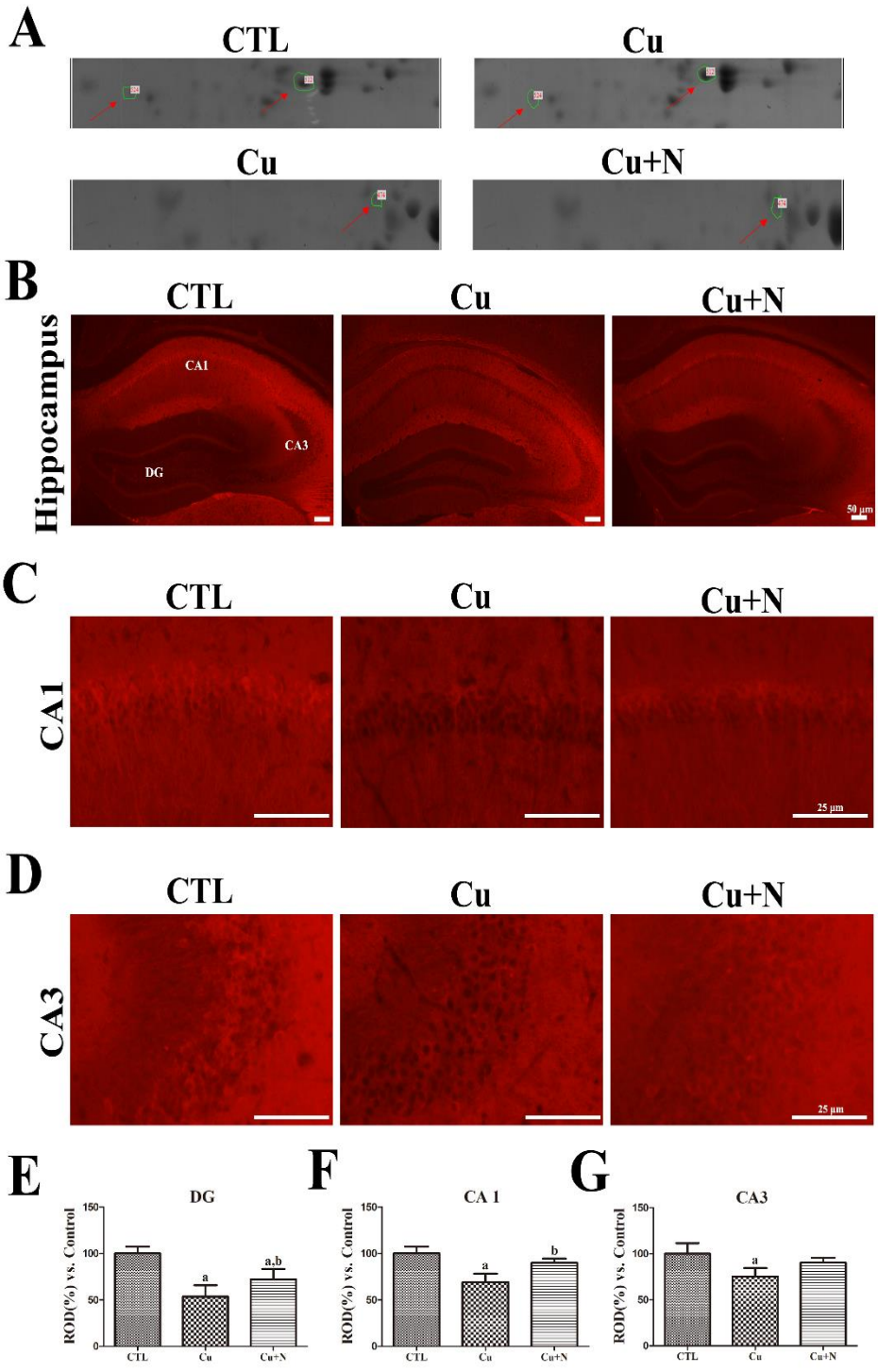
A
CTL
Cu
Cu
Cu+N
B
CTL
Cu
Cu+N
Hippocampus
CA1
CA3
DG
50 μm
C
CTL
Cu
Cu+N
CA1
25 μm
D
CTL
Cu
Cu+N
CA3
25 μm
E
DG
ROD(%) vs. Control
150
100
50
0
a
a,b
CTL
Cu
Cu+N
F
CA 1
ROD(%) vs. Control
150
100
50
0
a
b
CTL
Cu
Cu+N
G
CA3
ROD(%) vs. Control
150
100
50
0
a
CTL
Cu
Cu+N

Figure 11. CRYM expression in the hippocampus of group fed normal chow diet for 8 weeks (CTL), group fed CPZ diet for 8 weeks (Cu), and group fed normal diet for 3 weeks after CPZ diet for 5 weeks (Cu+N). CRYM detected on (A) 2DE gels of CTL *versus* Cu group and Cu *versus* Cu+N group. CRYM immunoreactivity in (B) the whole hippocampus and magnified (C) CA1 and (D) CA3 regions in all groups. (E, F, G) ROD is described as the percentage of CRYM immunoreactivity in the CTL group. Scale bar = 50 μm (B) and 25 μm (C, D). (n = 5 per group; $^{a}p < 0.05$, significantly different from the CTL group; $^{b}p < 0.05$, significantly different from the Cu group). All data are presented as mean ± standard deviation.

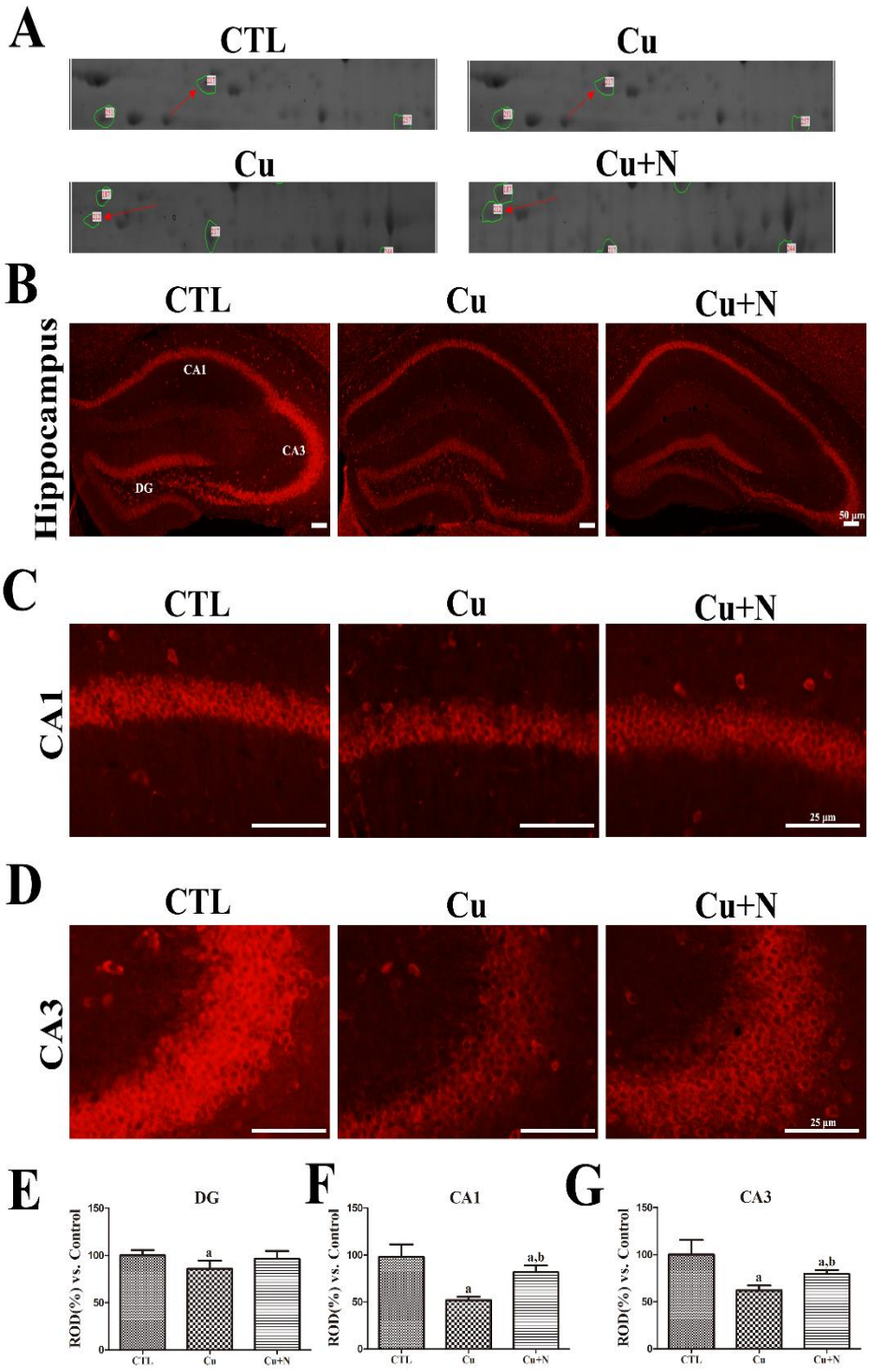
A
CTL
Cu
Cu
Cu+N
B
CTL
Cu
Cu+N
Hippocampus
CA1
CA3
DG
50 μm
C
CTL
Cu
Cu+N
CA1
25 μm
D
CTL
Cu
Cu+N
CA3
25 μm
E
DG
ROD(%) vs. Control
150
100
50
0
a
CTL
Cu
Cu+N
F
CA1
ROD(%) vs. Control
150
100
50
0
a
a,b
CTL
Cu
Cu+N
G
CA3
ROD(%) vs. Control
150
100
50
0
a
a,b
CTL
Cu
Cu+N

Figure 12. PDIA3 expression in the hippocampus in group fed normal chow diet for 8 weeks (CTL), group fed CPZ diet for 8 weeks (Cu), and group fed normal diet for 3 weeks after CPZ diet for 5 weeks (Cu+N). PDIA3 detected on (A) 2DE gels of CTL *versus* Cu group and Cu *versus* Cu+N group. PDIA3 immunohistochemistry in (B) the whole hippocampus and magnified (C) CA1 and (D) CA3 regions in all groups. (E, F, G) ROD is described as the percentage of PDIA3 immunoreactivity in the CTL group. Scale bar = 50 μm (B) and 25 μm (C, D). (n = 5 per group; $^{a}p < 0.05$, significantly different from the CTL group; $^{b}p < 0.05$, significantly different from the Cu group). All data are presented as mean ± standard deviation.

Table 7. Results of CRYM and PDIA3 immunostaining

Group \ Region	CRYM			PDIA3		
	DG	CA1	CA3	DG	CA1	CA3
Cu group	↓ ↓	↓ ↓	↓ ↓	↓ ↓	↓ ↓	↓ ↓
Cu+N group	↑ ↑	↑ ↑	↑	↑	↑ ↑	↑ ↑

The two arrows in the Cu group show significant results *versus* the CTL group. The two arrows in the Cu+N group indicate significant results *versus* the Cu group. One arrow indicates non-significant results.

Experiment II

Synthesis of Tat-CRYM and Tat-PDIA3 fusion proteins

CRYM and *PDIA3* genes were integrated to a Tat peptide expression vector to synthesize Tat-CRYM and Tat-PDIA3 fusion proteins, respectively, and the two fusion proteins were overexpressed in *E. coli*. For protein purification, $Ni^{b+} \rightarrow Ni^{2+}$-nitrilotriacetic acid sepharose affinity column and PD-10 column chromatography were applied. The purified Tat-PDIA3 and Tat-CRYM proteins were confirmed by western blotting for His-tag, and clear single bands were detected at ~37 and ~62 kDa, respectively (Figure 13A).

His-tag immunostaining was performed to determine whether His-Tat-CRYM and His-Tat-PDIA3 were delivered to the hippocampus (Figure 13B). His-tag-positive cells were observed in the SGZ of DG in the CTL and Cu groups but were rarely observed in the CA1 and CA3 regions. The percentage of ROD in the Cu group was 101.0%. However, in the Tat-CRYM- and Tat-PDIA3-treated groups, His-tag immunoreactivity was detected more prominently in all areas of the hippocampus than that in the CTL group. In addition, His-tag immunoreactivity was detected in the stratum lacunosum-moleculare of the CA1 region and mossy fibers of the CA3 region. Overall, His-tag immunoreactivity in the Tat-CRYM and Tat-PDIA3 groups was significantly elevated by respectively 151.2% and 153.5% compared with that in the CTL group (Figure 13B).

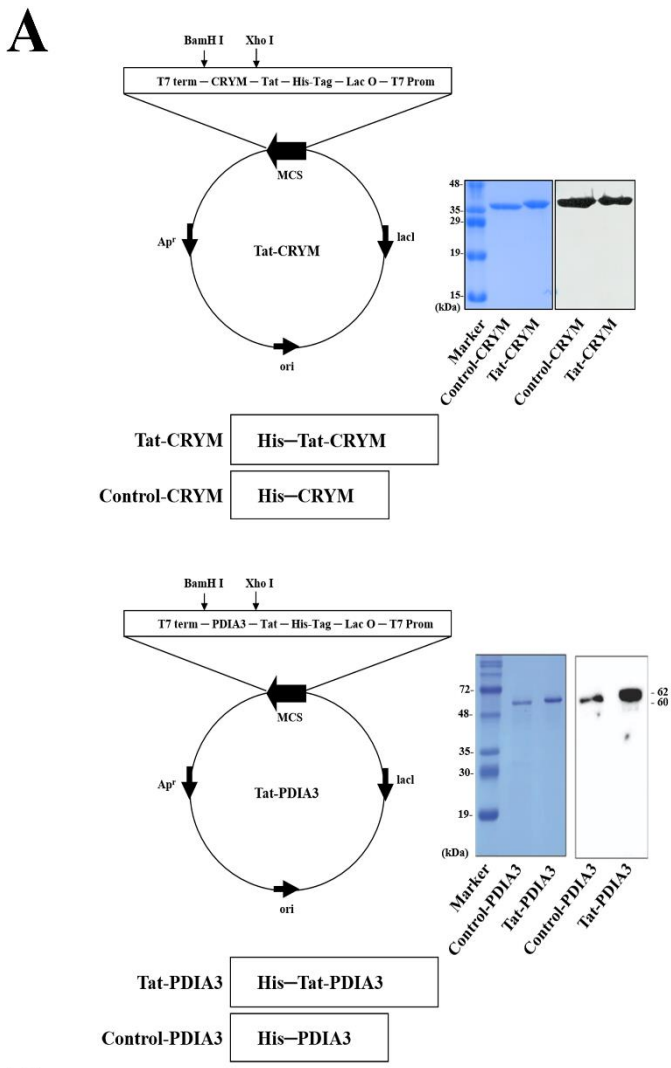
A
BamH I
Xho I
T7 term — CRYM — Tat — His-Tag — Lac O — T7 Prom
MCS
Ap^r
lacI
Tat-CRYM
ori
48-
35-
29-
19-
15-
(kDa)
Marker
Control-CRYM
Tat-CRYM
Control-CRYM
Tat-CRYM
Tat-CRYM
His—Tat-CRYM
Control-CRYM
His—CRYM
BamH I
Xho I
T7 term — PDIA3 — Tat — His-Tag — Lac O — T7 Prom
MCS
Ap^r
lacI
Tat-PDIA3
ori
72-
48-
35-
30-
19-
(kDa)
- 62
- 60
Marker
Control-PDIA3
Tat-PDIA3
Control-PDIA3
Tat-PDIA3
Tat-PDIA3
His—Tat-PDIA3
Control-PDIA3
His—PDIA3

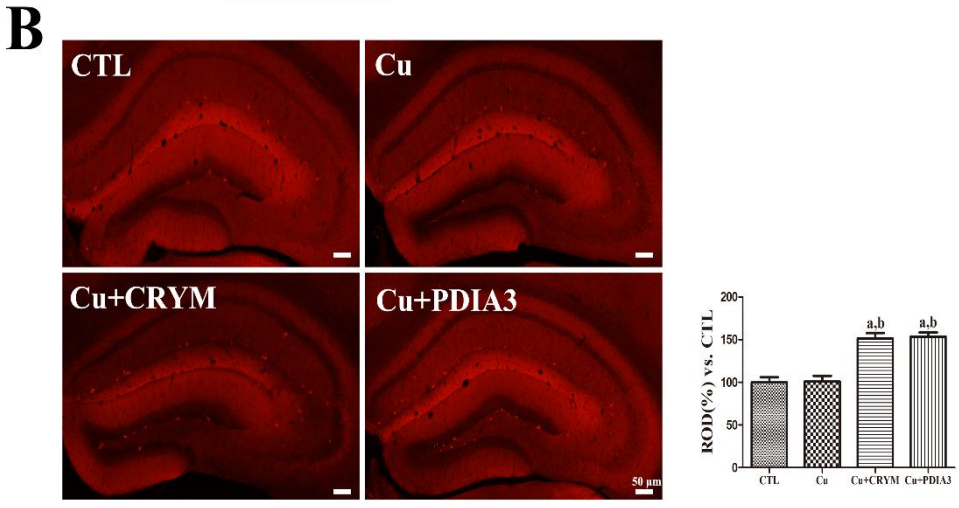
B
CTL
Cu
Cu+CRYM
Cu+PDIA3
50 μm
ROD(%) vs. CTL
200
150
100
50
0
a,b
a,b
CTL
Cu
Cu+CRYM
Cu+PDIA3

Figure 13. Overview of Tat-CRYM and Tat-PDIA3 fusion proteins and confirmation of the delivery of these proteins to the mouse hippocampus with immunohistochemical staining for His-tag. (A) Vector maps of Tat-CRYM and Tat-PDIA3 are shown; clear single bands were detected. (B) Immunohistochemical staining for His-tag in the hippocampus of group fed normal chow diet (CTL), group fed CPZ diet (Cu), group fed CPZ diet and administered Tat-CRYM injection (Cu+CRYM), and group fed CPZ diet and administered Tat-PDIA3 injection (Cu+PDIA3). ROD is described as the percentage of His-tag immunoreactivity in the DG in the CTL group. Scale bar = 50 μm (n = 5 per group; $^{a}p < 0.05$, significantly different from the CTL group; $^{b}p < 0.05$, significantly different from the Cu group). All data are presented as mean ± standard deviation.

Effects of Tat-CRYM and Tat-PDIA3 on CPZ-induced demyelination in the mouse hippocampus

To assess the effects of Tat-CRYM and Tat-PDIA3 on demyelination, MBP immunohistochemical staining was performed. In the CTL group, MBP immunoreactivity was detected in alveus and stratum-lacunosum moleculare of the CA1 region, mossy fibers of the CA3 region, and SGZ of the DG (Figure 14A). In the Cu group, weak MBP immunoreactivity was detected in all hippocampal regions, and MBP immunoreactivity in the Cu group was significantly reduced (43.3% of CTL) compared with that in the CTL group (Figure 14B and 14E). In the Cu+CRYM and Cu+PDIA3 groups, the distribution pattern of MBP immunoreactive structures was the same as that in the Cu group (Figures 14C and 14D), although immunoreactivity was higher in these groups by 70.1% and 73.8% of that in the CTL group. However, the difference achieved statistical significance only between the Cu+PDIA3 and Cu groups (Figure 14E).

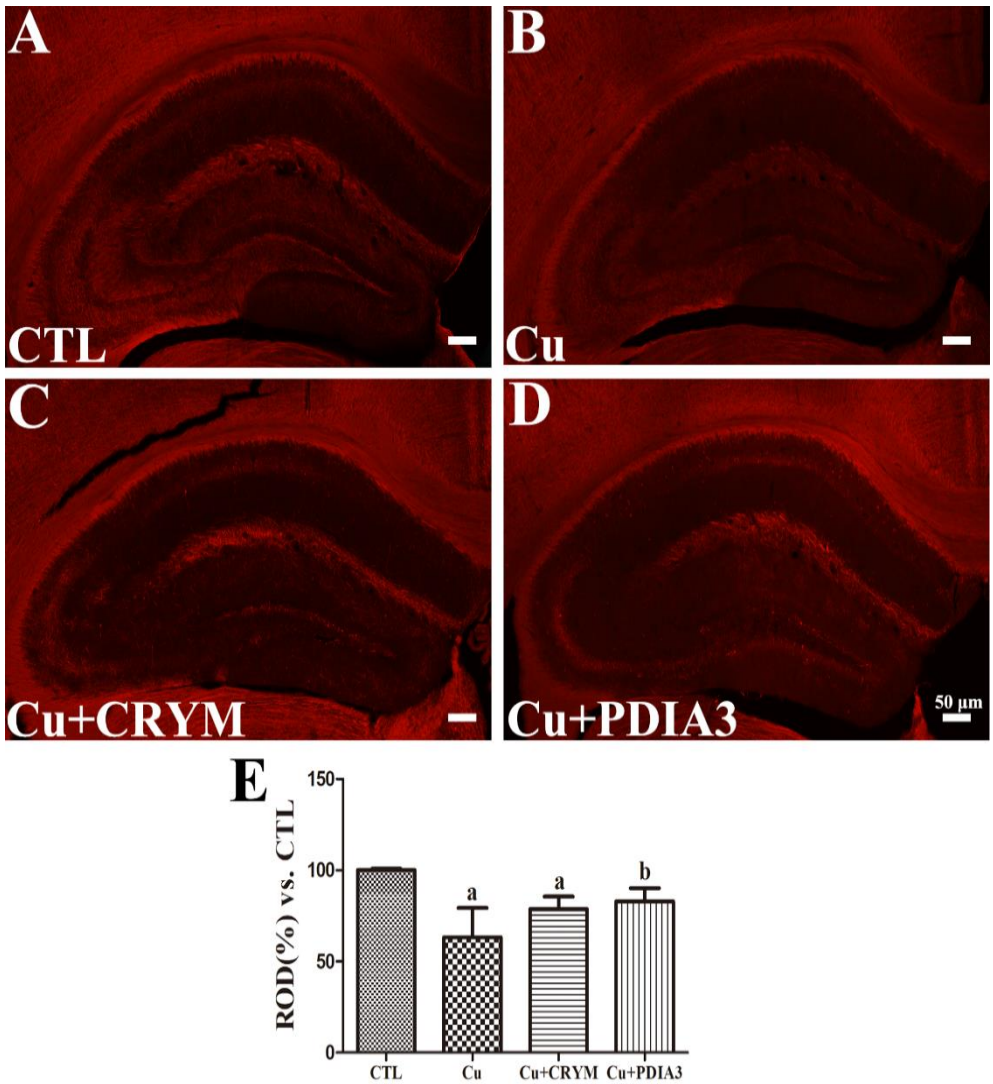

Figure 14. MBP immunohistochemical staining in the hippocampus of (A) group fed normal chow diet (CTL), (B) group fed CPZ diet (Cu), (C) group fed CPZ diet and administered Tat-CRYM injection (Cu+CRYM), and (D) group fed CPZ diet and administered Tat-PDIA3 injection (Cu+PDIA3). (E) ROD is described as the percentage of MBP immunoreactivity in the hippocampus in the CTL group. Scale bar = 50 μm. (n = 5 per group; $^{a}p < 0.05$, significantly different from the CTL group; $^{b}p < 0.05$, significantly different from the Cu group). All data are presented as mean ± standard deviation.

Effects of Tat-CRYM and Tat-PDIA3 on CPZ-induced microglial activation in the mouse hippocampus

Iba-1 immunostaining was performed to examine the effects of Tat-CRYM and Tat-PDIA3 on changes in microglial morphology in the hippocampus under CPZ-induced demyelination. In the CTL group, Iba-1-immunoreactive microglia were detected in all areas of the hippocampus, and their cytoplasm was small, with long processes (Figure 15A). In the Cu group, Iba-1-immunoreactive microglia presented hypertrophied cytoplasm with thickened processes, and their immunoreactivity was significantly increased to 129.1% of that in the CTL group (Figure 15B and 15E). In the Cu+CRYM and Cu+PDIA3 groups, the morphology of Iba-1-immunoreactive microglia was the same as that in the Cu group, but Iba-1 immunoreactivity was increased to respectively 124.8% and 129.1% of that in the CTL group; no significant differences were noted between the Cu+CRYM and Cu+PDIA3 groups and the Cu group (Figure 15C,15D, and 15E).

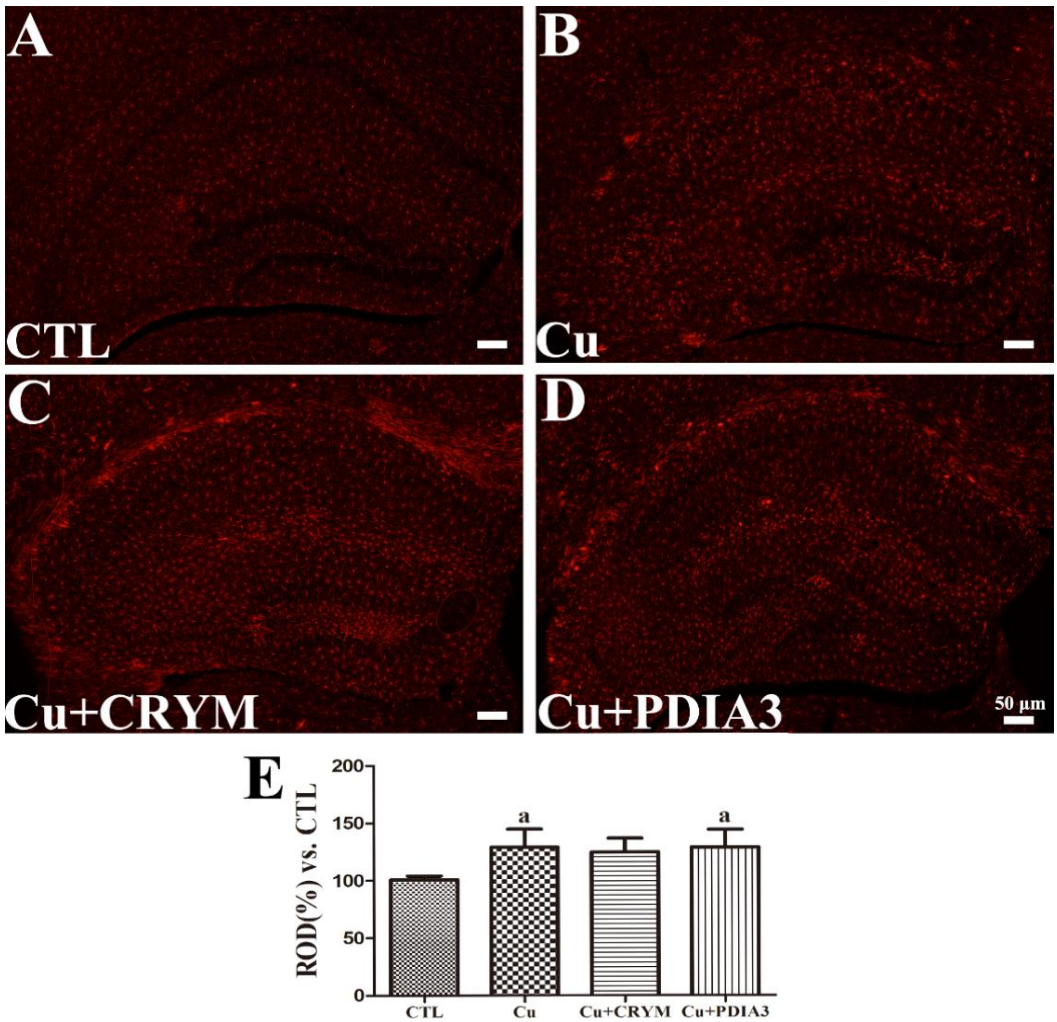

Figure 15. Iba-1 immunohistochemical staining in the hippocampus of (A) group fed normal chow diet (CTL), (B) group fed CPZ diet (Cu), (C) group fed CPZ diet and administered Tat-CRYM injection (Cu+CRYM), and (D) group fed CPZ diet and administered Tat-PDIA3 injection (Cu+PDIA3). (E) ROD is described as the percentage of Iba-1 immunoreactivity in the hippocampus in the CTL group. Scale bar = 50 μm (n = 5 per group; $^{a}p < 0.05$, significantly different from the CTL group; $^{b}p < 0.05$, significantly different from the Cu group). All data are presented as mean ± standard deviation.

Effects of Tat-CRYM and Tat-PDIA3 on CPZ-induced reduction in cell proliferation

Ki67 immunostaining was performed to observe proliferating cells in the DG. In the CTL group, Ki67-positive nuclei were detected in the SGZ of DG, and their mean number was 24 per section (Figure 16A and 16E). In the Cu group, few Ki67-positive nuclei were detected in the SGZ, and their mean number was significantly reduced to 1 per section compared with that in the CTL group (Figure 16B and 16E). In the Cu+CRYM and Cu+PDIA3 groups, a few Ki67-positive nuclei were detected in the SGZ of DG, and their number was significant increased (to 3.8 and 3.6 per section, respectively) compared with that in the Cu group (Figure 16C, 16D, and 16E).

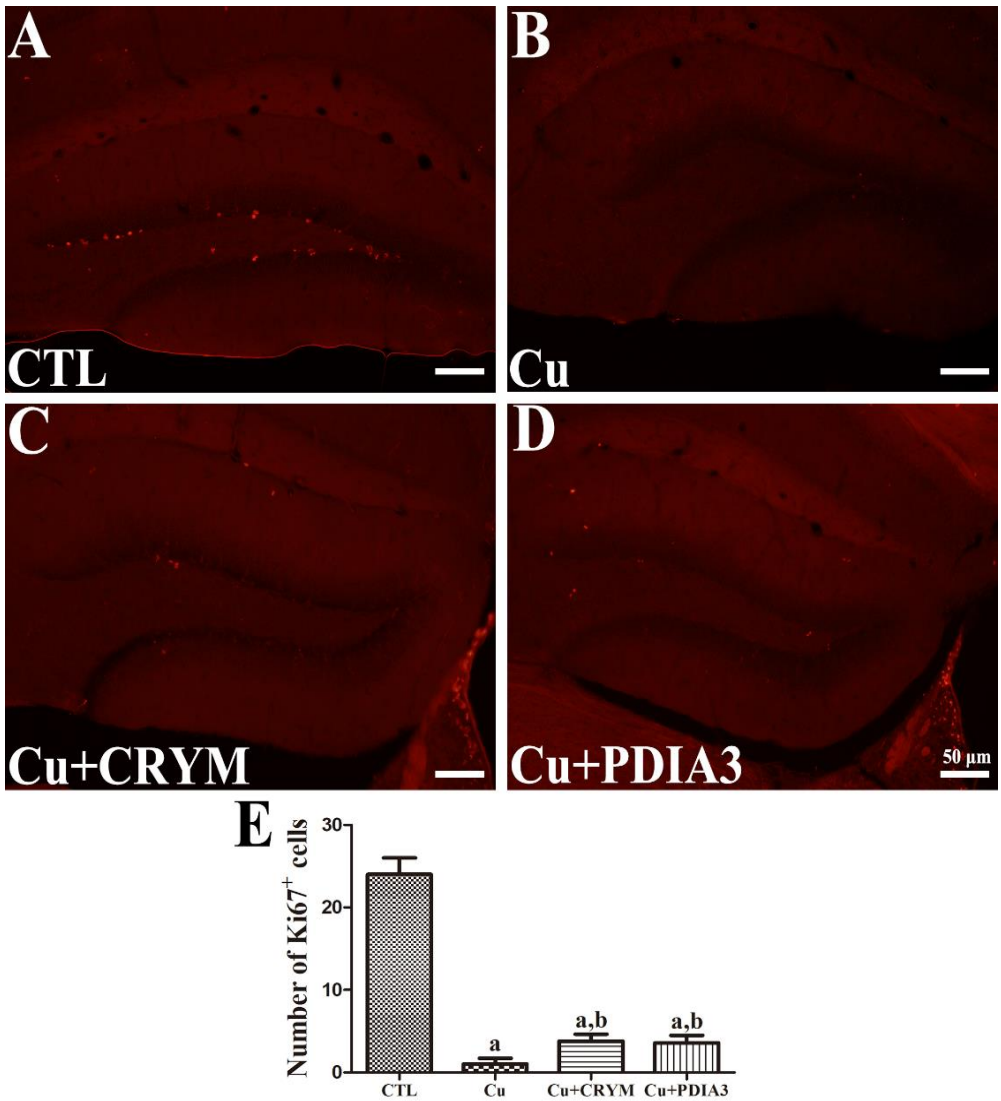

Figure 16. Ki67 immunohistochemical staining in the hippocampal DG of (A) group fed normal chow diet (CTL), (B) group fed CPZ diet (Cu), (C) group fed CPZ diet and administered Tat-CRYM injection (Cu+CRYM), and (D) group fed CPZ diet and administered Tat-PDIA3 injection (Cu+PDIA3). (E) The mean number of Ki67-postive nuclei in the SGZ of DG is shown. Scale bar = 50 μm (n = 5 per group; $^{a}p < 0.05$, significantly different from the CTL group). All data are presented as mean ± standard deviation.

Effects of Tat-CRYM and Tat-PDIA3 on CPZ-induced reduction in neuroblast differentiation

In the CTL group, DCX-immunoreactive neuroblasts were detected in the SGZ of the DG, and their dendrites extended to the ML of the DG (Figure 17A and 17E). In the Cu group, weaker DCX immunoreactivity was detected in the DG (Figure 17B and 17F), and it was significantly decreased to 30.4% of that in the CTL group (Figure 17I). In the Cu+CRYM and Cu+PDIA3 groups, a few DCX-immunoreactive neuroblasts were observed in the DG, and their dendrites were poorly developed than in those of neuroblasts in the CTL group (Figure 17C, 17G, 17D, and 17H). However, in these groups, DCX immunoreactivity was significantly increased compared with that in the Cu group (respectively 46.2% and 49.93% of that in the CTL group) (Figure 17I).

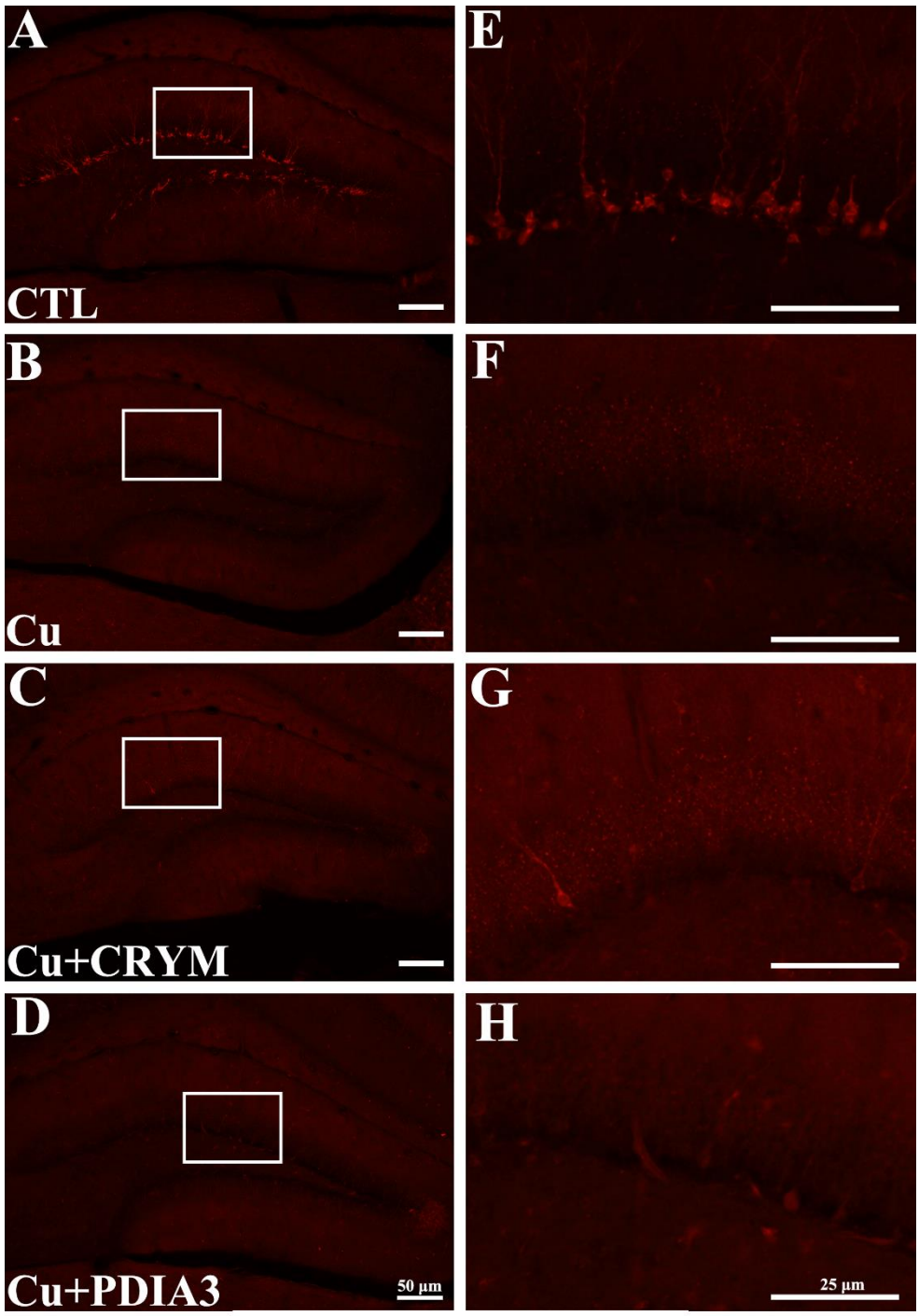
A
CTL
E
B
Cu
F
C
Cu+CRYM
G
D
Cu+PDIA3
50 μm
H
25 μm
I
ROD(%) vs. Control
150
100
50
0
a
a,b
a,b
CTL
Cu
Cu+CRYM
Cu+PDIA3

Figure 17. DCX immunohistochemical staining in the hippocampal DG of (A, E) group fed normal chow diet (CTL), (B, F) group fed CPZ diet (Cu), (C, G) group fed CPZ diet and administered Tat-CRYM injection (Cu+CRYM), and (D, H) group fed CPZ diet and administered Tat-PDIA3 injection (Cu+PDIA3). (E, F, G, H) High magnification of boxed areas. (I) ROD is described as the percentage of DCX immunoreactivity in the DG in the CTL group. Scale bar = 50 μm (A, B, C, D) and 25 μm (E, F, G, H). (n = 5 per group; $^{a}p < 0.05$, significantly different from the CTL group; $^{b}p < 0.05$, significantly different from the Cu group). All data are presented as mean ± standard deviation.

Effects of Tat-CRYM and Tat-PDIA3 on CPZ-induced reduction in CREB phosphorylation at Ser133 in the moue hippocampus

Phosphorylation of CREB was observed in the DG of hippocampus. Abundant pCREB-positive nuclei were detected in the CTL group, and their mean number was 105.6 per section (Figure 18A and 18E). In the remaining groups, some pCREB-positive nuclei were detected in the SGZ of DG, and their mean number was 17.6, 28.0, and 29.8 per section, respectively, indicating significantly reduction in the number compared with that in the CTL group (Figure 18B,18C, and 18D). Only in the Cu+PDIA3 group, the number of pCREB-positive nuclei was significantly higher than that in the Cu group (Figure 18E).

The results of changes in MBP immunoreactivity, microglia activation, cell proliferation, neuroblast differentiation, and CREB phosphorylation in each group are summarized in Table 8.

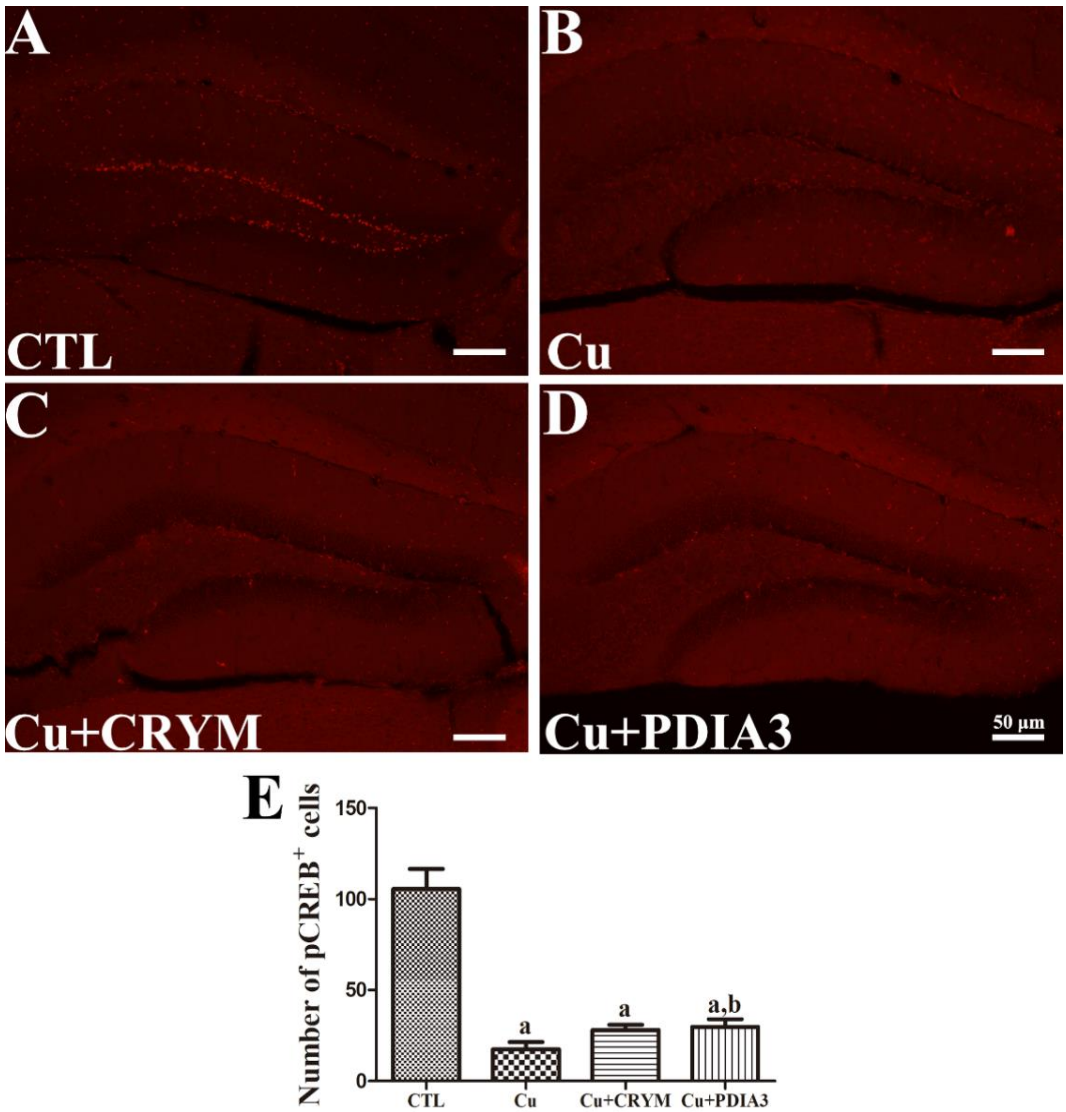

Figure 18. pCREB staining in the hippocampal DG of (A) group fed normal chow diet (CTL), (B) group fed CPZ diet (Cu), (C) group fed CPZ diet and administered Tat-CRYM injection (Cu+CRYM), and (D) group fed CPZ diet and administered Tat-PDIA3 injection (Cu+PDIA3). (E) Number of pCREB-positive cells per section. Scale bar = 50 μm (n = 5 per group; $^{a}p < 0.05$, significantly different from the CTL group; $^{b}p < 0.05$, significantly different from the Cu group). All data are presented as mean ± standard deviation.

Table 8. Changes in MBP immunoreactivity, microglial activation, cell proliferation, neuroblast differentiation, and CREB phosphorylation in each group

Group / Neurogenesis	Cu	Cu+CRYM	Cu+PDIA3
myelin	↓ ↓	↑	↑ ↑
microglia	↑ ↑	↓	=
proliferating cell	↓ ↓	↑ ↑	↑ ↑
neuroblast	↓ ↓	↑ ↑	↑ ↑
CREB signaling	↓ ↓	↑	↑ ↑

The two arrows in the Cu group indicate significant results compared with the CTL group. The two arrows in the Cu+CRYM and Cu+PDIA3 groups indicate significant results compared with the Cu group. One arrow indicates non-significant results. The '=' sign indicates the same value as that in the Cu group.

DISCUSSION

Experiment I

CPZ has been widely used to study demyelination mimicking the condition in MS in which the hippocampal DG is sensitive (Planche et al., 2018). Since MS is characterized by incomplete remyelination and remyelination failure, the major focus of MS treatment is complete remyelination.

Five-week exposure to CPZ diet suppressed mitochondrial activity in the hippocampus but promoted the release of inflammatory cytokines, such as interleukin 1β and tumor necrosis factor-α (Zhang et al., 2018). Replacing CPZ diet to normal chow diet after 6 weeks of normal chow intake led to over 60% recovery of the myelin sheath in the hippocampus (Dutta et al., 2013). Varying protocols and durations of demyelination and remyelination have been applied in studies on CPZ treatment. In the present study, CPZ diet administered for 5 weeks and then withdrawn for 3 weeks.

In the present study, exposure to CPZ significantly lowered MBP immunoreactivity, Ki67-positive proliferating cell count, DCX-immunoreactive neuroblast count, and pCREB-positive nuclear count in the hippocampus, consistent with previous reports (Hahn et al., 2022). When CPZ diet was switched to normal chow diet, the reduction in MBP immunoreactivity, Ki67-positive proliferating cell count, DCX-immunoreactive neuroblast count, and pCREB-positive nuclear count was significantly ameliorated. During the remyelination period, myelin synthesis has been reported in the hippocampus (Leicaj et al., 2018). In addition, neural progenitor cells are involved in the hippocampus of mature oligodendrocytes (Klein et al., 2020).

Proteomic analysis is one of the useful approaches to identify therapeutic targets for diseases (Partridge et al., 2015). However, there have been no comprehensive studies aimed at detecting the possible targets for CPZ-induced demyelination and remyelination in the hippocampus. Therefore, in the present experiment, proteins whose expression patterns were altered by over two-folds after demyelination and remyelination were investigated through 2DE and LC-MS/MS.

According to functions, the identified high-scoring proteins were grouped into the categories of energy production, genetic material, signaling pathways, metabolism, protein folding, cytoskeletal activity, synaptic protein, and other activities.

First, protein involved in energy production, such as glyceraldehyde-3-phosphate dehydrogenase, were downregulated following CPZ-induced demyelination. This protein plays important roles in glycolysis, cytoskeleton assembly (Füchtbauer et al., 1986), and membrane transport (Tisdale, 2001). In addition, it is associated with the transcriptional activation of neurons (Morgenegg et al., 1986), nuclear export of RNA (Singh and Green, 1993), and repair of DNA (Meyer-Siegler et al., 1991). Furthermore, glyceraldehyde 3-phosphate dehydrogenase is a critical part of diverse apoptotic pathways, which are implicated in neurodegenerative disease (Chuang et al., 2005). Moreover, ATP synthase subunit alpha plays a crucial role in the synthesis of ATP from ADP (Antes et al., 2003), and its expression was increased when the CPZ diet was switched to normal diet.

Second, the expression of proteins related to genetic material, such as transcriptional activator protein Pur-alpha and heterogenous nuclear ribonucleoprotein A2/B1, was decreased when the CPZ diet was switched to normal diet. Transcriptional activator protein Pur-alpha is a DNA-binding protein involved DNA replication initiation and

recombination (Kelm et al., 1999). Heterogenous nuclear ribonucleoprotein A2/B1 serves diverse functions of transcriptional regulation, such as RNA splicing, capping, and modification, among others (Wu et al., 2018).

Third, the expression of proteins involved in signaling pathways and signal transduction, such as ras-related protein Rab-1A isoform 1, was decreased in the Cu group. Ras-related protein Rab-1A isoform 1 plays a key role in intracellular membrane transport, and it regulates the transport of vesicles from the cell surface to the secretion of growth hormones (Wang et al., 2010). In the group switched to normal diet after CPZ diet, the expression of other proteins related to signal transduction, such as 14-3-3 epsilon, was increased, while that of guanine nucleotide-binding protein G(q) and tyrosine 3-monooxygenase/tryptophan 5-monooxygenase activation protein, zeta polypeptide was decreased. Previously, 14-3-3 protein epsilon has been reported to mediate signal transduction and implicated in various cellular activities, such as cell growth, apoptosis, and migration, in various types of cancer (Gan et al., 2020). Moreover, it is a multifunctional protein that is highly expressed in the brain during development and has recently been recognized as a key regulator of neurodevelopmental processes (Cornell and Toyo-oka, 2017). Guanine nucleotide-binding protein G(q) is involved in the transmission of signals to the cell nucleus upon cellular stimulation (Hurowitz et al., 2000). It interferes with the circulation of adrenaline monophosphate or cAMP-dependent pathway, primarily through the glutamatergic and GABAergic synaptic pathways (Lu et al., 2020).

Fourth, the expression of proteins involved in metabolism, such as CRYM, was decreased in the CPZ group. CRYM is involved in NADPH binding (Borel et al.,

2014) and thyroid hormone catabolism (Visser et al., 2010). The expression of other protein, such as PDIA3, was increased in the group switched to normal diet after CPZ diet. PDIA3 activity is part of glycoprotein-specific quality control machinery involved in the folding of cysteine-rich glycoproteins and serves an important function in cellular signaling (Zhang et al., 2006). The expression of fructose-bisphosphate aldolase A isoform 2 was decreased in the group switched to normal diet after CPZ diet. This protein is involved in glycolysis, glucose synthesis, and fructose metabolism (Salvatore et al., 1986)

Fifth, the expression of proteins involved in protein folding, such as HSP10, was decreased after the intake of CPZ diet as well as after switch to normal diet after CPZ diet. HSP10 is a co-chaperonin involved in mitochondrial protein import and polymer assembly (Cheng et al., 1989). Furthermore, the expression of T-complex protein 1 subunit beta was increased upon switch to normal diet after CPZ diet. This protein serves as a molecular chaperone in actin and tubulin folding (Wu et al., 2015).

Sixth, the expression of proteins involved in cytoskeletal activity, such as beta-actin, was increased after the intake of CPZ diet. This is a cytoskeletal protein involved in cellular structure and motility (Sikand et al., 2012). Moreover, the expression of LIM and SH3 domain protein 1 was decreased after the withdrawal of CPZ diet. These are actin-binding proteins that regulate actin-based cytoskeletal actions. In a previous study, axonal growth was significantly reduced in LIM- and SH3 domain protein 1-knockdown mice (Pollitt et al., 2020).

Seventh, the expression of synaptic proteins, such as dynamin 1 and glial fibrillary acid protein isoform 2, was increased following the withdrawal of CPZ diet. Dynamin 1 is a synaptic protein involved in clathrin-mediated endocytosis at the

synapse, and significantly lower degree of dynamin immunoreactivity and protein levels were noted in elderly mice than in adult mice (Yoo et al., 2016). In addition, the expression of dynamin 1 was reduced in an animal model of Alzheimer's disease (Ciavardelli et al., 2010). The expression of this protein in the remyelination state is considered a meaningful result related to demyelination disease. Glial fibrillary acidic protein isoform 2 is a long-term synaptic-strengthening protein and a specific marker that distinguishes astrocytes from other nervous system cells during central nervous system development (Yang and Wang, 2015).

Finally, proteins involved in other activities were classified, because it was difficult to combine their functions of into a single category. The expression of MICOS complex subunit Mic60 isoform 1 was decreased in the Cu group. This is a protein complex on the inner mitochondrial membrane, and it is involved in the formation and maintenance of the crista structure in the mitochondria (Kozjak-Pavlovic, 2017). In addition, the expression of guanosine diphosphate dissociation inhibitor 1 was decreased in the Cu group; this protein is present in neural and sensory tissues and involved in vesicular trafficking of molecules between organelles (Kumamoto and Oshio, 2013). The expression of stathmin was decreased in the Cu+N group. This protein is part of the cytoplasmic structure and involved in the maintenance and breakdown of microtubules (Belmont and Mitchison, 1996).

In summary, during the demyelination process, proteins involved in cytoskeletal activity were upregulated, while proteins related to energy production, signal transduction pathways and processes, metabolic processes, protein folding, and other activities were upregulated in mitochondrial membrane involvement (e.g., MICOS complex subunit Mic60 isoform 1 protein) and downregulated in vesicle transport

(e.g., guanosine diphosphate dissociation inhibitor). Meanwhile, during the remyelination process, proteins related to energy production were upregulated, while proteins related genetic material, cytoskeletal activation, and cytoplasmic activity (e.g., stathmin) were downregulated.

Furthermore, among these identified proteins, those whose expression decreased during demyelination and increased during remyelination were identified, because the deficiency of these proteins may be related to damage to the myelin sheath and targeting these protein may ameliorate the demyelination damage induced by CPZ. Accordingly, CRYM and PDIA3 in the hippocampus were analyzed as the candidates using immunostaining, and consistent results were obtained. CRYM immunoreactivity was decreased in hippocampal DG, CA1, and CA3 during demyelination and increased in DG and CA1 during remyelination. According to previous studies, CRYM expression peaks at first and then decreases following extensive expression in immature neurons of hippocampal CA1 after birth (Hommyo et al., 2018). In the present experiment, CRYM, which was upregulated in hippocampal CA1 after remyelination, may play a similar role during hippocampal neuronal development. Furthermore, PDIA3 immunoreactivity was decreased in DG, CA1, and CA3 in the demyelinated state and increased in CA1 and CA3 in the remyelinated state. The increase in PDIA3 expression in the remyelinated state in the present experiment is supported by a previous finding that mutant PDIA3 exhibited impaired neurogenesis function (Bilches Medinas et al., 2022). PDIA3 and CRYM immunoreactivity was significantly increased in the hippocampal CA1 region during remyelination. Therefore, immunohistochemical results for PDIA3 and CRYM in the hippocampus indicated that the expression of these proteins

decreases upon demyelination and increases upon remyelination. Overall, the results of proteomic analysis and protein validation were consistent.

Experiment II

In experiment I, I confirmed that the expression of CRYM and PDIA3 decreased during demyelination and increased during remyelination. CRYM is known as the NADPH-dependent p38 cytosolic T3-binding protein (Vié et al., 1997). Although it is highly expressed in the brain, its neurobiological function remains unknown (Suzuki et al., 2007). The PDI group proteins are upregulated in various neurological disorders as well as in Alzheimer's, Huntington's, and Parkinson's diseases (Andreu et al., 2012; Hwang et al., 2005). PDIA3 is a molecular chaperone belonging to the PDI group (Kozlov et al., 2010); however, the effects of Tat-CRYM or Tat-PDIA3 on myelin damage, cell proliferation, neuroblast differentiation, and CREB phosphorylation in the hippocampus during demyelination or remyelination remain unknown.

As long-term (8 weeks) exposure to CPZ induces strong demyelination in the brain (Koutsoudaki et al., 2009), CPZ was administered for 8 weeks. In addition, neuroblasts and immature neurons have been reported to express DCX by 4 weeks after birth (Couillard-Despres et al., 2005).

The elucidate the effect of Tat-CRYM or Tat-PDIA3 on CPZ-induced demyelination, immunohistochemical staining of MBP, the major component of myelin sheath, was performed. In the present study, only Tat-PDIA3 efficiently ameliorated CPZ-induced demyelination in the hippocampus.

Next, inflammatory response was visualized to detect microglia in the hippocampus, because microglia, which are involved in the inflammatory response of the central nervous system, are one of the major cell types (Saijo et al., 2009). These cells contribute to brain damage repair and brain development under normal physiological conditions (Bachiller et al., 2018; Harry and Kraft, 2012). CPZ-induced demyelination activates microglia, with hypertrophied cytoplasm and thickened processes. Likewise, abnormal microglial activation has been observed in several neurodegenerative diseases that affect cognition and memory, such as Parkinson's and Alzheimer's diseases (Joers et al., 2017; Wang et al., 2015). However, in the present study, no CPZ-induced microglial activation was observed following Tat-PDIA3 and Tat-CRYM treatment.

To assess the effects of Tat-PDIA3 and Tat-CRYM on CPZ-induced reduction in AHN, proliferating cells and differentiated neuroblasts were visualized through immunohistochemical staining for Ki67 and DCX. Consistent with previous reports (Hahn et al., 2022; Kim et al., 2019), CPZ diet reduced the number of proliferating cells and differentiated neuroblasts in the DG. However, Tat-PDIA3 and Tat-CRYM treatment significantly mitigated these effects in the DG even during demyelination. These findings are supported by a previous report that Tat-PDIA3 administration further increased the number of proliferating cells and neuroblast in the hippocampal DG under ischemic damage (Yoo et al., 2019).

The maturation, survival, and integration of newly generated neurons in the hippocampus is controlled by CREB-dependent signaling (Merz et al., 2011; Ortega-Martínez, 2015), and the number of proliferating cells and neuroblasts is positively correlated with pCREB levels in the hippocampus after CPZ administration (Hahn

et al., 2022; Kim et al., 2019). CPZ-induced demyelination significantly decreased the number of pCREB-positive nuclei in the SGZ of DG, while only Tat-PDIA3 treatment exerted an ameliorative effect on the suppression of CREB signaling under demyelination.

In previous studies, downregulation of CRYM mRNA was reported in animal models of neurodegenerative disorders (Brochier et al., 2008; Hodges et al., 2006), and CRYM was reported to exert neuroprotective effects in the striatum in a mouse model of Huntington's disease (Francelle et al., 2015). In addition, PDIA3 downregulation led to acute motor dysfunction with synaptic loss (Woehlbier et al., 2016). Furthermore, neuroprotective effects of PDIA3 against toxicity induced by methamphetamine, a neurotoxic drug, have been demonstrated in a neuroblastoma cell line (Pendyala et al., 2012). Thus, increased CRYM and PDIA3 expression may be the one of the compensatory mechanisms to protect the neurons from demyelination induced by CPZ exposure. Taken together, the improvement of neurogenesis and CREB signaling suggests that PDIA3 serves as an essential modulation target in hippocampal neurogenesis during demyelination and remyelination.

In the present study, the mechanism of Tat-PDIA1 remains to be elucidated, although several hypotheses can be proposed. As the PDI family is involved in redox folding, the misfolded substrates go through the refolding cycle in conjunction with another chaperone calnexin (CNX) (Medinas et al., 2022). In particular, PDIA3 is involved in the oxidative folding of CNX and glycoproteins (Kanemura et al., 2020), and deficiency of this protein may lead to the misfolding and dysfunction of myelin protein zero, which is one of the major myelin components (Jung et al., 2011).

Additionally, a previous study has shown that CNX is involved in the folding of myelin proteins (Dickson et al., 2002). Therefore, PDIA3 and CNX are synergistically involved in myelin regeneration and, ultimately, nerve regeneration. Corroborating the speculations of Castillo et al. (2015) that PDIA3 is a central component of the CNX–calreticulin cycle and serves relevant functions in maintaining glial protein degradation, this protein may contribute to the maintenance of the myelin structure.

CONCLUSION

CPZ induced demyelination and activated microglia in the hippocampus, significantly suppressing cell proliferation, neuroblast differentiation, and CREB phosphorylation in the DG. Meanwhile, switch to normal diet from CPZ diet reversed the damage to the myelin sheath and suppression of cell proliferation, neuroblast differentiation, and CREB phosphorylation.

Further, significantly altered protein profiles were assessed through 2DE and LC-MS/MS after the intake of CPZ diet and after switch to normal diet. Specifically, the expression of CRYM and PDIA3 was decreased after the intake of CPZ diet and increased after switch to normal diet. Consistent with the findings of proteomic analyses, the expression of PDIA3 and CRYM in the hippocampal DG was significantly decreased during demyelination and increased during remyelination.

After validating the above results, the Tat-CRYM and Tat-PDIA3 proteins were prepared. Treatment with both proteins alleviated the suppression of cell proliferation and neuroblast differentiation in the hippocampus, while treatment with Tat-PDIA3 alone mitigated the damage to the myelin sheath and suppression of CREB signaling during demyelination. Therefore, PDIA3 may be useful to prevent demyelination-induced impairments in neurogenesis.

REFERENCES

Amaral, D.G., Scharfman, H.E., and Lavenex, P. (2007). The dentate gyrus: fundamental neuroanatomical organization (dentate gyrus for dummies). Prog Brain Res. *163*, 3-22.

Andreu, C.I., Woehlbier, U., Torres, M., and Hetz, C. (2012). Protein disulfide isomerases in neurodegeneration: from disease mechanisms to biomedical applications. FEBS Lett. *586*, 2826-2834.

Antes, I., Chandler, D., Wang, H., and Oster, G. (2003). The unbinding of ATP from F1-ATPase. Biophys J. *85*, 695-706.

Bachiller, S., Jiménez-Ferrer, I., Paulus, A., Yang, Y., Swanberg, M., Deierborg, T., and Boza-Serrano, A. (2018). Microglia in neurological diseases: a road map to brain-disease dependent-inflammatory response. Front Cell Neurosci. *12*, 488.

Beckervordersandforth, R., Zhang, C.L., and Lie, D.C. (2015). Transcription-factor-dependent control of adult hippocampal neurogenesis. Cold Spring Harb Perspect Biol. *7*, a018879.

Belmont LD, Mitchison TJ. (1996). Identification of a protein that interacts with tubulin dimers and increases the catastrophe rate of microtubules. Cell. *84*, 623-631.

Bilches Medinas D, Malik S, Yıldız-Bölükbaşı E, et al. (2022) Mutation in protein disulfide isomerase A3 causes neurodevelopmental defects by disturbing endoplasmic reticulum proteostasis. EMBO J. *41*, e105531.

Borel, F., Hachi, I., Palencia, A., Gaillard, M.-C., and Ferrer, J.-L. (2014). Crystal structure of mouse mu-crystallin complexed with NADPH and the T3 thyroid hormone. FEBS J. *281*, 1598-1612.

Brochier, C., Gaillard, M.-C., Diguet, E., Caudy, N., Dossat, C., Ségurens, B., Wincker, P., Roze, E., Caboche, J., Hantraye, P.*, et al.* (2008). Quantitative gene expression profiling of mouse brain regions reveals differential transcripts conserved in human and affected in disease models. Physiol Genomics.*33*, 170-179.

Castilla-Ortega, E., Pedraza, C., Estivill-Torrús, G., and Santín, L.J. (2011). When is adult hippocampal neurogenesis necessary for learning? evidence from animal research. Rev Neurosci *22*, 267-283.

Castillo V, Oñate M, Woehlbier U, Rozas P, Andreu C, Medinas D, Valdés P, Osorio F, Mercado G, Vidal RL, Kerr B, Court FA, Hetz C. (2015). Functional role of the disulfide isomerase ERp57 in axonal regeneration. PLoS One.*10*, e0136620.

Cheng, M.Y., Hartl, F.U., Martin, J., Pollock, R.A., Kalousek, F., Neupert, W., Hallberg, E.M., Hallberg, R.L., and Horwich, A.L. (1989). Mitochondrial heat-shock protein hsp60 is essential for assembly of proteins imported into yeast mitochondria. Nature *337*, 620-625.

Chuang, D. M., Hough, C., & Senatorov, V. V. (2005). Glyceraldehyde-3-phosphate dehydrogenase, apoptosis, and neurodegenerative diseases. Annu Rev Pharmacol Toxicol. *45*, 269–290.

Ciavardelli, D., Silvestri, E., Del Viscovo, A., Bomba, M., De Gregorio, D., Moreno, M., Di Ilio, C., Goglia, F., Canzoniero, L. M., & Sensi, S. L. (2010). Alterations of brain and cerebellar proteomes linked to Aβ and tau pathology in a female triple-transgenic murine model of Alzheimer's disease. Cell Death Dis. *1*, e90.

Cornell, B., and Toyo-oka, K. (2017). 14-3-3 proteins in brain development: neurogenesis, neuronal migration and neuromorphogenesis. Front Mol Neurosci.*10*, 318.

Couillard-Despres, S., Winner, B., Schaubeck, S., Aigner, R., Vroemen, M., Weidner,

N., Bogdahn, U., Winkler, J., Kuhn, H.G., and Aigner, L. (2005). Doublecortin expression levels in adult brain reflect neurogenesis. Eur J Neurosci. *21*, 1-14.

Dickson KM, Bergeron JJ, Shames I, Colby J, Nguyen DT, Chevet E, et al. (2002) Association of calnexin with mutant peripheral myelin protein-22 ex vivo: a basis for "gain-of-function" ER diseases. Proc Natl Acad Sci U S A. *99*, 9852-9857

Dutta, R., Chomyk, A.M., Chang, A., Ribaudo, M.V., Deckard, S.A., Doud, M.K., Edberg, D.D., Bai, B., Li, M., Baranzini, S.E.*, et al.* (2013). Hippocampal demyelination and memory dysfunction are associated with increased levels of the neuronal microRNA miR-124 and reduced AMPA receptors. Ann Neurol. *73*, 637-645.

Eichenbaum, H. (2017). The role of the hippocampus in navigation is memory. J Neurophysiol. *117*, 1785-1796.

Francelle, L., Galvan, L., Gaillard, M.-C., Guillermier, M., Houitte, D., Bonvento, G., Petit, F., Jan, C., Dufour, N., Hantraye, P.*, et al.* (2015). Loss of the thyroid hormone-binding protein Crym renders striatal neurons more vulnerable to mutant huntingtin in Huntington's disease. Hum Mol Genet. *24*, 1563-1573.

Füchtbauer, A., Jockusch, B.M., Leberer, E., and Pette, D. (1986). Actin-severing activity copurifies with phosphofructokinase. Proc Natl Acad Sci U S A. *83*, 9502-9506.

Gage, F.H. (2002). Neurogenesis in the adult brain. J Neurosci. *22*, 612.

Gan, Y., Ye, F., and He, X.-X. (2020). The role of YWHAZ in cancer: a maze of opportunities and challenges. J Cancer. *11*, 2252-2264.

Guimarães, J., and Sá, M.J. (2012). Cognitive dysfunction in multiple sclerosis. Front Neurol. *3*, 74.

Hahn, K.R., Kim, W., Jung, H.Y., Kwon, H.J., Kim, D.W., Hwang, I.K., and Yoon, Y.S. (2022). Comparison of the effects of cuprizone on demyelination in the corpus callosum and hippocampal progenitors in young adult and aged mice. Neurochem Res. *47*, 1073-1082.

Harry, G.J., and Kraft, A.D. (2012). Microglia in the developing brain: a potential target with lifetime effects. Neurotoxicology. *33*, 191-206.

Hodges, A., Strand, A.D., Aragaki, A.K., Kuhn, A., Sengstag, T., Hughes, G., Elliston, L.A., Hartog, C., Goldstein, D.R., Thu, D.*, et al.* (2006). Regional and cellular gene expression changes in human Huntington's disease brain. Hum Mol Genet. *15*, 965-977.

Hommyo, R., Suzuki, S.O., Abolhassani, N., Hamasaki, H., Shijo, M., Maeda, N., Honda, H., Nakabeppu, Y., and Iwaki, T. (2018). Expression of CRYM in different rat organs during development and its decreased expression in degenerating pyramidal tracts in amyotrophic lateral sclerosis. Neuropathology. *38*, 247-259.

Hurowitz, E.H., Melnyk, J.M., Chen, Y.-J., Kouros-Mehr, H., Simon, M.I., and Shizuya, H. (2000). Genomic characterization of the human heterotrimeric G Protein α, β, and γ subunit genes. DNA Res. *7*, 111-120.

Hwang, I.K., Yoo, K.-Y., Kim, D.W., Han, B.H., Kang, T.-C., Choi, S.Y., Kim, J.S., and Won, M.H. (2005). Protein disulfide isomerase immunoreactivity and protein level changes in neurons and astrocytes in the gerbil hippocampal CA1 region following transient ischemia. Neurosci Lett. *375*, 117-122.

Joers, V., Tansey, M.G., Mulas, G., and Carta, A.R. (2017). Microglial phenotypes in Parkinson’s disease and animal models of the disease Prog Neurobiol. *155*, 57-75.

Jung, H.Y., Kim, W., Hahn, K.R., Kwon, H.J., Nam, S.M., Chung, J.Y., Yoon, Y.S., Kim, D.W., Yoo, D.Y., and Hwang, I.K. (2020). Effects of pyridoxine deficiency on

hippocampal function and its possible association with V-Type proton ATPase Subunit B2 and heat shock cognate Protein 70. Cells *9*, 1067.

Jung, H.Y., Kwon, H.J., Kim, W., Nam, S.M., Kim, J.W., Hahn, K.R., Yoo, D.Y., Won, M.-H., Yoon, Y.S., Kim, D.W.*, et al.* (2019). Phosphoglycerate mutase 1 promotes cell proliferation and neuroblast differentiation in the dentate gyrus by facilitating the phosphorylation of cAMP response element-binding protein. Neurochem Res. *44*, 323-332.

Jung J, Coe H, Michalak M. (2011) Specialization of endoplasmic reticulum chaperones for the folding and function of myelin glycoproteins P0 and PMP22. FASEB J. *25*, 3929–37

Kanemura S, Matsusaki M, Inaba K, Okumura M. (2020) PDI family members as guides for client folding and assembly. Int J Mol Sci. *21*, 9351.

Kelm, R.J., Jr., Cogan, J.G., Elder, P.K., Strauch, A.R., and Getz, M.J. (1999). Molecular interactions between single-stranded DNA-binding proteins associated with an essential MCAT element in the mouse smooth muscle alpha-actin promoter. J Biol Chem. *274*, 14238-14245.

Kempermann, G., Kuhn, H.G., and Gage, F.H. (1997). Genetic influence on neurogenesis in the dentate gyrus of adult mice. Proc Natl Acad Sci U S A. *94*, 10409-10414.

Kempermann, G., Song, H., and Gage, F.H. (2015). Neurogenesis in the adult hippocampus. Cold Spring Harb Perspect Biol. *7*, a018812.

Kim, W., Hahn, K.R., Jung, H.Y., Kwon, H.J., Nam, S.M., Kim, J.W., Park, J.H., Yoo, D.Y., Kim, D.W., Won, M.H.*, et al.* (2019). Melatonin ameliorates cuprizone-induced reduction of hippocampal neurogenesis, brain-derived neurotrophic factor, and phosphorylation of cyclic AMP response element-binding protein in the mouse

dentate gyrus. Brain Behav. *9*, e01388.

Klein, B., Mrowetz, H., Kreutzer, C., Rotheneichner, P., Zaunmair, P., Lange, S., Coras, R., Couillard-Despres, S., Rivera, F.J., and Aigner, L. (2020). DCX(+) neuronal progenitors contribute to new oligodendrocytes during remyelination in the hippocampus. Sci Rep. *10*, 20095.

Koutsoudaki, P.N., Skripuletz, T., Gudi, V., Moharregh-Khiabani, D., Hildebrandt, H., Trebst, C., and Stangel, M. (2009). Demyelination of the hippocampus is prominent in the cuprizone model. Neurosci Lett. *451*, 83-88.

Kozjak-Pavlovic V. (2017). The MICOS complex of human mitochondria. Cell Tissue Res. *367*,83-93.

Kozlov, G., Määttänen, P., Thomas, D.Y., and Gehring, K. (2010). A structural overview of the PDI family of proteins. FEBS J. *277*, 3924-3936.

Kumamoto, T., and Oshio, S. (2013). Effect of fetal exposure to bisphenol A on brain mediated by X-chromosome inactivation. J Toxicol Sci. *38*, 485-494.

Lassmann H. (2018). Multiple sclerosis pathology. Cold Spring Harb Perspect Med. 8, a028936.

Leicaj, M.L., Pasquini, L.A., Lima, A., Gonzalez Deniselle, M.C., Pasquini, J.M., De Nicola, A.F., and Garay, L.I. (2018). Changes in neurosteroidogenesis during demyelination and remyelination in cuprizone-treated mice. J Neuroendocrinol. *30*, e12649.

Lu, Z., Yang, G., Qin, Z., Shen, H., Zhang, M., Shi, F., Li, J., Sarath Babu, V., and Lin, L. (2020). Glutamate related osmoregulation of guanine nucleotide-binding protein G (I) α2 from giant freshwater prawn (Macrobrachium rosenbergii) during molting and salinity stress. Aquaculture. *521*, 735000.

Matsushima, G.K., and Morell, P. (2001). The neurotoxicant, cuprizone, as a model to study demyelination and remyelination in the central nervous system. Brain Pathol. *11*, 107-116.

Medinas DB, Rozas P, Hetz C. (2022). Critical roles of protein disulfide isomerases in balancing proteostasis in the nervous system. J Biol Chem. *298*,102087.

Meyer-Siegler, K., Mauro, D.J., Seal, G., Wurzer, J., deRiel, J.K., and Sirover, M.A. (1991). A human nuclear uracil DNA glycosylase is the 37-kDa subunit of glyceraldehyde-3-phosphate dehydrogenase. Proc Natl Acad Sci U S A. *88*, 8460-8464.

Morgenegg, G., Winkler, G.C., Hübscher, U., Heizmann, C.W., Mous, J., and Kuenzle, C.C. (1986). Glyceraldehyde-3-phosphate dehydrogenase is a nonhistone protein and a possible activator of transcription in neurons. J Neurochem. *47*, 54-62.

Mu, Y., Zhao, C., and Gage, F.H. (2011). Dopaminergic modulation of cortical inputs during maturation of adult-born dentate granule cells. J Neurosci. *31*, 4113-4123.

Omotoso, G.O., Olajide, O.J., Gbadamosi, I.T., Adebayo, J.O., Enaibe, B.U., Akinola, O.B., and Owoyele, B.V. (2019). Cuprizone toxicity and Garcinia kola biflavonoid complex activity on hippocampal morphology and neurobehaviour. Heliyon *5*, e02102.

Ortega-Martínez, S. (2015). A new perspective on the role of the CREB family of transcription factors in memory consolidation via adult hippocampal neurogenesis. Front Mol Neurosci. *8*, 46.

Park, K.S., Kim, H., Kim, N.G., Cho, S.Y., Choi, K.H., Seong, J.K., and Paik, Y.K. (2002). Proteomic analysis and molecular characterization of tissue ferritin light chain in hepatocellular carcinoma. Hepatology. *35*, 1459-1466.

Partridge, M.A., Myers, S.J., Gopinath, S., and Coorssen, J.R. (2015). Proteomics of a conundrum: Thoughts on addressing the aetiology versus progression of multiple sclerosis. Proteomics Clin Appl. *9*, 838-843.

Paxinos, G. and Franklin, K.B.J. (2001) The Mouse Brain in Stereotaxic Coordinates. 2nd Edition, Academic Press, San Diego.

Pendyala, G., Ninemire, C., and Fox, H.S. (2012). Protective role for the disulfide isomerase PDIA3 in methamphetamine neurotoxicity. PLoS One *7*, e38909.

Planche, V., Koubiyr, I., Romero, J.E., Manjon, J.V., Coupé, P., Deloire, M., Dousset, V., Brochet, B., Ruet, A., and Tourdias, T. (2018). Regional hippocampal vulnerability in early multiple sclerosis: Dynamic pathological spreading from dentate gyrus to CA1. Hum Brain Mapp.*39*, 1814-1824.

Pollitt, S.L., Myers, K.R., Yoo, J., and Zheng, J.Q. (2020). LIM and SH3 protein 1 localizes to the leading edge of protruding lamellipodia and regulates axon development Mol Biol Cell. *31*, 2718-2732.

Saijo, K., Winner, B., Carson, C.T., Collier, J.G., Boyer, L., Rosenfeld, M.G., Gage, F.H., and Glass, C.K. (2009). A Nurr1/CoREST pathway in microglia and astrocytes protects dopaminergic neurons from inflammation-induced death. Cell *137*, 47-59.

Salvatore, F., Izzo, P., and Paolella, G. (1986). Aldolase gene and protein families: structure, expression and pathophysiology. Horiz Biochem Biophys. *8*, 611-665.

Sen, M.K., Almuslehi, M.S.M., Shortland, P.J., Mahns, D.A., and Coorssen, J.R. (2021). Proteomics of multiple sclerosis: Inherent issues in defining the pathoetiology and identifying (Early) biomarkers. Int J Mol Sci. *22*, 7377.

Sikand, K., Singh, J., Ebron, J.S., and Shukla, G.C. (2012). Housekeeping gene selection advisory: glyceraldehyde-3-phosphate dehydrogenase (GAPDH) and β-

actin are targets of miR-644a. PLoS One *7*, e47510.

Singh, R., and Green, M.R. (1993). Sequence-specific binding of transfer RNA by glyceraldehyde-3-phosphate dehydrogenase. Science *259*, 365-368.

Skripuletz, T., Manzel, A., Gropengiesser, K., Schafer, N., Gudi, V., Singh, V., Salinas Tejedor, L., Jorg, S., Hammer, A., Voss, E.*, et al.* (2015). Pivotal role of choline metabolites in remyelination. Brain *138*, 398-413.

Suzuki, S., Suzuki, N., Mori, J., Oshima, A., Usami, S., and Hashizume, K. (2007). micro-Crystallin as an intracellular 3,5,3'-triiodothyronine holder in vivo. Mol Endocrinol. *21*, 885-894.

Szilagyi, G.T., Nawrocki, A.M., Eros, K., Schmidt, J., Fekete, K., Elkjaer, M.L., Hyrlov, K.H., Larsen, M.R., Illes, Z., and Gallyas, F. (2020). Proteomic changes during experimental deand remyelination in the corpus callosum. PLoS One *15*, 1-21.

Tisdale, E.J. (2001). Glyceraldehyde-3-phosphate dehydrogenase is required for vesicular transport in the early secretory pathway. J Biol Chem. *276*, 2480-2486.

Toni, N., and Schinder, A.F. (2015). Maturation and functional integration of new granule cells into the adult hippocampus. Cold Spring Harb Perspect Biol. *8*, a018903.

Vié, M.P., Evrard, C., Osty, J., Breton-Gilet, A., Blanchet, P., Pomérance, M., Rouget, P., Francon, J., and Blondeau, J.P. (1997). Purification, molecular cloning, and functional expression of the human nicodinamide-adenine dinucleotide phosphate-regulated thyroid hormone-binding protein. Mol Endocrinol. *11*, 1728-1736.

Visser, W.E., Wong, W.S., van Mullem, A.A., Friesema, E.C., Geyer, J., and Visser, T.J. (2010). Study of the transport of thyroid hormone by transporters of the SLC10

family. Mol Cell Endocrinol. *315*, 138-145.

Wang, C., Yoo, Y., Fan, H., Kim, E., Guan, K.-L., and Guan, J.-L. (2010). Regulation of Integrin β 1 recycling to lipid rafts by Rab1a to promote cell migration. J Biol Chem. *285*, 29398-29405.

Wang, W.-Y., Tan, M.-S., Yu, J.-T., and Tan, L. (2015). Role of pro-inflammatory cytokines released from microglia in Alzheimer's disease. Ann Transl Med. *3*, 7.

Werner, S.R., Saha, J.K., Broderick, C.L., Zhen, E.Y., Higgs, R.E., Duffin, K.L., and Smith, R.C. (2010). Proteomic analysis of demyelinated and remyelinating brain tissue following dietary cuprizone administration. Journal of Molecular Neuroscience. *42*, 210-225.

Woehlbier, U., Colombo, A., Saaranen, M.J., Pérez, V., Ojeda, J., Bustos, F.J., Andreu, C.I., Torres, M., Valenzuela, V., Medinas, D.B.*, et al.* (2016). ALS-linked protein disulfide isomerase variants cause motor dysfunction. EMBO J. *35*, 845-865.

Wu, B., Su, S., Patil, D.P., Liu, H., Gan, J., Jaffrey, S.R., and Ma, J. (2018). Molecular basis for the specific and multivariant recognitions of RNA substrates by human hnRNP A2/B1. Nat Commun. *9*, 420.

Wu, C.-Z., Chang, L.-C., Lin, Y.-F., Hung, Y.-J., Pei, D., and Chen, J.-S. (2015). Chaperonin-Containing t-Complex Protein-1 Subunit β as a Possible Biomarker for the Phase of Glomerular Hyperfiltration of Diabetic Nephropathy. Dis Markers. *2015*, 548101.

Yang, Z., & Wang, K. K. (2015). Glial fibrillary acidic protein: from intermediate filament assembly and gliosis to neurobiomarker. Trends Neurosci. *38*, 364–374.

Yoo, D.Y., Cho, S.B., Jung, H.Y., Kim, W., Choi, G.-M., Won, M.-H., Kim, D.W., Hwang, I.K., Choi, S.Y., and Moon, S.M. (2017). Tat-protein disulfide-isomerase A3:

a possible candidate for preventing ischemic damage in the spinal cord. Cell Death Dis. *8*, e3075-e3075.

Yoo, D.Y., Cho, S.B., Jung, H.Y., Kim, W., Lee, K.Y., Kim, J.W., Moon, S.M., Won, M.-H., Choi, J.H., Yoon, Y.S.*, et al.* (2019). Protein disulfide-isomerase A3 significantly reduces ischemia-induced damage by reducing oxidative and endoplasmic reticulum stress. Neurochem Int. *122*, 19-30.

Yoo, D.Y., Jung, H.Y., Kim, J.W., Yim, H.S., Kim, D.W., Nam, H., Suh, J.G., Choi, J.H., Won, M.H., Yoon, Y.S.*, et al.* (2016). Reduction of dynamin 1 in the hippocampus of aged mice is associated with the decline in hippocampal-dependent memory. Mol Med Rep. *14*, 4755-4760.

Zhang, J., Yang, L., Fang, Z., Kong, J., Huang, Q., and Xu, H. (2018). Adenosine promotes the recovery of mice from the cuprizone-induced behavioral and morphological changes while effecting on microglia and inflammatory cytokines in the brain. J Neuroimmune Pharmacol. *13*, 412-425.

Zhang, Y., Baig, E., and Williams, D.B. (2006). Functions of ERp57 in the folding and assembly of major histocompatibility complex class I molecules. J Biol Chem. *281*, 14622-14631.

국문 초록

다발성경화증(multiple sclerosis)은 수초의 손상을 특징으로 하는 자가면역성 질환이다. 이러한 특징 때문에, 탈수초 현상을 일으키는 큐프리존(cuprizone) 모델은 다발성경화증 연구에 널리 사용되고 있다. 이번 실험의 목적은 큐프리존을 통한 탈수초화 및 재수초화 과정에서 해마에서 유의적으로 변화하는 단백질을 확인하고, 몇 가지의 단백질을 통해 탈수초화 억제를 유도할 수 있는 단백질을 도출하고자 하였다.

5주령 마우스에 8주간 큐프리존이 첨가된 사료 섭취 또는 5주간 큐프리존 사료 섭취 및 3주 정상 사료 섭취를 통해 수초화 및 탈수초화 모델을 유도하였다. 큐프리존 섭취로 인해 해마에서 수초의 손상이 유도되었으며, 해마의 과립 밑 구역에서 세포증식, 신경모세포 분화 및 CREB 신호를 유의적으로 감소시키는 것을 확인할 수 있었다. 반면에, 큐프리존 섭취를 중단하고 일반사료로 전환한 결과로 수초, 세포증식, 신경모세포 및 CREB 신호전달이 해마에서 유의적으로 개선되는 것을 확인할 수 있었다.

이후에, 단백질 발현을 조사하기 위해 2차원 겔 전기영동(2DE) 및 액체크로마토그래프-질량분석기(LC-MS/MS) 기반 정량화 방법을 사용하였다. 큐프리존 식이 중 발현된 단백질과 큐프리존 섭취를 중단

후 발현된 단백질 중에서 유의적으로 변화하는(2배 이상 증가 또는 감소) 리스트를 확인하였으며, 그중에서 큐프리존 식이를 할 때는 발현이 감소하고 큐프리존 식이를 중단했을 때 발현이 증가하는 단백질들을 확인하였다. 그 이유는, 이러한 변화 경향을 보이는 단백질이 탈수초화 및 수초화에 직접 관여할 것으로 생각했기 때문이다. 케티민환원효소 뮤-크리스탈린(CRYM)과 단백질 이황화이소머라제 A3 전구체(PDIA3)를 확인할 수 있었으며, 정확한 조직 내에서 변화를 확인하기 위하여, CRYM와 PDIA3에 대한 면역조직화학염색을 수행하였다. 그 결과 탈수초화 시 해마의 CA1에서 유의하게 감소하고 재수초화 시 증가한 것을 확인할 수 있었으며, 단백질 분석 및 면역염색의 결과는 같았다.

이 두 단백질을 큐프리존 식이 중에 실험 동물에게 직접 투여하여 해마에서 수초화, 신경세포재생 등의 변화를 확인하였다. 단백질의 혈관뇌 투과성 및 세포 내 투과성을 높이기 위하여, Tat-융합단백질인 Tat-CRYM 및 Tat-PDIA3를 제조하였다. 실험동물군은 대조군, 큐프리존 식이군, 큐프리존 식이와 Tat-CRYM을 투여한 군, 그리고 큐프리존 식이와 Tat-PDIA3를 투여한 군으로 나누었으며, 큐프리존을 함유한 식이는 8주간, Tat-CRYM 및 Tat-PDIA3 단백질은 마지막 4주간 복강 내로 하루에 1회 투여를 하였다. 면역염색 결과, Tat-CRYM과 Tat-PDIA3를 각각 투여한 그룹에서 큐프리존 식이군 대비 해마의 세포증식과 신경모세포 분화가 유의적으로 증가하였다. 반면,

Tat-PDIA3 투여군에서만 수초와 CREB 신호가 증가한 것을 확인할 수 있었다. 이러한 결과는 Tat-PDIA3가 CREB 신호의 인산화를 증가시킴으로써 해마에서 큐프리존 유도 탈수초화 및 해마 신경 생성의 감소를 개선한다는 것을 시사한다.

결론적으로, 큐프리존 급여는 탈수초화를 유도하며, 이와 함께 해마에서 세포증식, 신경모세포분화를 억제하며, 이는 CREB 신호를 억제하는 것과 연관이 있었다. 반면, 큐프리존 식이를 중단함으로써 재수초화 과정에서 해마에서는 수초화, 세포증식, 신경모세포분화, CREB 신호가 개선되는 것을 확인할 수 있었다. 탈수초화와 재수초화 과정을 단백질 분석을 통해 탈수초화시에는 발현이 감소가 되고 재수초화시에 발현이 증가하는 단백질로 CRYM과 PDIA3의 존재를 확인하였다. 탈수초화 상태에서 CRYM과 PDIA3를 투여한 결과, 두 투여군 모두 해마의 세포증식과 신경모세포 분화가 개선되었으며 PDIA3에서만 말이집과 CREB 신호가 개선되는 것을 확인할 수 있었다. 이상의 결과를 종합해 볼 때, PDIA3는 탈수초화 및 재수초화에서 매우 중요한 역할을 하며, 이러한 단백질은 탈수초화의 예방 또는 치료를 위한 접근 방식이 될 수 있다. 이러한 결과로 PDIA3의 다발성경화증 치료제의 가능성을 제시할 수 있다.

주요어: 신경세포재생, 해마, 다발성경화증, 큐프리존, 탈수초화, 재수초화, 케티민환원효소 뮤-크리스탈린, 단백질 이황화이소머라제 A3 전구체

학 번: 2016-21756